Self-Induced Cracking Problems in Hardening Concrete Structures

Daniela Bosnjak

Department of Structural Engineering
The Norwegian University of Science and Technology
Trondheim

December 2000

Acknowledgement

This work has been prepared during my Ph.D. study carried out at Department of Structural Engineering, Norwegian University of Science and Technology. It is related to two research programmes:
The national project NOR-IPACS supported by the Norwegian Research Council (NFR), with the following partners: Selmer ASA, Elkem ASA Materials, Norcem A/S, Fesil ASA, Norwegian Public Roads Directorate and the Norwegian University of Science and Technology (NTNU),
The European Brite-Euram program IPACS with the partners from Sweden (Scancem AB, TU Luleå, NCC AB, Skanska, Teknik AB), Norway (Selmer ASA, Norwegian Public Roads Directorate, Elkem ASA Materials, Norcem AS and NTNU), Italy (ENEL and Ismes), Germany (TU Braunschweig) and The Netherlands (TU Delft).
The financial support has come from the following sources:

- 2.5 years dr.ing. individual stipend from NFR
- The Brite-Euram project IPACS
- The NFR-project NOR-IPACS
- The NFR-project “Material modelling for structural analysis”

First of all I want to express my gratitude to my supervisor Terje Kanstad. Without his professional support, his permanent encouragement and his enthusiasm in research, this work have not been possible.

I am also grateful to my colleagues at the Department of Structural Engineering, especially to Prof. Erik Sellevold for the fruitful discussions, Øyvind Bjøntegaard, who has let me use his experimental results, and Jan Øverli who has never hesitated to give me computer advice. Also thanks to the rest of the Concrete group for a pleasant and good working environment.

As a part of this research I spent 3 months at TNO Construction and Building Research, Department of Engineering Mechanics and Information Technology, Rijswijk, The Netherlands. I want to thank the staff in the Group for Computational Mechanics for support and good working conditions during my stay and for valuable help with the source code of the finite element program DIANA. Particularly I appreciate the assistance of Rob ter Steeg and Max Hendrix.

Finally, I want to thank my family - my parents and sisters for taking care of my children, Jan and Una, during the last part of my study. And Zeljko whose love has been essential for my peace of mind during these years.

Abstract

This thesis deals with prediction of early age cracking caused by restrained temperature dilation and autogenous deformation. Traditionally, prediction of early-age cracking has been based on temperature criteria. The temperature criteria alone are, however, not sufficiently accurate for cracking prediction. Stress-strain criteria are more reliable because they consider all the crucial factors: thermal dilation, autogenous deformation, mechanical properties and restraint conditions.

The purpose of this dr.ing. project is to extend the general applicability of stress/strain based curing technology, and to contribute to better understanding and better prediction of stresses during hardening of concrete structures.

In the first part of the thesis the major features of hardening concrete are described and mathematical descriptions of the phenomena are given. Different models are discussed, and on the basis of such discussion, new models have been implemented in the FE program DIANA. First, the equivalent time was introduced in parallel to the degree of hydration, so that all material properties may be considered equivalent-time dependent. It is shown that the simpler and more common equivalent-time based model for the heat of hydration development can describe temperature development with the same accuracy as the degree of hydration based model. Further, the activation energy is made temperature dependent instead of being constant. A modified CEB equation for E-modulus development is implemented. The temperature influence on creep is modified by introducing a thermal transitional creep term.

A mathematical description of stress- and strain development in hardening concrete structures is presented, and special attention given to the viscoelastic behaviour of concrete. The influence of creep on self-induced stresses is examined. The emphasis is put on creep importance in different periods of the hardening process. In externally restrained structures, prone to through cracking, creep in the early period (heating phase) reduces the compressive stresses, and consequently increases the tensile stresses in the subsequent cooling period, thus increasing the cracking risk. For internally restrained structures, prone to surface cracking in the early period, creep obviously reduces the cracking risk. In the cooling phase creep reduces the tensile stresses. For externally restrained structures, the effects of creep in the cooling and heating phases are counteracting, and in some cases they annul each other. The present results do not diminish the importance of creep on thermal stresses, to the contrary, it emphasises the necessity of correct prediction of creep during the whole period of hardening.

Three creep models for young concrete are compared: Double Power Law, Maxwell chain model and Burgers model. The models are calibrated against the same experimental data and used in calculation of thermal stresses. The temperature dependency of the models is

also investigated. A good agreement between the Double Power Law and the Maxwell chain was obtained, whereas the Burgers model, which consists of one Kelvin unit and one viscous damper, gave different results. Although the major reason for the deviation is due to the simplicity of the Burgers model, the deviation is also caused by different descriptions of the temperature dependence, and the nature of the test data used in the calibration. Test methods are also discussed, with special weight on the Temperature Stress Testing Machine tests. Although this type of test is indispensable, and very useful to check the validity of the material models and the calculation methods, the shortcomings by using it to predict the creep model parameters are also shown.

Restraint conditions and their influence on thermal stresses were also investigated. Different ways of modelling the structure and the interaction with the subgrade were analysed and compared. Influence of the stiffness of the ground and the structural geometry on thermal stresses and cracking risk was investigated by means of 3D analyses.

The last part of the work is numerical simulation of temperature and stress/strain development in a real structure, the Maridal culvert in Oslo. A comprehensive laboratory test program was performed at NTNU to identify material parameters. Both thermal and mechanical properties were tested. Material models were checked in the TSTM for three different realistic temperature histories. Within the Brite-Euram project IPACS a large field instrumentation programme has been carried out to measure temperature and strain development in the culvert. 3D analyses of the foundations and walls in two of the instrumented sections of this structure were performed with DIANA and calculated results are compared to measurements. Deviation between calculated and measured temperature is within range of $\pm 5^{0}C$. Deviation between calculated and measured strains is about $\pm 50 \times 10^{-6}$. Possible reasons of disagreement between calculations and measurements are discussed. When all uncertainties in material modelling and measuring methods are considered it is concluded that results of the simulation are satisfying.

Contents

Chapter 1

Introduction

1.1 Background

In all concrete structures the concrete is exposed to the volume changes caused by hydration reactions in the first period of hardening. These volume changes are always restrained in a structure to some extent, either externally by adjoining structures, or internally due to temperature variations. As a consequence, stresses are generated during hardening: in the most typical cases, first, compressive stresses in the heating period then tensile stresses in the cooling period. If the tensile stresses exceed the tensile strength, which still can be low, cracking may occur.

Cracking is always undesirable in concrete structures because it jeopardizes structures durability, functionality and appearance. Many deterioration mechanisms depend on water or aggressive substances entering from the outside through the surface layer: sulphate and acid attack, alkali attack, frost attack, chloride penetration, carbonation. All of them are accelerated and enhanced by cracking. Prevention and limitation of early age cracking is therefore of vital importance.

Recently, durability has become of more and more interest in the design of structures and to meet the increasing demands, new types of concrete have been designed, called high performance concrete (HPC). Although these concretes have proved to be better than normal quality concrete in many cases, they have some unfavourable properties. During the hardening they develop a high autogenous deformation, which, in many cases enhances tensile stresses thus increasing the risk of cracking. In recent years, awareness about influence of autogenous deformation on cracking risk has grown, and more and more attention is paid to this phenomenon. The term thermal cracking, traditionally used to describe cracks which develop due to restrained deformation in the hardening period, is thus out-of-date and misleading, and the term self-induced cracking is therefore preferred.

In the past, prediction of early age cracking has been almost exclusively based on temperature criteria. The temperature development in the young concrete was calculated and cracking predicted from the maximal temperature difference in a structure. To avoid cracking, limitations were applied to maximum temperature, temperature difference between the surface and the centre of the structure, and between the new and the older adjoining structure. These limitations were based on practical experience and experience from the laboratory.

The main drawback of the temperature based crack risk estimation is that the other important factors in stress calculation are not considered: restraint conditions, material proper-

ties and shrinkage. It is assumed that cracking risk at early ages depends only on temperature.

Several researchers, f.i. (Emborg 1989) and (Bernander 1994) have shown that there is no general correlation between stresses and temperature. Whether young concrete will crack or not, depends very much on restraint conditions and material properties.

Three most important factors in prediction of early age cracking are:

- the temperature and shrinkage development
- the development of material properties
- restraint conditions

The restraint is a precondition for stress generation - the stress starts developing only if the volume changes are restrained. Due to the different restrained conditions one concrete element may crack and the other may remain uncracked even though they have the same temperature history.

The material properties are also crucial factors in stress generation in hardening concrete. In the first period after casting during the temperature rise, the concrete will expand, and if this expansion is restrained, compressive stresses are generated. If the material properties of hardening concrete were constant in time, compressive stresses would vanish after cooling down to the fresh concrete temperature, and no cracks would occur. The problem arises because of the development of material properties: in the first, heating, period Young's modulus is very low, and the relaxation very high, so that low compressive stresses are generated. In the cooling period, due to increased Young's modulus and reduced relaxation, the compressive stresses are turned into relatively high tensile stresses, and cracking may occur. The problem becomes even more complex if non-uniform development of material properties across the concrete section is taken into account due to non-uniform temperature and maturity distribution. Non uniformity of material properties results in internal restraint causing different relative deformation between different parts of a structure.

The discussion above clearly demonstrates the insufficiency and inaccuracy of temperature criteria. For a reliable crack prediction at early ages stress-strain criteria must be applied. This calls for well-documented material models. In recent years an increased interest in cracking of hardening concrete has led to extensive research on this subject. A large number of material models for young concrete have been presented and implemented in computer programs for the simulation of stress development. The use of these numerical tools has contributed to better understanding of the behaviour of concrete structures at early ages. Numerical analysis may be used not only for crack prediction and investigation of the efficiency of different measures taken with regard to crack control, but also for explanation of different effects in young concrete.

To be reliable, simulation of hardening structures has to take into account temperature development due to hydration, development of material properties and shrinkage, and restraint conditions of the particular structure. Today there exist several commercially available computer programs capable of calculating the temperature and stress development in hardening concrete structures, some of them very powerful. Within the IPACS project a Round Robin calculation has been performed with the aim to map and compare

the existing programs for concrete structure at early ages (Olofsson 1999). Five different programs have been used to simulate temperature and stress development in two examples of hardening concrete structure. All calculations were based on the same set of laboratory test results describing specific concrete properties. Nevertheless, the scatter between their results was significant, see Figure 1.1 .

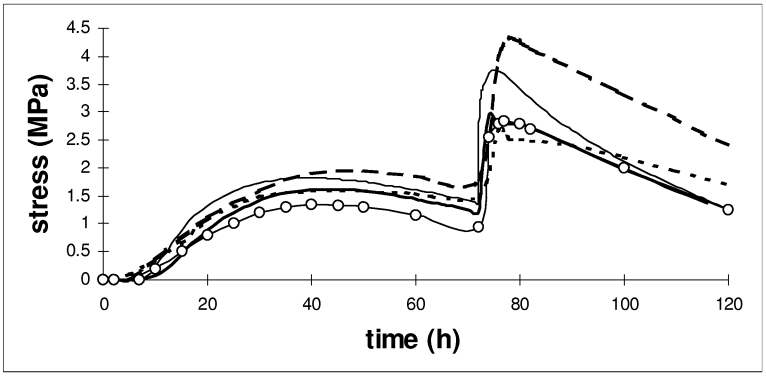

Figure 1.1: Stress development in hardening concrete slab calculated with different programs.

The deviation between the results obtained by different programs may be explained by differences in material modelling, modelling of geometry and restraint conditions. The deviations were considerable even in the case of stress simulation of hardening specimen in the TSTM with well defined temperature and restraining conditions, i.e. when the material modelling was the only reason for disagreement. The different material models were calibrated to the same experimental data, but in simulation of total behaviour of a structure they gave different results. The comparison gave rise to several questions. To which accuracy do material models have to be calibrated against experimental data? What kinds of tests are most appropriate for characterization of different material properties? Which factors are most important for calculation of self-induced stresses? What is most important: That different material models are able to describe material properties separately, or that the combination of all models are able to describe the total behaviour of hardening concrete structure?

It is obvious that a thorough understanding of modelling of hardening concrete behaviour is lacking, and that more research is necessary to bridge the gap between mathematical description of different phenomena on one hand, and their application in practical design on the other hand.

1.2 Objective and scope of the thesis

The main objective of the present work is to extend the general applicability of stress/strain based curing technology and to contribute to better understanding and better prediction of stress and strain development in concrete structures during hardening.

The particular aims are defined as follows:

- To study material models for early age concrete behaviour, their experimental and theoretical background
- To improve existing programs for simulation of temperatures and stresses in hardening concrete structures, and make it more applicable for the engineering practice
- To clarify the influence of creep/relaxation on self-induced stresses, to compare different creep models, and to give some recommendations regarding calibration of creep models
- To clarify the influence of restraint conditions on stresses in hardening structure
- To examine to what extent different simplifications in structural modelling affect calculated results and, if possible, give some recommendations regarding modelling of the structure and interaction with the ground
- To simulate temperature, stress and strain development in a real structure and to check the validity of the calculations results by comparing them with measurements. On the basis of that comparison, possible reasons of disagreement should be identified.

1.3 Organization of the thesis

This thesis starts with an introductory chapter, where the background of the problem concerning cracking in hardening concrete structures is described. The aim and scope of this work are given, together with its significance to engineering practice. The content of the thesis is briefly outlined.

In Chapter 2 the main features and mechanisms of young concrete behaviour are described and their contribution to self-induced stresses is briefly discussed. Experimental results from the literature on the development of the material properties are presented. This chapter serves as basis for the subsequent chapter where mathematical modelling of the phenomena is given.

In Chapter 3, the mathematical description of the temperature and stress development in hardening concrete is given. Special attention is paid to the viscoelastic behaviour of young concrete. A brief overview of the most commonly used models for different material properties is given. Existing models are discussed, and on the basis on this discussion, new implementations and improvements in the FE program DIANA are made. Equivalent time is introduced to describe the state of the hydration process and a new equation for the E-modulus development is implemented. The transient thermal creep is included in the stress calculation to take into account the increase in creep due to temperature changes.

In Chapter 4 a numerical solution of the mathematical formulation is given. The finite element method is adopted to solve the governing set of differential equations. Since the thermomechanical problem is decoupled, the finite element formulation and the iterative solution of the two sets of equations are elaborated separately. Special attention is given to the numerical integration of the viscoelastic constitutive relation.

Creep is a very important factor in the stress simulation and it is the subject of Chapter 5. First, the importance of creep in different periods of hardening is examined. The creep coefficient is varied in different periods of hardening of an externally restrained structure,

and stresses are compared. To get more insight into the complicated nature of creep effects, TSTM tests are used, and strain components are identified for various temperature histories and various creep properties. Further, three creep models for young concrete are compared: Maxwell chain, Burgers model and the Double Power Law. On the basis of this comparison, both the creep models and the creep tests are discussed, and some practical recommendations regarding calibration of the creep models are given.

In Chapter 6 different methods for analyses of hardening structures are presented and discussed, and some of them are compared. The influence of parameters describing the effects of geometry and stiffness of the ground on stresses in a hardening structure is investigated. Three-dimensional nonlinear analyses are used for that purpose. Finally, some recommendations for design of concrete structure with regard to restraint are given.

In Chapter 7 temperature and stress/strain development in a real structure, the Maridal culvert in Oslo is simulated. A comprehensive laboratory test program was performed at NTNU to identify the material parameters. Both thermal and mechanical properties were tested. Material models were checked in the Temperature-stress testing machine (TSTM). A large field instrumentation program has been carried out to measure temperature and strain development in the culvert. Three-dimensional analyses of the walls in two section are performed with DIANA. Calculated results are compared to measurements.

Finally, in Chapter 8 some conclusions are given together with suggestions for further research.

Chapter 2

Features of Young Concrete Behaviour

2.1 General

The behaviour of young concrete in a real structure is complex due to the fact that the microstructure is being formed while a load is applied, in addition to the effects of varying temperature and humidity. Immediately after mixing concrete behaves as a liquid. During the first hours stiffening takes place due to the cement hydration, and material properties start developing. Heat liberated by chemical reactions cannot be passed on rapidly enough to the surroundings, and the temperature rise in hardening concrete may be considerable. The temperature is the main cause of volume changes at early ages, but not the only one. Another important mechanism is autogenous deformation, specially for concrete with low water to binder ratio. If concrete is not restrained, these volume changes will occur freely without any stresses being generated. However, this never happens in practice as the concrete in a structure is always restrained to some degree. As a consequence, compressive and tensile stresses develop and if tensile stresses exceed the tensile strength of hardening concrete, cracks are formed.

The major contributors to time dependent deformation and stresses in young concrete are: temperature development, shrinkage, development of material properties, and restraint conditions. In this chapter these parameters are briefly presented and their contributions to the stresses in young concrete are discussed. The intention is not to give a complete summary of the state-of-the-art knowledge on young concrete, but to give a basis for the formulation of the numerical models in the subsequent chapter.

2.2 Temperature development

The temperature development in a newly cast structure is determined by the balance between the development of heat due to hydration and the exchange of heat with the surroundings. The most important factors for temperature development in hardening concrete are:

1. Thermal properties of concrete (hydration heat, conductivity, heat capacity)
2. Geometry and size of the structure
3. Boundary conditions (air temperature, wind, solar radiation, temperature of adjoining structures, formwork, insulation, etc.)
4. Initial conditions (fresh concrete temperature, casting history etc.)

A state of the art of the determination of temperature development in hardening concrete is given, among others, in (Breugel 1994).

2.2.1 Thermal properties

Concrete thermal properties are determined by the concrete mixture (type and amount of cement, type and amount of aggregate, water to binder ratio, amount and type of additions and admixtures), and also depend on temperature and moisture conditions. Complexity of the problem lies in the mutual dependency of temperature and thermal properties: for example temperature rise in hardening concrete depends on heat generation, but at the same time, the rate of heat generation is highly influenced by temperature.

Experimental determination of thermal properties is reported in (Khan 1998).

Heat of hydration is obviously the most important property affecting temperature development in hardening concrete. According to (Breugel 1994), the rate and magnitude of heat generation depends on the type of cement (chemical composition, fineness and particle size distribution), water to binder ratio, type and amount of chemical additives, and temperature. The total quantity of heat generated in concrete is directly proportional to the amount of cement. Heat of hydration may be measured from different types of tests: isothermal tests, adiabatic tests and semi-adiabatic tests. Isothermal tests are usually applied to cement paste and do not take into account temperature influence on the hydration process. Therefore adiabatic and semi-adiabatic tests are preferred. In (Morabito 1994) results of a Round Robin test program were presented, where adiabatic and semi-adiabatic curves obtained from different types of calorimeters were compared. Factors that influence test results were identified. None of these two methods were generally recommended; which test should be performed depends on the reasons why the test is being carried out. For temperature analysis of mass concrete where the temperature conditions are close to the adiabatic ones, adiabatic input curves are preferred. For slender concrete structures, with large temperature exchange with surroundings, semi-adiabatic input curves are more appropriate.

Thermal conductivity of concrete describes the rate of heat transfer in concrete due to temperature gradient. According to (Breugel 1994) the coefficient of thermal conductivity depends on the temperature and moisture conditions, type and content of aggregate, porosity, density and age. For normal concrete it varies between 1.2 and 3.0 W/mK.

Contradictory results on thermal conductivity of concrete at early ages are reported in the literature. (Byfors 1980) did not observed any significant change in conductivity with age. Increase of the conductivity with age has been found by (Marechal 1972), whereas (Brown 1970) reported decreasing conductivity during hardening.

Specific heat of concrete indicates how much energy moving through the concrete will be absorbed and used to raise concrete temperature. For ordinary concrete the specific heat varies between 0.85 and 1.15 kJ/kgK. For a given concrete mix the specific heat depends on the water content and temperature: it increases with increase in temperature and increase in water (Breugel 1994), (Khan 1998).

A decrease in specific heat with age was reported by several authors: (Breugel 1980), (Freiesleben 1978) and (Brown 1970)

2.2.2 Boundary conditions

The heat transfer between a surface and the environment can be described by the coefficient of heat transfer and depends on the type and thickness of the formwork and insulation, the time of the formwork removal, the ambient temperature, wind velocity, and solar radiation. The effects of wind and the solar radiation on temperature development in young concrete is significant, and must be taken into account in numerical simulations (Breugel 1994). In practice the wind velocity and solar radiation are rarely if ever recorded on construction sites. In addition, they are difficult to take into account in a proper way: one part of the structure may be exposed to the wind or solar radiation more than the other part, depending of structural geometry, position, environmental conditions etc.

2.2.3 Geometry and size of the structure

Geometry and size of the structure influence temperature history in hardening concrete, but they are more difficult to alter then other parameters. If possible, thermal effect should be taken into consideration when geometry and size of the structure are selected.

In massive concrete structures the generated heat does not pass easily to the surroundings and hardening conditions are almost adiabatic. The problems related to massive concrete structure are high maximal temperature and large temperature difference between the interior and the surface (internal restraint).

In the case of a slender concrete structure, the temperature field is highly influenced by exchange of heat with the surroundings, and temperature difference between hardening concrete and adjoining structures is of concern. In this type of structures through cracking is likely to occur.

2.2.4 Initial conditions

Fresh concrete temperature is an important parameter influencing hardening concrete temperature. High casting temperature accelerates the cement hydration and results in a higher and earlier maximal temperature. Consequently, the thermal contraction due to cooling is increased, which leads to higher cracking risk. Unlike many other parameters, casting temperature can be influenced significantly on site.

The casting history is also important for massive concrete structures. Lift heights and the time between the placement of lifts have effect on the temperature distribution in the structure. In massive concrete structures long periods between the placement of two lifts allow heat dissipation, thus reducing maximal temperature in the structure. In slender concrete structures a long casting times increase temperature gradients, and cracking risk due to the higher internal restraint. In addition, when considering the aging of concrete, the long casting time is unfavourable, because the previously cast concrete will be stiffer providing more restraint to the newly cast concrete. In the case of external restraint - casting of concrete against previously cast sections, temperature difference between new and old concrete is of essential importance. If the new section is cast while the old concrete is still warm due to its own heat of hydration, this difference is reduced, which significantly reduces the risk of through cracking.

2.3 Volume changes

2.3.1 Thermal dilation

Thermal strains caused by temperature changes are predicted by the thermal dilation coefficient. For hardened concrete the value varies from 5×10^{-6} to 15×10^{-6} /^{0}C and it is influenced by concrete mix design, especially type and amount of aggregate, water content and temperature. Traditionally, a constant value of 10×10^{-6} /^{0}C is used in calculations.

There is no general agreement on thermal dilation coefficient at early ages. In (Byfors 1980) experimental data on thermal dilation coefficient from literature were reported which showed that the coefficient of thermal dilation decreased rapidly the first 8 hours after mixing achieving a value of 12×10^{-6} /^{0}C (Figure 2.1).

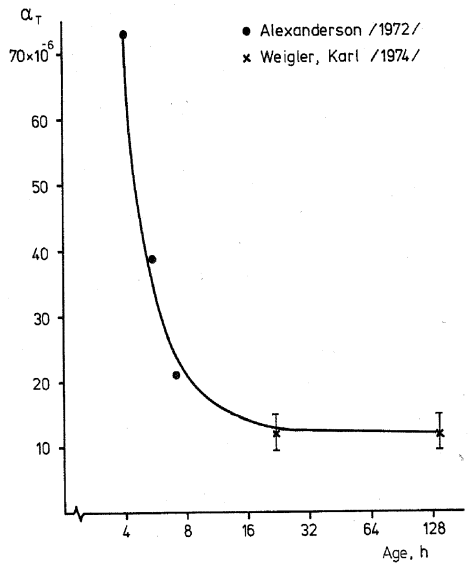

Figure 2.1: Age dependency for the coefficient of thermal expansion based on data from the literature (from Byfors 1980)

(Emborg 1989) found that the coefficients of thermal expansion and contraction were different. Constant values of those two coefficients were assumed even though test results showed a slight age dependence. The same assumption was done in (Westman 1995) and (Hedlund 1996) for high performance concrete and values of $10-12\times10^{-6}$ /^{0}C was reported for thermal expansion coefficient and $7-9\times10^{-6}$ /^{0}C for thermal contraction coefficient, see Figure 2.2.

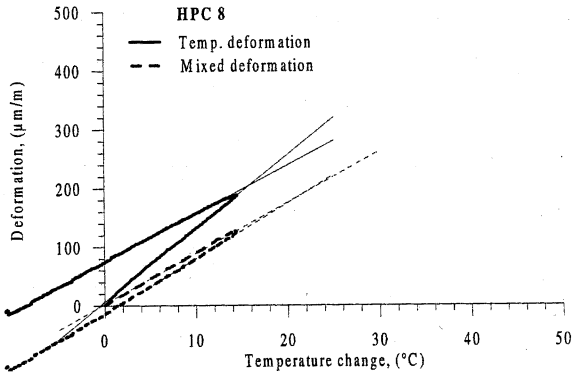

Figure 2.2: Deformation versus temperature change for a high performance concrete. Mixed deformation is the sum of thermal deformation and autogenous deformation (from Hedlund 1996)

Difference between thermal dilation coefficient in expansion and contraction was also found in (Gutsch 1998), but with the opposite range: the thermal contraction coefficient was measured greater than the thermal expansion coefficient.

For high performance concrete the main problem seems to be the separation between autogenous and thermal deformation for realistic temperature histories. That was one of the main topics in (Bjøntegaard 1999) where development of the thermal dilation coefficient of high performance concrete through the hydration phase was investigated. Figure 2.3 shows development of the thermal dilation coefficient versus time: after drop from a high value (about $20\times10^{-6}/^{0}$C) to a minimum value (about $7\times10^{-6}/^{0}$C) during the first 12-14 hours, the thermal dilation coefficient gradually increases with a rate which depends on temperature history.

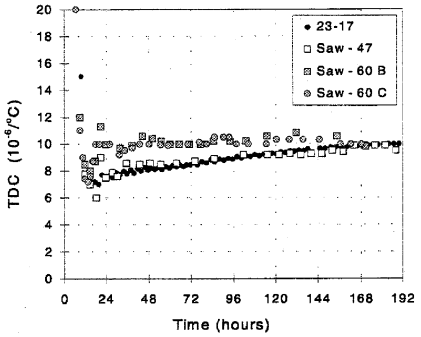

Figure 2.3: Development of the thermal dilation coefficient versus time measured in different temperature tests (from Bjøntegaard 1999)

According to (Bjøntegaard 1999) increase of the thermal dilation coefficient is caused by selfdesiccation during hardening - if the concrete is immersed in water later, then the thermal dilation coefficient is reduced by as much as 50%. Bjøntegaards comprehensive results demonstrate clearly the interdependence of thermal and autogenous deformations at early ages. However, a simple way to handle the problem is not yet available, except that to measure the sum of the two for a given temperature history is easy.

Contradictory results in the literature reflects a high degree of uncertainty in the knowledge on the thermal dilation coefficient in young concrete, which is quite surprising having in mind the importance of the thermal dilation coefficient in stress generation in hardening structures.

2.3.2 Shrinkage

Shrinkage is the traditional term describing the volume change of unloaded concrete due to the moisture exchange with surroundings, cement hydration or carbonation (Neville 1987). Several types of shrinkage exist:

Autogenous deformation is all the external volume change of the concrete under conditions of no moisture exchange with surroundings and after correcting for the movements caused by thermal dilation (Bjøntegaard 1999). It generally occurs as shrinkage, but expansion has also been observed, and therefore the term "autogenous deformation" is preferred. Autogenous deformation is a consequence of chemical shrinkage - the fact that the products of cement hydration have smaller volume than the reactants. Its magnitude depends on degree of self-desiccation - reduction of the relative humidity due to the use of water for hydration. Low water to binder ratios gives high autogenous deformation.

Autogenous deformation of $500 - 800 \cdot 10^{-6}$ has been measured in high performance concrete during the first week of hardening. The nature of the phenomenon, driving mechanisms, measuring etc. are thoroughly described in (Bjøntegaard, 1999).

Drying shrinkage is volume change of the concrete caused by moisture loss to the surroundings.

Plastic shrinkage is drying shrinkage taking place at the surface of newly cast (still plastic) concrete caused by evaporation of water or by suction to the concrete below.

Carbonation shrinkage is contraction of concrete caused by carbonation - the reaction of CO_2 with the hydrated cement. In practice it of course occurs simultaneously with drying shrinkage.

When shrinkage is considered, drying shrinkage dominates in the normal quality concrete, and if concrete is exposed to drying at relatively high age for very long period. Traditionally, more attention has been paid to the drying shrinkage, whereas autogenous deformation has often been neglected. During the last years the development and use of high performance concrete has increased significantly and it has become clear that the autogenous deformation is important contribution to the stress development in hardening high performance concrete. Drying shrinkage may be neglected in simulation of concrete behaviour at early ages for several reasons:

Drying shrinkage takes place over long periods (many years), and may be neglected in the relatively short hardening period, which rarely exceeds more than a couple of weeks. In

the large concrete members only the surface is drying, whereas the internal part of the structure remains unaffected. In the most cases, even that is prevented or reduced at early ages by means of formwork, plastic foil or some kind of insulation.

In this study only autogenous deformation and its contribution to the stresses at early ages is considered.

2.4 Mechanical properties

Mechanical properties important in the analysis of hardening concrete are: E-modulus, creep/relaxation and strength. In young concrete the development of these properties as functions of time and temperature history is of great concern. One simple and commonly used approach is to use the equivalent age concept. The equivalent age or maturity is the concrete age at which the hydration at the reference temperature (20^0C) has reached the same stage. This is comprehensively discussed in Section 3.2 .

2.4.1 Compressive strength

When modelling mature concrete the compressive strength is one of the most fundamental properties. In the analysis of concrete at early ages, compressive strength is not very important since the compressive stresses are low, and cracking occurs due to high tensile stresses. However, compressive strength is of interest because of its correlation with the other mechanical properties. Since experimental determination of compressive strength is more simple than of E-modulus or tensile strength, it is desirable to use compressive strength in estimation of other properties.

Compressive strength is determined by short-term testing of specimens prepared and cured under standardized conditions. Size and shape of specimens influence results, what is taken into account by means of different corrective factors. The same methods for compressive strength determination may be used for hardening concrete.

Development of the compressive strength in hardening concrete has been investigated by many authors, for instance (Freiesleben Hansen 1977), (Byfors 1980), (Jonasson 1984), (Laube 1990), etc.

2.4.2 Tensile strength

The tensile strength of concrete is a very important parameter in early-age cracking prediction. It may be determined directly in a uniaxial tensile test or indirectly in the splitting tensile strength test or bending tests. The uniaxial tensile test is more difficult to perform, but the result is the true tensile strength of concrete. Practical difficulties connected to this type of test are described for instance in (Hauggard 1997), (Andersen 1995), (Kanstad 1999). The main problem is to obtain uniform stress field without stress concentration and eccentricities. Because of these difficulties the uniaxial tensile test is most commonly replaced by the tensile splitting test. To convert the tensile splitting strength to the uniaxial tensile strength different correlations between them are proposed in the literature together with correlations between tensile strength and compressive strength (CEB/FIP MC90), (EC2 1991), (Byfors 1980), (Oluokun 1991a and b), etc.

At early ages the tensile strength develops faster than the compressive strength (Laube 1990), (Kanstad 1999). Figure 2.6 shows the relative development of the compressive strength, tensile strength and E-modulus (Kanstad 1999).

2.4.3 Modulus of elasticity

The modulus of elasticity may be determined in tension or compression. It is usually assumed that the E-modulus is the same in tension and compression both for mature and young concrete even though contradictory results may be found in literature. In (Onken 1995) it was found that E-modulus in tension after 28 days is 15% larger than the corresponding value of E-modulus in compression.

Figure 2.4 from (Kanstad 1999) shows the relationship between the E-modulus in tension and compression, for different concrete ages determined in Norwegian test program.

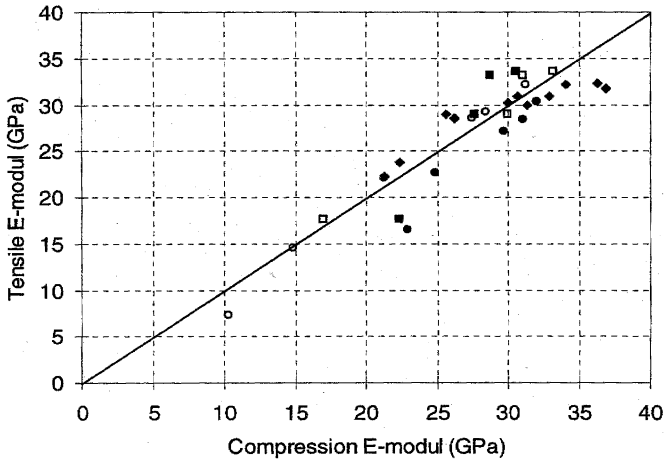

Figure 2.4: Modulus of elasticity tested in compression and tension. Each mark represents the average results for two or three test specimens (from Kanstad 1999).

The influence of the hydration on the development of the E-modulus has ben investigated by many researches, for instance (Byfors 1980), (Laube 1990), (Schutter 1996), etc. Figure 2.5 (Kanstad 1999) presents development of E-modulus versus equivalent time. It can be seen that E-modulus increases rapidly during the first day of hydration. Similarly to the tensile strength, this increase is not proportional to that for compressive strength. Therefore the relations between E-modulus, tensile strength and compressive strength for mature concrete are not valid for young concrete.

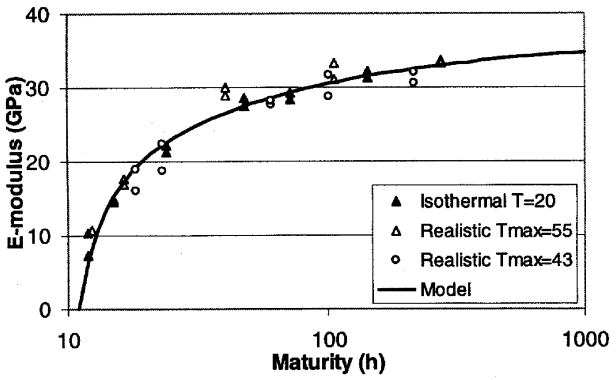

Figure 2.5: Development of E-modulus vs. maturity (from Kanstad 1999)

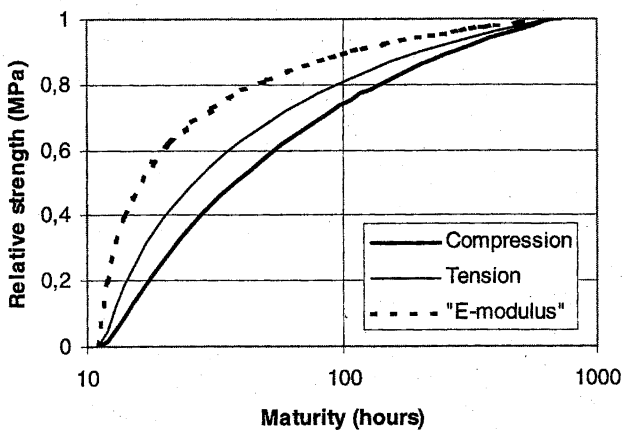

Figure 2.6: Relative development of the E-modulus, compressive and tensile strength (from Kanstad 1999)

2.4.4 Effective mechanical properties in structure

Mechanical properties are determined on specimens which are fabricated and cured in laboratory according to specified standards. The difference between concrete in the laboratory and in a real structure is taken into account by use of the effective strength in the structure.

To investigate the effective mechanical properties in hardening concrete structures comprehensive experimental studies were performed at TU Braunschweig (Rostasy 2000). Mechanical properties were determined on specimens cast in the laboratory and on speci-

mens extracted from structures and from large size structural elements cast in laboratory. The laboratory specimens were cured under same temperature history as measured in large size elements. The following relations between the effective values and laboratory test specimen values for the different mechanical properties were found:

- for tensile strength:

$$f_{cte} \approx 0.75 f_{ct} \tag{2.1}$$

- for compressive strength:

$$f_{ce} \approx 0.85 f_{c} \tag{2.2}$$

- for E-modulus:

$$E_{ce} \approx E_{c} \tag{2.3}$$

It was aslo found that these values were independent on the concrete age.

2.4.5 Temperature effect

Temperature affects mechanical properties indirectly: high temperature accelerates the hydration process, which leads to faster development of E-modulus and strength. On the other hand, it is generally agreed that high curing temperature may reduce strength and E-modulus at later ages, for instance (Byfors 1980). This fact is explained by the temperature effect on microstructure of the hydration products.

The effect of temperature on mechanical properties is usually investigated on specimens exposed to high constant temperatures, which are not representative for real structures. In (Kanstad 1999) the effect of different temperature histories on mechanical properties of high performance concrete was investigated. Concrete specimens were exposed to realistic temperature histories (gradual heating from 20^0C to 55^0C followed by realistic cooling to 20^0C). Compressive strength, tensile splitting strength and E-modulus were tested after 28 days and compared to the corresponding values for concretes cured at constant temperature of 20^0C. It was shown that the loss of 28 days strength and E-modulus for high performance concrete due to elevated curing temperature was less than 8%. The uniaxial tensile strength was more sensitive to the elevated temperature. These results agree with (Lindgård 1993), who also found that high performance concrete was more robust to elevated curing temperature than normal quality concrete.

Further, concrete specimens were exposed to the constant temperatures of 5^0C, 20^0C and 50^0C - the temperature was changed abruptly just after mixing and kept constant until testing. Comparison of compressive strengths showed that effect of that rough procedure on compressive strength was considerably larger than the effect of a gradual, realistic temperature history. This was confirmed by (Helland 2000).

2.4.6 Creep (relaxation)

Time dependent behaviour of concrete is described by means of the basic phenomena, creep and relaxation. Creep is time dependent deformation of concrete subjected to sus-

tained load and relaxation is a decrease in stress with time in concrete subjected to constant deformation, as shown in Figure 2.7.

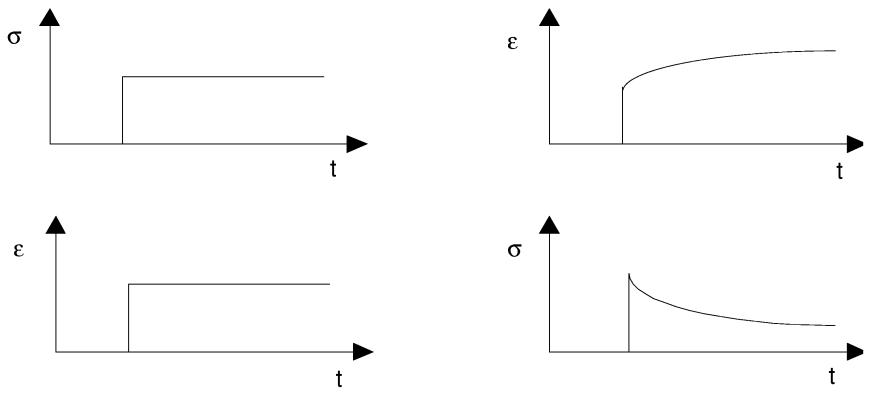

Figure 2.7: Creep and relaxation

Creep and relaxation are two alternative descriptions of the same phenomenon. The separation between creep and relaxation is possible almost only in the laboratory. In most cases, concrete in a structure is both loaded and restrained to some extent, and its behaviour is a combination of creep and relaxation. Very commonly, the term creep is used to denote both creep and relaxation and their combination. Description of concrete behaviour by means of relaxation is rarely adopted since relaxation tests are more difficult to perform than creep tests.

If a sustained load is removed after some time, the strain decreases immediately and this instantaneous recovery is defined as the elastic strain, see Figure 2.8. This strain is smaller than the strain at loading due to the increase of E-modulus with age. A gradual decrease of strain follows, with a higher rate than that of the creep curve. One part of the creep deformation is irreversible, which means that creep recovery cannot be modelled as a negative creep (creep due to the stress with opposite sign).

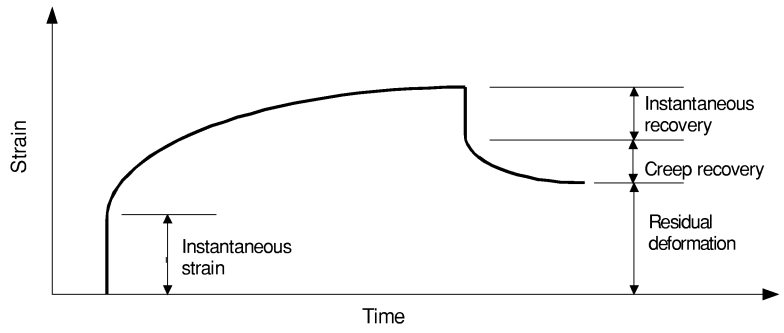

Figure 2.8: Creep recovery

If creep and shrinkage take place simultaneously, the observed deformation is larger then the sum of the drying shrinkage deformation of the unloaded specimen and of the deformation of the loaded specimen which does not dry. The phenomenon is called the Pickett effect and the increase of deformation is regarded either as increase of creep due to drying (drying creep) or as load-induced shrinkage.

Creep has different effects in a structure, which may be both beneficial and detrimental:

- redistribution of the stresses caused by external loads and increase of the deformations
- reduction of internal stresses caused by non-uniform volume changes (young concrete)
- reduction of concrete stresses due to prestressing
- redistribution of internal stresses (composite structures)
- reduction of strength of structures due to large deformation (buckling problems)

Creep is a very important mechanical property of concrete, but it is at the same time one of the least understood. The scatter of test results is larger than for strength and elastic modulus. The complexity of creep is a consequence of the many and complex physico-chemical processes which determine concrete behaviour. Creep depends on many factors, intrinsic and external, and it is very sensitive to the conditions of the tests. Influence of intrinsic factors (factors dictated by the concrete mix) and external factors (temperature and moisture, age of loading, level of loading etc.) are given in detail in (Neville 1983).

Creep of hardening concrete is even more complicated issue due to the effects of varying temperature and humidity. High creep at early loading ages, temperature and humidity influence on creep and creep at high tensile stresses are some of the relevant aspects for creep in young concrete. A relatively small number of tests that investigate these aspects are reported in literature.

Most data on creep reported in the literature refer to the creep in compression. It is partly due to the fact that creep tests in compression are much easier to perform than creep tests in tension. For young concrete creep in tension is very relevant. Commonly, creep in tension is assumed to be equal to creep in compression, and parameters for creep model are determined by compressive tests. At early ages concrete dries internally due to hydration (selfdesiccation), which means that simultaneous creep and shrinkage are always present. Drying creep is different in tension and compression, and when the autogenous deformation measured on unloaded specimen is substracted from the total deformation, different values for creep strain may be obtained in tension and compression.

(Umehara 1994) reported different creep in tension and in compression for young concrete and proposed different models for creep in tension and creep in compression. (Rostasy 1993) fitted the creep model for young concrete to the creep tests in tension.

In this study creep in tension and compression are assumed to be equal.

Temperature influence on creep

Temperature affects creep in two ways: directly, influencing creep rate, and indirectly, influencing aging and maturity of concrete. These effects are competing: higher temperature accelerates the creep rate, and at the same time it accelerates the chemical reaction of cement hydration, which leads to faster hardening, and, thus, reduced creep.

(Umehara 1994) has measured creep of early age concrete at different temperature levels and shown that the resulting effect of increased temperature is an acceleration of creep, see Figure 2.9. (Gutsch 1998) reported similar results.

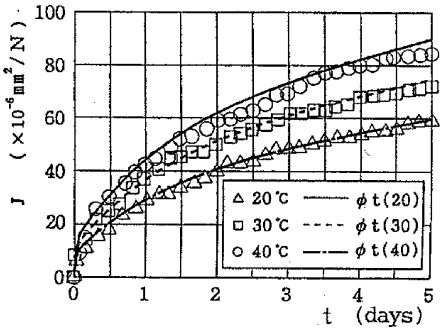

Figure 2.9: Effect of temperature on tensile creep strain. Age of loading is 3 days (from Umehara 1994)

Another temperature effect is increase of creep due to temperature change, regardless of it being cooling or heating, so-called transitional thermal creep. The phenomenon was discovered by Hansen and Erikson in 1966, but Illston and Sanders were first to report it in details in (Illston 1973), and called it 'transitional thermal creep'. Influence of changing temperature on creep in young concrete has been investigated by (Hauggaard 1997b) and is shown in Figure 2.10. The experimental results show an apparent increase of creep strain due to transient temperature.

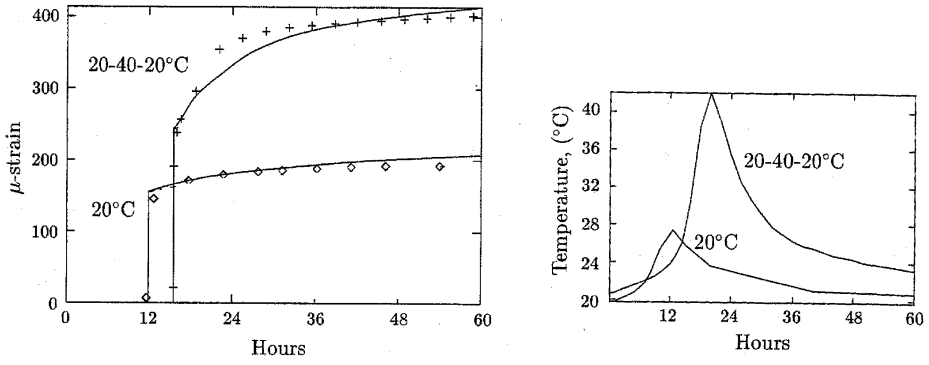

Figure 2.10: Creep of concrete specimen exposed to the transient temperature (from Hauggaard 1997)

2.4.7 Couplings

The hydration process is governed by two diffusion processes: temperature development and development of the water distribution. They influence development of mechanical properties and stress generation. In (Haugaard 1997) the overall couplings of different factors in hardening concrete are considered, see Figure 2.11.

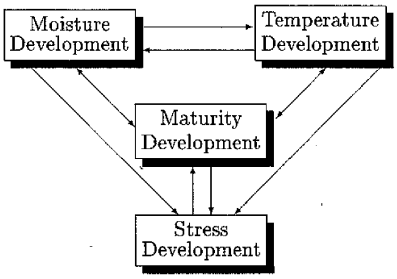

Figure 2.11: Couplings of the processes in hardening concrete, from (Haugaard 1997)

According to (Haugaard 1997) two-way coupling between temperature development and moisture development exists: diffusing water transports a large amount of heat, and the diffusion coefficient is dependent on the relative humidity.

The influence of moisture development and temperature development on mechanical properties and stress generation is well known, but also a certain influence of stresses on the hydration process is observed. Some of these effects are mentioned bellow.

The influence of cracking due to high stresses on heat and moisture flow is probably the most obvious coupling effect (Wittmann 1995).

Increase of strength due to applied load has been observed by several researchers, see (Neville 1983). (Coutinho 1977) explained the phenomenon by the increased hydration due to external load. Accelerated ageing due to loading was also investigated by (Bazant 1979) who used it as explanation for the phenomenon low-stress nonlinearity. (Rostasy 1993) investigated the same phenomenon for young concrete in tension, and did not find any strength gain due to loading.

Another cross-effect which was investigated, among others, by (Bazant 1974b) is named stress-induced shrinkage. It is assumed to be the main reason of the Pickett effect.

However, the effects of mechanical load and stresses on the hydration process and temperature and moisture conditions is uncertain and not satisfactorily verified by laboratory tests. Therefore a common assumption is that the hydration process and the temperature development are independent of stresses. Another common assumption is that the influence of the development of water distribution on hydration process may be neglected and only influence of temperature is considered. Hence, the behaviour of early age concrete is considered as a thermomechanical problem, which may be decoupled.

2.5 Restraint conditions

Uniform volume changes of concrete will not produce any stresses if the concrete is unrestrained. However, this case never happens in practice: a part of structure is always externally restrained to some degree, and volume changes are in general not uniform due to non uniform temperature distribution. Regardless of wether it is internal or external, restraint impedes free volume changes and produces tensile or compressive stresses.

Traditionally, it has been differentiated between two types of restraint conditions which may cause two different types of cracks:

- internal restraint
- external restraint

Internal restraint is used to describe the effect of a non-uniform distribution of the temperature and moisture field across the structure. That results in variation of volume changes and material properties over a cross section and cause self-equilibrating stresses which may lead to the surface cracking in the heating period. Surface cracks will partly close again in the following cooling period.

External restraint is present if the free volume changes of the hardening concrete are prevented externally by adjoining structures: old concrete, ground, etc. In that case compressive stresses develop in the heating phase and they are turned into tensile stresses in the subsequent cooling phase. They may cause through cracks which may remain open permanently.

As the surface cracks normally close in the cooling phase, and through cracks usually remain open, the main attention in the early-age cracking prediction is paid to the external restraint. However, surface cracking is also of interest in the case of aggressive environments because of its effect on structure's durability. According to some authors (Bernander 1994) surface cracking may initiate through cracks, which may not have developed otherwise.

Nearly all structures are both internally and externally restrained to some degree and the stresses are the results of both effects. In spite of this fact, the previous classification is justified, since in most cases one of these two effects dominates.

Restraint has often been described by a restraint factor. According to (ACI Comitee 207 1973) the strain is equal to the product of the degree of restraint existing at the point in question and the strain which would occur if the concrete were not restrained. The restraint in a structures is not uniform but varies with the location. It also changes during the hardening period.

When considering externally restrained structures, two types of restraint are of interest: restraint from the ground and restraint from the adjoining structure (construction joints).

Restraint from the ground depends on dimensions and geometry of the structure, stiffness and flexibility of the ground and the quality of the bond between the structure and the subgrade.

Restraint from the adjoining structure depends on the geometry, dimensions and stiffness of the restraining structure, length and quality of the joints and amount of through reinforcement in the joints.

Stresses at a decisive point in a structure are the results of both types of restraints. A more comprehensive discussion of modelling of supports conditions and restraint will be given in Chapter 7.

Chapter 3

Mathematical Modelling of Early Age Concrete

3.1 General

Assuming that the mechanical behaviour of concrete does not influence the thermal and hydration processes, the thermomechanical problem in young concrete behaviour may be decoupled. The hydration process and the temperature development are assumed to be independent of stresses, and are calculated first. The results are used in the subsequent stress calculations. Another assumption is that the influence of the moisture conditions on the hydration process and mechanical behaviour may be neglected, and only the influence of temperature is considered. This significantly simplifies numerical simulation of concrete behaviour at early ages.

In this chapter mathematical description of the temperature and stress development in hardening concrete is given. The starting point is a differential equation that describes the thermal response. Next, a mathematical description for the mechanical response is given in the form of the constitutive equations for different strain components. Special attention is paid to the viscoelastic behaviour of young concrete. A macroscopical approach is adopted for both thermal and mechanical response, first of all because of the absence of a full understanding of the processes and mechanisms at the micro level, also because of its practical applicability and relevance.

A brief overview of the most used models for different material properties is given. Existing models are discussed, and on the basis on this discussion, new implementations and improvements in FE program DIANA are made.

3.2 Temperature calculation

The temperature development in hardening concrete due to hydration may be described by the Fourier differential equation for heat conduction in a homogenous and isotropic body:

$$k \cdot \left(\frac{\partial^2 T}{\partial x^2} + \frac{\partial^2 T}{\partial y^2} + \frac{\partial^2 T}{\partial z^2} \right) + Q = \rho \cdot c \cdot \frac{\partial T}{\partial t}, \tag{3.1}$$

where k is the thermal conductivity, T is the temperature, ρ is the mass density, c is the specific heat, Q is the rate of internal heat generation per unit volume, t is time, and x, y, z are coordinates.

Boundary conditions are described by convection heat transfer:

$$q = h(T_f - T) \ , \tag{3.2}$$

where q is the heat flux, h is the heat transfer coefficient, T is the boundary temperature, and T_f is the temperature of the surroundings.

The mathematical modelling of the rate of heat generation caused by hydration process Q is a central part in temperature calculation of early age concrete.

Traditionally, two parameters are used to describe the state of the hydration process: degree of hydration and equivalent age.

3.2.1 Degree of hydration

Several definitions of degree of hydration are present in literature, see (Byfors 1980). The two most used definitions are:

- Degree of hydration is the ratio of the amount of cement reacted at time t to the original amount of cement.
- Degree of hydration is the ratio of the chemically bounded water at the time t to the chemically bounded water at complete hydration.

In practice it is difficult to determine the amount of reacted cement and reacted water. Since there is a good correlation between the amount of cement that has reacted and amount of liberated heat (Byfors 1980), (Breugel 1994), developed heat may be used to indicate the state of the reaction process. Hence, degree of hydration is defined as the ratio of the amount of heat liberated at time t, $Q(t)$, to the amount of heat at complete hydration, Q_{max}.

$$r(t) = \frac{Q(t)}{Q_{max}} \tag{3.3}$$

Total heat corresponding to the complete hydration is impossible to measure because the hydration takes very long time (several years). Therefore in practice it is replaced by Q_{max} determined from the adiabatic tests. Degree of hydration determined in this way is not the true degree of hydration and should only be considered as a model parameter. This should be kept in mind when modelling other properties as functions of the degree of hydration.

3.2.2 Maturity concept and equivalent age

For concrete the maturity concept was introduced in the 1950's to take into account temperature influence on the hydration process. It is based on the assumption that the rate of hydration at a given degree of hydration is a function of temperature only. Mathematically, it can be expressed as:

$$\frac{dr}{dt} = g(r) \cdot f(T) \tag{3.4}$$

where $g(r)$ is the function of the degree of hydration and $f(T)$ is the function of the temperature.

A great number of different functions $f(T)$ describing temperature influence on the rate of the chemical reaction was proposed in literature (Byfors 1980). The function proposed by (Freiesleben and Pedersen 1977) gave the best agreement with measurements within very wide temperature range (from -10^{0}C to 90^{0}C). It is based on the Arrhenius' equation and includes the activation energy as a model parameter.

$$f(T) = k \cdot \exp\left(-\frac{E_a}{RT}\right) \tag{3.5}$$

where k is a proportionality constant, E_a activation energy (J/mol), R universal gas constant = 8.314 (J/mol^{0}K), and T concrete temperature (^{0}K).

The activation energy describes the effect of temperature on the rate of hydration. Since cement hydration consists of many individual processes with different rates, activation energy for concrete is a result of the temperature dependency of all existing processes and mechanisms. This 'average' parameter is therefore often termed apparent activation energy.

According to (Freiesleben 1977) activation energy for concrete is a function of temperature and may be described as:

For $T \geq 20^0 C \quad E_a = A$

$$\text{For } T \leq 20^0 C \quad E_a = A + B \cdot (20 - T) \tag{3.6}$$

where A and B are constants which f. i. may be determined from the compressive strength tests, see Section 7.3.1 .

(Jonasson 1984) proposed the following alternative expression for the activation energy:

$$\frac{E_a}{R} = \Theta_{ref} \cdot \left(\frac{30}{T + 10}\right)^{\kappa_3}, \tag{3.7}$$

where Θ_{ref} and κ_3 are empirical constants depending on the type of cement.

The consequence of the Eq.(3.5) is that hydration process at an arbitrary temperature history may be compared to the process at reference temperature (usually $T_{ref} = const$ = 20^{0}C) with the same degree of hydration. First, the rate factor is defined as a relation between speed of hydration at reference temperature T_{ref} [^{0}K], and the speed at T [^{0}K]:

$$H(T) = \frac{speed at\, T}{speed at\, T_{ref}} = \frac{f(T)}{f(T_{ref})} = \exp\left[\frac{E_a}{R}\left(\frac{1}{T_{ref}} - \frac{1}{T}\right)\right] \tag{3.8}$$

Then comparison between two processes is done by calculating the equivalent age of the concrete. The equivalent age of a concrete, frequently denoted maturity, is the age at which the hydration at the reference temperature (20^{0}C) has reached the same stage. It is determined as:

$$t_{eq} = \int_0^t H(t)dt \tag{3.9}$$

The relation between degree of hydration and equivalent age is given in (Jonasson 1984):

$$r = \exp\left(-\lambda_1\left[\ln\left(1+\frac{t_{eq}}{t_1}\right)\right]^{-\kappa_1}\right), \tag{3.10}$$

where λ_1, t_1 and κ_1 are fitting parameters. It should be noted again that r is not a true value of degree of hydration, but a convenient parameter.

A disadvantage of the maturity concept is that it predicts only positive effect of temperature on the rate of hydration and material properties closely linked to the progress of hydration, for instance strength. This is, however, not the case as curing at high temperature may reduce the final strength, as discussed in Section 2.4.5 .

3.2.3 Hydration heat development

Modelling the heat development due to hydration is a very important part in the temperature calculation. The fact that the hydration process is a self-accelerating process (the produced heat increases the rate of hydration) makes this modelling more complicated.

Different models are reported in literature, two of them will be briefly presented here.

(Reinhardt 1982) proposed a model based on the degree of hydration:

$$Q(t) = \int_0^t q(t,T)\cdot dt\ , \tag{3.11}$$

$$q(t,T) = \gamma\cdot q(r)\cdot q(T) \tag{3.12}$$

where $q(t,T)$ is the rate of heat production, γ is the maximum rate of the heat production, $q(r)$ is the normalized heat production rate depending on the degree of reaction, $q(T)$ is the heat production rate depending on temperature:

$$q(T) = \exp\left(-\frac{b}{T}\right), \tag{3.13}$$

b is the Arrhenius' constant, T is absolute temperature [K].

$$b = \frac{E_a}{R}.$$

$q(r)$ can be determined from an adiabatic curve as a multi linear function of degree of hydration together with γ (Reinhardt 1982).

The degree of hydration is in this case defined as:

$$r = \frac{Q(t)}{Q_{max}} = \frac{c \cdot (T(t) - T_0)}{c \cdot (T_{max} - T_0)} = \frac{T(t) - T_0}{T_{max} - T_0} , \tag{3.14}$$

where Q_{max} determined from adiabatic test is used instead of total heat at complete hydration since the latter cannot easily be measured. c is the specific heat of concrete, T_0 is the initial mixure temperature, T_{max} is the maximum value of concrete temperature measured in adiabatic test.

A simpler and more commonly used approach in engineering practice is the three parameter equation proposed by (Freiesleben 1977) based on equivalent age:

$$Q(t_{eq}) = Q_\infty \cdot \exp\left[-\left(\frac{\tau}{t_{eq}}\right)^\alpha\right] \tag{3.15}$$

where Q_∞, τ and α are model parameters that can be determined from adiabatic curve.

Although related to the degree of hydration, the model (3.12) is also based on the maturity principle, and thereby suffers from the same shortcomings as mentioned in the previous section. On the other hand, modelling of the hydration process and material properties by means of degree of hydration is not common in engineering practice and an additional effort is usually made to transform degree of hydration to equivalent age. This transformation, for instance using Eq.(3.10), requires experimental data from an adiabatic test, which are not always available to the user. To make DIANA program more applicable to the engineering practice, the model in Eq.(3.15) is implemented. The degree of hydration is replaced by the equivalent age, and consequently, all material properties are made dependent on equivalent age. In addition, a constant activation energy is replaced by a temperature dependent activation energy calculated according to expression (3.6).

Two models for the evolution of hydration heat (3.12) and (3.15) are used to calculate temperature development in a wall cast on a previously cast foundation. The wall, which is a part of the Stalsberg Culvert at Gardermoen, was instrumented by temperature sensors at six points in the middle of the wall, and the temperature was monitored from the time of casting (Vinorum 1996). The cross section of the wall is shown in Figure 3.1-a. In Figure 3.1-b. calculated temperature in two points are presented and compared to measurements. It can be seen that equivalent age can be used to describe temperature development in a hardening concrete structure with the same accuracy as degree of hydration, as expected.

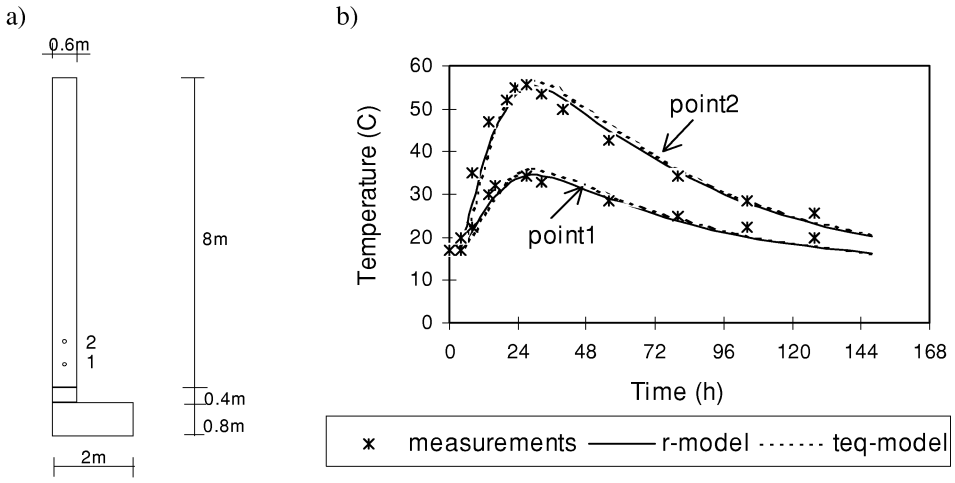

Figure 3.1: a) Cross section of the wall. Length of the wall is 14 m. b) Temperature development in two points of the wall. Calculation results based on two models for evolution of hydration heat are compared to measurements

In addition to the three-parameter equation, the function for heat development $Q(t_e)$ may be given as a discrete function of equivalent age. If the experimental data from the adiabatic test are available, tabular input of the heat development is recommended.

3.3 Stress calculation

Description of the constitutive behaviour of hardening concrete is a very complex task, since it must include all phenomena important for stress generation at early ages: development of mechanical properties, thermal dilation and autogenous deformation, temperature influence on concrete behaviour, and finaly, cracking. To simplify this description, it is assumed that the strain rate may be decomposed as follows:

$$\dot{\varepsilon} = \dot{\varepsilon}_e + \dot{\varepsilon}_c + \dot{\varepsilon}_{th} + \dot{\varepsilon}_{sh} + \dot{\varepsilon}_{crack}, \tag{3.16}$$

where ε_e is the elastic strain, ε_c the creep strain, ε_{th} the thermal strain, ε_{sh} the shrinkage and ε_{crack} is the cracking strain. In this way, the constitutive law for each component may be defined independently. Such a separate approach is adopted in the absence of a full understanding of the microstructural processes in hardening concrete.

3.3.1 Thermal dilation and autogenous deformation

Thermal strain is modelled as follows:

$$\varepsilon_{th} = \alpha_T \cdot \Delta T, \tag{3.17}$$

where α_T is the thermal dilation coefficient, and ΔT the temperature gradient.

At present there are no generally accepted models for thermal dilation coefficient and autogenous deformation. Neither is there agreement on whether they can be presented as functions of equivalent age (or degree of hydration) or not. Modelling of the thermal dilatation and autogenous deformation necessitates their separation, because it is always the sum of the two effects that is measured, the problem which is discussed in detail in (Bjøntegaard 1999). Determination of thermal dilation depends on the assumptions that are made about autogenous deformation and visa versa.

In (Emborg 1989) two different values for thermal dilation coefficient were used: thermal expansion coefficient and thermal contraction coefficient. The same assumption has made by (Hedlund 1996) for high performance concrete, where autogenous deformation has been modelled as function of equivalent age, and thermal dilation has been determined by substracting autogenous deformation from the total measured deformation. (Tazawa 1994) also used maturity principle to predict autogenous deformation. A comprehensive literature review on autogenous deformation and thermal dilation is given in (Bjøntegaard 1999). In the same work it was shown that autogenous deformation cannot be modelled as function of equivalent age. Accordingly, input data for stress calculation at the present state of knowledge can only be given by the total deformation measured on the realistic temperature history.

In calculations, only the total deformation is of concern, i. e. each combination of thermal dilation and autogenous deformation that gives the "true" total deformation is accepted. The problem arising here is that such a combination is valid only for that particular temperature history, which is very inconvenient having in mind the temperature variation existing in one structure.

Lack of models for thermal dilation and autogenous deformation is a consequence of poor understanding of the fundamental microstructural processes in hardening concrete. It is obviously necessary with more research on this topic.

3.3.2 Modelling of mechanical properties

Modulus of elasticity and strength.

As previously mentioned, compressive strength is often used in estimation of tensile strength and E-modulus, because the tensile strength test and E-modulus test are more complicated to perform than compressive strength test. The correlation between these properties is therefore an important topic.

In the literature there exist a large number of mathematical expressions and models for compressive strength based on different concepts, such as: porosity, gel-space ratio, degree of hydration, equivalent age concept, etc. Very often, tensile strength and E-modulus are expressed in terms of the compressive strength. Different correlation between them are proposed in literature, some of them are listed in (Byfors 1980), (Emborg 1994) and (Andersen 1995). In (Emborg 1994) different expressions for compressive strength's, tensile strength's and E-modulus' development were compared and large scatter was found, especially for early ages. Therefore it was recommended to calibrate formulas against measured values for actual concrete before calculation. That is reasonable since E-modulus of aggregate has large effect on E-modulus of concrete, but not on concrete strength.

Commonly, E-modulus, compressive and tensile strength are modelled as functions of equivalent age or degree of hydration. The limitation of that approach is that direct influence of the temperature on the material properties is not taken into consideration. Temperature influence on material properties is included only by equivalent age or degree of hydration, with the consequence that high curing temperatures cause increase of strength and E-modulus. This is contradictory to the observations, see previous chapter. To model the loss of the final strength due to high curing temperature, different empirical correction factors are proposed in literature, (Jonasson 1994), (Emborg 1989), (Laube 1990). In these investigations only compressive strength results were used in calibration of the correction factors, and the temperature sensitivity of the tensile strength was not considered explicitly. In (Emborg 1989) temperature sensitivity of the tensile strength was taken into account via correlation between compressive and tensile strength. The recent observations (Kanstad 1999) have shown different temperature sensitivities for the E-modulus, tensile and compressive strength. It was also found that the loss of the final strength and E-modulus is less pronounced for high performance concrete and realistic temperature histories.

In this study E-modulus and strength are modelled by means of the following expressions (Kanstad 1999):

$$f_c(t_e) = f_c(28) \cdot \exp\left[s \cdot \left(1 - \sqrt{\frac{28}{t_e - t_0}}\right)\right]$$

$$f_t(t_e) = f_t(28) \cdot \left\{\exp\left[s \cdot \left(1 - \sqrt{\frac{28}{t_e - t_0}}\right)\right]\right\}^{n_t}$$

$$E_c(t_e) = E_c(28) \cdot \left\{\exp\left[s \cdot \left(1 - \sqrt{\frac{28}{t_e - t_0}}\right)\right]\right\}^{n_E} \tag{3.18}$$

$f_c(28)$, $f_t(28)$ and $E_c(28)$ are compressive strength, tensile strength and E-modulus of concrete at 28 days, s, t_0, n_t and n_E are the model parameters.

The parameters s and t_0 are set to be equal for all three properties, and therefore may be determined from the simple compressive strength tests. The parameters n_t and n_E are used to describe different time (maturity) dependence for the tensile strength and E-modulus, and may be determined from the tensile strength and E-modulus tests, respectively. The basic idea was to make the test program more efficient by using compressive strength tests to estimate some parameters for tensile strength and E-modulus. Thus the test program on mechanical property development is considerably reduced (Kanstad 1999).

The expressions (3.18) are based on the CEB-FIP MC90 equation for E-modulus, which is modified by introducing the parameters t_0, n_t, n_E. t_0 is a concrete age at which stiffness achieves value high enough to produce measurable stresses. It is assumed that before t_0 volume changes do not induce any stresses, so t_0 is a "zero-point" for stress calculation. The concept of concrete age t_0 below which no stresses can be generated is shown to be convenient for several reasons. Models with t_0 more clearly describe development of material properties in very early ages and are therefore more robust against the conse-

quences of an insufficient amount of experimental data (Bjøntegaard 1998). In this paper the above model for E-modulus development is compared to the model proposed by (Freiesleben 1977):

$$E_c(t_e) = E_\infty \cdot \exp\left(\frac{t_e}{\tau}\right)^\alpha \tag{3.19}$$

where E_∞, τ and α are the model parameters.

The models are calibrated against two sets of experimental data with the same accuracy. If there is a lack of experimental data, model (3.19) becomes much more inaccurate than model (3.18), as shown in Figure 3.2.

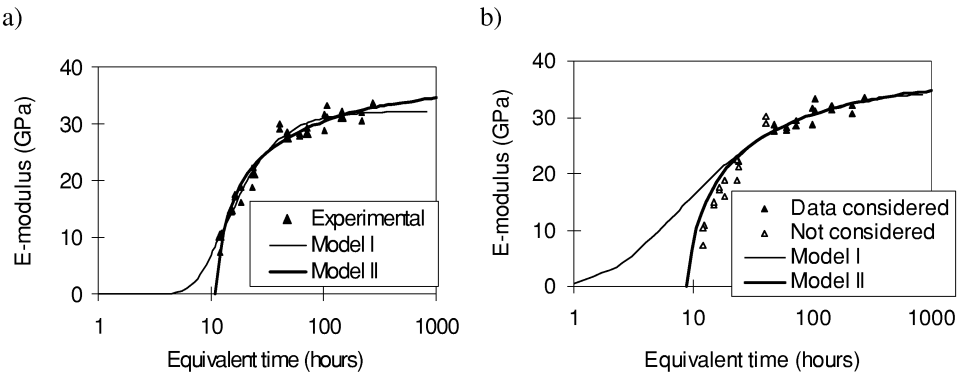

Figure 3.2: a) E-modulus development, experimental data and models. Model I is proposed by (Freiesleben 1977), model II is modified CEB-FIP MC90 equation.
b) E-modulus data generated before 48 hours were not considered (from Bjøntegaard 1999)

Furthermore, the t_0 concept is convenient if the creep is modelled by the Double Power Law, see the next section.

An analogue approach is the assumption of an initial degree of hydration (Laube 1990), (Breugel 1990).

The model (3.18) is implemented in the FE program DIANA and used in connection with the Double Power Law creep model.

3.3.3 Viscoelasticity

Time dependent behaviour of concrete is described by the theory of linear viscoelasticity for aging materials. The sum of elastic (ε_e) and creep (ε_c) strain is replaced by the viscoelastic strain ε_{ve} as follows:

$$\varepsilon_{ve} = \varepsilon_e + \varepsilon_c \tag{3.20}$$

According to the linear theory, the strain is proportional to the applied stress. It means that the strain at time t caused by constant uniaxial stress σ applied at time t' is given by:

$$\varepsilon(t) = \sigma \cdot J(t, t') \tag{3.21}$$

where $J(t,t')$ is the compliance function (or creep function), which represents the strain at time t produced by unit constant stress applied at time t'. An important property of the compliance function of concrete is that it is a function of two variables, the current age t and age at loading t', which takes age dependence into account.

For a variable stress history, the principle of superposition is assumed to be valid. For aging materials such as concrete the principle of superposition was originally formulated by Maslov and McHenry (Neville 1983): strains produced at any time t by a stress increment applied at age $t' < t$ are independent of the effects of any stress applied earlier or later.

It means that total strain at time t of a concrete subjected to varying stress is the accumulation of the strains caused by each stress increment $\Delta\sigma(t')$.

$$\varepsilon(t) = \sum_{t' = t_0}^{t} \Delta\sigma(t') J(t, t') \tag{3.22}$$

If the stress varies continuously, the strain becomes:

$$\varepsilon(t) = \int_{t_0}^{t} J(t, t') d\sigma(t') \tag{3.23}$$

In the same way the stress can be expressed as a function of a prescribed strain history:

$$\sigma(t) = \int_{0}^{t} R(t, t') d\varepsilon(t') \tag{3.24}$$

where $R(t,t')$ is the relaxation function, which represents the stress at any time t caused by unit constant strain applied at time t', $t' < t$.

The linear superposition principle is valid for concrete under the following conditions (Bazant 1982):

1. The stress is less than about 40% of the strength
2. The strains do not decrease in magnitude (but the stresses can)
3. There is no significant drying during creep
4. There is no large increase of the stress magnitude after initial loading

(3.25)

Proportionality between stresses and strains are provided by fulfilment of restrictions (1) and (3), whereas the principle of superposition requires the additional restrictions (2) and (4). More about nonlinearities will be given in the next section.

Creep properties within the linear range are fully characterized by the creep or relaxation functions. A great number of creep functions for concrete is proposed in literature, such as: Double Power Low (Bazant 1975), Triple Power Low (Bazant 1985b), Bazant-Panula model (Bazant 1978), etc. They are normally obtained from fit of test data, with some exceptions (Bazant-Panula model) where the creep function is given as a function of the mix proportions. Another large group of creep functions has resulted from attempts to

simulate concrete behaviour by means of ideal rheological models (spring /dashpot combinations). Here two approaches may be noted:

- time dependent deformation of concrete is described by rheological model in such a way that a specific part of concrete deformation has been assigned to a given element of the model
- rheological models are used simply to approximate the observed deformation without any physical meaning.

The latter approach is used usually to simplify the solution of the integral (3.23) by converting it into differential equations, see e.g. (Bazant 1982).

Detailed reviews of creep models is given in e.g. (Neville 1983).

Regarding modelling of creep at early ages, most of the proposed models are only modification of the creep models for mature concrete. With such modifications researchers have tried to describe special aspects of creep behaviour for young concrete, such as: pronounced ageing effects and high creep at very early ages, temperature influence on creep, and high stress nonlinearity.

To express temperature influence and strong ageing effect (Bazant 1982) proposed Kelvin and Maxwell chain model with equivalent age dependent moduli and viscosities. (Pedersen 1994) applied the same approach to the Burgers model with the only difference that the ratio between modulus and viscosity, i. e. the retardation time was not kept constant, but age dependent. If the Maxwell model with age dependent relaxation times is used, the constitutive relations are given by differential equations known as rate-of-creep method, or the Dischinger method.

To be able to model high creep at very early ages (Emborg 1989) modified the Triple Power Low supplementing it with two additional functions. To the same purpose (de Borst 1995) used an increasing, instantaneous E-modulus instead of a constant material parameter E_0 in the Double Power Law, originally proposed by (Bazant 1975) for mature concrete. (Jonasson 1994) used an age-dependent Maxwell chain model with additional terms for high-stress nonlinearity and temperature and humidity effects.

Some authors proposed new creep models for young concrete, among them (Rostasy 1993), later modified by (Gutsch 1998), then (Schutter 1997), (Lokhorst 1994), etc.

Nonlinear effects.

Measurements of creep deviate from the principle of superposition when some of the requirements (3.25) are violated. If the basic creep is considered (requirement 3 is fulfilled), these deviations are due to high-stress nonlinearity (requirement 1 violated), and low-stress nonlinearity (requirements 2 and 4 are violated).

Pickett effect.

At simultanous drying the deformation of a loaded concrete specimen is larger than the sum of creep and shrinkage when measured separately. The phenomenon is called Pickett effect and cannot be accounted for with the principle of superposition. There is no general agreement how this increase of deformation may be regarded: as increase of creep due to drying (drying creep) or as increase of shrinkage due to loading.

A common approach is to assume that the total deformation consists of shrinkage (equal to that of an unloaded specimen), basic creep (creep of a specimen which is not allowed to dry) and drying creep (the increase of creep due to shrinkage). This approach is simple, but not correct since creep and shrinkage influence each other and are not independent phenomena which may be separated.

For hardening concrete, the situation is ever more complicated: external drying is not relevant (see Section 2.3.2), but internal drying due to hydration (self-desiccation) cannot be prevented and simultaneous creep and shrinkage are always present. To be strictly correct, the term basic creep as it is used for hardened concrete should not be applied here.

In the present study, however, the Pickett effect is disregarded and creep and autogenous shrinkage are considered to be independent phenomena. The basic creep is defined as the creep under conditions of constant reference temperature (20^0C) and no moisture exchange with surroundings corrected for the autogenous deformation measured on unloaded specimen.

High-stress nonlinearity.

Measured creep under high stresses is higher than predicted by the principle of superposition. This phenomenon is well known and documented for hardened concrete, both in compression and in tension. This nonlinear creep behaviour is mainly due to microcracking.

For hardening concrete, experimental data are more scarce. Nonlinear concrete behaviour in compression at early ages is reported at the stress level as low as 40% of compressive strength (Schutter 1997). (Han 1997) investigated creep of high performance concrete (HPC) at early ages, and also concluded that young HPC has a lower limit of linear behaviour in compression (50%) than hardened HPC (70%). Decreasing of the limit of linearity with decreasing age is reported by (Brameshuber and Hilsdorf 1987).

Data on non-linearity in tension are even more limited. (Hauggaard 1997) performed tensile stress tests which showed that the limit of linearity is somewhere between 60% and 80% of the tensile strength. (Laube 1990) found that this limit is about 50% of the tensile strength.

In concrete structures at early ages the compressive load level is normally far below 40% of the compressive strength. Therefore the nonlinearity due to high compressive stresses is not relevant for self-induced stresses. On the other hand, the tensile stress level is high, and in prediction of cracking, nonlinearity in tensile stresses is of great interest.

Nonlinear behaviour in tension is usually considered before and after the tensile stress exceeds the tensile strength, so-called pre- and post-peak behaviour. Pre-peak behaviour may be modelled by nonlinear stress-strain relationship (Jonasson 1994), (Laube 1990). When the major principal tensile stress exceeds the tensile strength, a crack is initiated. The post-peak behaviour is then modelled by fracture energy parameters. The total strain rate is decomposed into a concrete strain rate and crack strain rate, and each of these components is governed by its own constitutive low. The values describing concrete behaviour after cracking, fracture energy and ultimate strain, are age dependent for young concrete. Fracture mechanics parameters for young concrete have been investigated by, among others, (Brameshuber and Hilsdorf 1987), (Laube 1990) and (Gutch 1998).

Very commonly, pre-peak nonlinear behaviour is neglected, and concrete is modelled as viscoelastic material prior to cracking, what is a conservative assumption. After cracking, smeared crack model is often used and the relation between the stress increment and the crack strain increment is defined by strain softening diagram. There are also other approaches in modelling high-stress nonlinearity in tension in young concrete, for instance a coupled elastoplastic creep models (Liang 1997).

In this study high-stress nonlinearity is not considered.

Low-stress nonlinearity.

Another deviation from the principle of superposition is stiffening of a previously loaded concrete when it is loaded again. It occurs within the service stress range and therefore is called low-stress nonlinearity. It is observed when a sudden load (positive or negative) is imposed on the already loaded concrete. The measured creep strain is then reduced compared to the principle of superposition. This phenomenon has been investigated on hardened concrete in compression, see for instance (Neville 1983) or (Bazant 1982). Sometimes it has been taken into account by adjusting existing creep models to data from the tests with stepwise loading (Jordaan 1977). According to (Bazant and Kim 1979), the consequence is a poor approximation of all other behaviour within the linearity range, and since it is a nonlinear phenomenon, it should be modelled by a nonlinear theory. Bazant explained the phenomenon as a compression-accelerated aging and stiffness' increase due to the compressive load, and modelled it by replacing the equivalent age with an equivalent hydration period and by introducing a stress-dependent function in Eq.(3.23). Thus:

$$\dot{\varepsilon}(t) = \int_0^t \dot{J}(t, t_e') \cdot \frac{\mathrm{d}\sigma(t')}{1 + a(t')} \tag{3.26}$$

$$t_e = \int \beta_T \beta_\sigma dt, \tag{3.27}$$

where β_T corresponds to $H(T)$ in Eq.(3.8), the function $a(t)$ and stress dependent factor β_σ is given by (Bazant 1979).

To the knowledge of this author, there are no investigations about low stress nonlinearity in tension reported in literature. There is also a lack of experimental evidence on the low-stress nonlinearity at early ages. As already mentioned, deviation from linearity is observed when a *sudden* load is imposed on the already loaded concrete and, according to (Neville 1983) it vanishes as the duration of the first load step diminishes. It is thus unclear what happens if the stresses vary continuously and shift from compression to tension, like thermal stresses.

More research on low stress nonlinearity at early ages is necessary before eventual modelling can be carried out. The phenomenon is ignored in the present study.

3.3.4 Temperature effects

Creep at constant temperature.

Temperature affects creep in two ways: directly, influencing the creep rate, and indirectly, influencing aging and maturity of concrete. Very often it has been considered that in young concrete the former effect always dominates, and therefore, only this effect is taken into account in creep models for young concrete in most calculation programs. The temperature effect on aging is usually modelled by replacing concrete age t' with equivalent age t_{eq}'.Consequently, all parameters which are functions of concrete age become functions of equivalent age.

The direct temperature influence on creep, i. e. the change of creep rate, is usually included by means of empirical factors on the creep parameters. For instance, the viscosities in the Kelvin and Maxwell chain model are reduced (Bazant 1988):

$$\eta_\mu(t) = \frac{\tau_\mu E_\mu(t)}{\phi_T}, \tag{3.28}$$

where τ_μ are retardation/ relaxation times and E_μ are elasticity modulii in the Kelvin/ Maxwell chain model (see the next chapter), ϕ_T corresponds to $H(T)$ in Eq.(3.8):

$$\phi_T = \exp\left(\frac{E_a}{R}\left(\frac{1}{T_{ref}} - \frac{1}{T}\right)\right) \tag{3.29}$$

According to (Bazant 1982), the compliance function $J(t,t')$ at any temperature kept constant after time t' may be obtained by the following replacements:

$$t' \rightarrow t_e' \quad t - t' \rightarrow (t - t')\phi_T$$

In this study the direct temperature effect on creep is not considered.

Creep at changing temperatures.

Increase of creep of hardened concrete at changing temperature, so-called transient creep, has been investigated by several researchers. A comprehensive historical overview is given in (Khoury 1985). According to (Thelanderson 1987), who investigated concrete at elevated temperature, the name 'creep' is confusing, since transient thermal creep is a quasi-instantaneous response to temperature change, similar to that of free thermal strain. He interpreted it as an interdependence between temperature response and mechanical response, and suggested that thermal strain rate should be made dependent on the current stress state:

$$\Delta\varepsilon_T = \alpha_T \Delta T \cdot \left(1 + \rho \cdot \frac{\sigma}{f_c'}\right), \tag{3.30}$$

where f_c' is the uniaxial compressive strength at the reference temperature, and a value of $\rho = 2.35$ was found to fit best to the experimental results.

To explain the nature of the problem, (Bazant 1985a) assumed that the viscosity coefficient, which characterizes the creep rate, depends on the the micro diffusion of water between the macropores and the micropores in the cement gel. Since the microdiffusion is driven by a humidity- and temperature gradient, the viscosity depends on a gradient of pore humidity $\dot{h}$ and temperature $\dot{T}$. Bazant proved mathematically (Bazant 1986) that this theory is equivalent to the assumption about stress-induced shrinkage and stress-induced thermal strain, and the viscosity being independent of temperature and pore humidity:

Hence, thermal and shrinkage strain are described as:

$$\Delta\varepsilon_T = \alpha_T \Delta T \cdot (1 + \rho \cdot \frac{\sigma}{f_t'} \cdot sign(\Delta H)) \tag{3.31}$$

$$\Delta\varepsilon_h = k\Delta h \cdot (1 + r \cdot \frac{\sigma}{f_t'} \cdot sign(\Delta H)) \tag{3.32}$$

$$\Delta H = \Delta h + c\Delta T \tag{3.33}$$

where c is positive constant.

$$sign(\Delta H) = \frac{\Delta H}{|\Delta H|}$$

Analysis of different test data showed that r is between 0.1 to 0.6, and ρ is between 2 and 2.5

(Jonasson 1994) was the first who applied this theory to young concrete. Assuming that for young concrete the temperature change dominates, he stated:

$$sign(\Delta H) = sign(\Delta T), \tag{3.34}$$

and consequently, the stress-induced thermal strain is:

$$\Delta\varepsilon_T^0 = \alpha_T \Delta T \cdot \rho \cdot \frac{\sigma}{f_{ct}} \cdot sign(\Delta T), \tag{3.35}$$

where f_{ct} is tensile strength dependent on maturity. Hence, stress-induced thermal strain for young concrete is made age (maturity) dependent. That is a reasonable assumption having in mind that for mature concrete at high temperatures this strain rate is probably caused by microstructural changes in the cement paste during heating. Age dependence of transient thermal creep for ages less then about three months is also reported in (Parrot 1979).

(Hedlund 1996) found from the experiments that value for ρ varied for different concrete mixtures from 0.1 to 0.7.

Transient creep in young concrete was also considered by (Hauggaard 1997). He used a conceptually different approach, modelling transient creep as modification of the creep model. He added an extra dashpot in the rheological model whose viscosity was a function of microprestresses.

(Gutsch 1998) modelled the temperature influence on creep by introducing the equivalent time under load instead of real time. Creep and relaxation curves under changing elevated temperature thus may be transformed into creep curve under isothermal temperature T = 20^0C with an identical degree of hydration at first loading.

At present, physical mechanism behind transient creep is not known. But there is no doubt that the phenomenon exists and has a such significance that it must be considered in analysis of concrete structures. Difficulties connected to modelling of transient creep, especially for young concrete, is that the experimental data are rather scarce, and therefore could be fitted equally well by different models.

In DIANA both the direct temperature influence on the creep rate and the transient creep are neglected. Aging effect is taken into account only by maturity of concrete at loading time, for Maxwell and Kelvin chain - by equivalent age (degree of hydration) dependency of E-moduli, and for Double Power Law by equivalent age (degree of hydration) dependency of E-modulus. Temperature history after loading time has no effect on creep. In other words, two concrete specimens under constant load exhibit equal creep strain if they have equal maturity at loading time, regardless of temperature after loading.

To include influence of transient temperature on creep, model in Eq.(3.31) is implemented in FE program DIANA. Work of (Takacs 1999) was used here as a starting point. A transient creep term is added in Eq.(3.16) which now reads:

$$\dot{\varepsilon} = \dot{\varepsilon}_e + \dot{\varepsilon}_c + \dot{\varepsilon}_{trc} + \dot{\varepsilon}_{th} + \dot{\varepsilon}_{sh} + \dot{\varepsilon}_{crack} \tag{3.36}$$

The adjustment factor ρ in the transient creep term may be determined from the creep test under changing temperature, or TSTM test, see the next Chapter.

In the following, TSTM tests from (Bjøntegaard 1999) are used in the calibration of the transient creep term for the BASE concrete. Five tests with different temperature histories have been carried out. Fully restrained specimen in the TSTM and unrestrained specimen in the free deformation rig were exposed to the same temperature histories, which are typical for hardening concrete structures. Stress generation in the specimen in the TSTM was recorded, and in a free deformation rig free movement was measured. To avoid cracking, the 100% restraint was turned off after approximately two days, and a more realistic stress history of a partly restrained structure was obtained. The deformation after this time was recorded in the TSTM, and used in calculation. For more detailed description of the test set-up, see (Bjøntegaard 1999). E-modulus and creep model parameters were determined from independent tests. The adjustment factor ρ in transient creep is found by fitting calculated stresses to the measurements. In Figure 3.3 results of numerical simulation are presented together with the experimental results from TSTM tests. Calculations were performed with and without transient creep. It can be seen that transient creep reduces stresses, thus having the same effect on thermal stresses as the increased creep rate. Generally, agreement between calculation results and experimental data is better when transient creep is taken into account. The parameters used in calculation are given in Appendix 1.

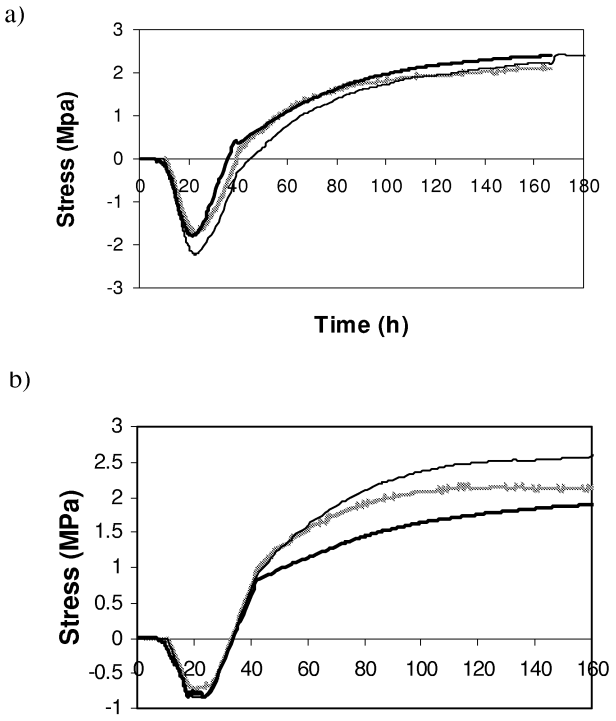

Figure 3.3: Experimental and calculated stress development for the BASE concrete specimen in the TSTM with different temperature histories: a) $T_{max} = 62^0C$, b) $T_{max} = 47^0C$

Chapter 4

Numerical Solution

4.1 General

Because the influence of the mechanical response on the temperature development in hardening concrete is small, the thermal and mechanical problem may be separated. The thermal problem must be solved first, and results are used as input for the subsequent stress calculation which is based on development of early-age concrete properties, thermal and shrinkage induced strain and cracking. The finite element method is adopted to solve the governing set of differential equations. Since the problem is decoupled, the finite element formulation and the iterative solution of the equations are elaborated separately.

4.2 Solution of thermal problem

4.2.1 Finite element formulation

The temperature development in hardening concrete due to hydration may be described by the Fourier differential equation for heat conduction in a homogenous and isotropic body, see e.g. (Zienkiewicz 1977) or (Cook1989):

$$div\boldsymbol{q} + \rho c\dot{T} = Q, \qquad (4.1)$$

$$\boldsymbol{q} = -\boldsymbol{K}\nabla T$$

where $\boldsymbol{q}$ is the heat flux, T the temperature, $\dot{T}$ the rate of temperature, ∇T the temperature gradient, ρ the mass density, c the specific heat, Q the rate of internal heat generation per unit volume, and $\boldsymbol{K}$ the conductivity matrix, which is diagonal for isotropic body.

Boundary conditions may be:

- essential, with a prescribed boundary temperature:

  $T = T_B$

- natural, with a prescribed boundary flux:

  $\boldsymbol{q} \cdot \boldsymbol{n} = -q_B$

- convective, with a given convection heat transfer:

  $\boldsymbol{q} \cdot \boldsymbol{n} = h(T_f - T)$,

where $\boldsymbol{n}$ is the vector pointing outwards normal to the boundary, h is the heat transfer coefficient, T is boundary temperature, and T_f is temperature of surroundings.

In order to complete the formulation of the thermal response, initial conditions have to be added to the differential equation and boundary conditions. Because the differential equation is of first order in time, only one initial condition is sufficient:

$$T = T_0$$

The Finite Element formulation can be derived using the Galerkin weighting procedure. Eq.(4.1) is multiplied by a test function v and integrated over the considered volume V:

$$\int_V v\, div\boldsymbol{q}\, dV + \int_V v\rho c\dot{T}\, dV = \int_V vQ\, dV \tag{4.2}$$

To reduce the order of the differential equation and introduce boundary conditions, the Gauss theorem is applied:

$$\int_V div\boldsymbol{q}\, v\, dV + \int_V \boldsymbol{q}\nabla v\, dV = \int_B (\boldsymbol{q}\cdot\boldsymbol{n})\, v\, dB. \tag{4.3}$$

With the Gauss theorem and boundary conditions, Eq.(4.2) may be written:

$$\int_V (-\boldsymbol{K}\nabla T)\nabla v\, dV = \int_B (h(T-T_f) - q_B)\, v\, dB + \int_V \rho c\dot{T}\, v\, dV - \int_V Qv\, dV \tag{4.4}$$

If the flux is prescribed at the part of the boundary B_N and convection heat transfer on another part B_C, Eq.(4.4) may be rewritten as follows:

$$\int_V \boldsymbol{K}\nabla T\, \nabla v\, dV + \int_{B_C} hTv\, dB_c + \int_V \rho c\dot{T}v\, dV = \int_{B_C} hT_f v\, dB_c + \int_{B_N} q_B v\, dB_n + \int_V Qv\, dV \tag{4.5}$$

In the Finite Element Method domain is divided into finite elements. In each element the temperature field is approximated as a linear function of the values of element nodes:

$$T = \boldsymbol{NT}$$

$$\nabla T = \nabla \boldsymbol{NT} = \boldsymbol{BT}, \tag{4.6}$$

where $\boldsymbol{N}$ is a matrix of element interpolation functions, and $\boldsymbol{T}$ the vector of nodal temperatures. The weight function is chosen to be of the same class as the interpolation functions $\boldsymbol{N}$.

Application of Eq.(4.5) to each finite element gives:

$$(\boldsymbol{K} + \boldsymbol{K}_c)\boldsymbol{T} + \boldsymbol{C}\dot{\boldsymbol{T}} = \boldsymbol{R}_Q + \boldsymbol{R}_q + \boldsymbol{R}_h\ , \tag{4.7}$$

where

$$\boldsymbol{K} = \int_V \boldsymbol{B}^T \boldsymbol{K} \boldsymbol{B}\, dV \tag{4.8}$$

is the thermal conductivity matrix,

$$\boldsymbol{K}_c = \int_{B_c} h \boldsymbol{N}^T \boldsymbol{N}\, dB_c \tag{4.9}$$

is the convection matrix,

$$\boldsymbol{C} = \int_V \rho c \boldsymbol{N}^T \boldsymbol{N}\, dV \tag{4.10}$$

is the heat capacity matrix, and

$$\boldsymbol{R} = \int_{B_c} \boldsymbol{N}^T h T_f\, dB_c + \int_{B_n} \boldsymbol{N}^T q_B\, dB_n + \int_V \boldsymbol{N}^T Q\, dV \tag{4.11}$$

is the load vector containing contributions from heat convection, prescribed flux and internal heat production.

After assembling all elements, the equation for a structural system is obtained:

$$\left[\boldsymbol{K}_T\right] \cdot \{\boldsymbol{T}\} + \left[\boldsymbol{C}\right] \cdot \{\dot{\boldsymbol{T}}\} = \{\boldsymbol{R}\}, \tag{4.12}$$

$$\left[\boldsymbol{K}_T\right] = \left[\boldsymbol{K}\right] + \left[\boldsymbol{K}_c\right] \tag{4.13}$$

$$\{\boldsymbol{R}\} = \{\boldsymbol{R}_Q\} + \{\boldsymbol{R}_q\} + \{\boldsymbol{R}_h\} \tag{4.14}$$

where $\left[\boldsymbol{K}\right]$ is the structural conductivity matrix, $\left[\boldsymbol{K}_c\right]$ is the structural convection matrix, $\left[\boldsymbol{C}\right]$ is the structural heat capacity matrix, $\{\boldsymbol{T}\}$ is the global nodal temperature vector, $\{\boldsymbol{R}_Q\}$ is the heat flux in structural nodes from internal heat generation, $\{\boldsymbol{R}_q\}$ is the prescribed heat flux in structural nodes, $\{\boldsymbol{R}_h\}$ is the heat flux in structural nodes from convectivity.

4.2.2 Time integration

To eliminate time derivatives of temperature from Eq.(4.12) a direct integration method is used, and differential equation is transformed into the set of usual linear equations:

$$\left(\frac{1}{\Delta t}\boldsymbol{C} + \beta \boldsymbol{K}_T\right) \cdot \boldsymbol{T}_{n+1} = \left(\frac{1}{\Delta t}\boldsymbol{C} - (1-\beta)\boldsymbol{K}_T\right) \cdot \boldsymbol{T}_n + (1-\beta)\boldsymbol{R}_n + \beta \boldsymbol{R}_{n+1} \tag{4.15}$$

where $\boldsymbol{T}_{n+1}$ and $\boldsymbol{T}_n$ are two temperature states, separated by time increment Δt, β is an integration parameter, $0 \le \beta \le 1$.

If $\beta = 0$ and $\boldsymbol{C}$ is a diagonal matrix, $\boldsymbol{T}_{n+1}$ may be calculated directly from the $\boldsymbol{T}_n$, and such scheme is known as explicit. If $\beta \neq 0$ the non-diagonal system of equations must be solved, and such integration schemes are called implicit. Among implicit methods the most popular are: Crank-Nicolson method ($\beta = 1/2$), Galerkin method ($\beta = 2/3$) and backward difference method ($\beta = 1$). It can be shown that recurrence schemes with $\beta \geq 1/2$ are unconditionally stable (Zienkiewicz 1977). When $0 < \beta < 1/2$, stability is conditional, requiring limited time steps. From unconditionally stable schemes Crank-Nicolson method ($\beta = 1/2$) is the most accurate. But it may produce oscillatory results at abrupt temperature changes. The Galerkin scheme with $\beta = 2/3$ is then recommended.

Since the internal heat generation, heat capacity and conductivity depends on the maturity age and temperature, Eq.(4.15) is nonlinear and an incremental-iterative solution procedure is used.

4.3 Solution of mechanical response

4.3.1 Finite element formulation

The starting point for the finite element formulation is the incremental formulation of the Principle of the Virtual Work:

$$\int_V \delta\varepsilon^T \sigma dV = \int_V \delta u^T b dV + \int_A \delta u^T t dA \tag{4.16}$$

where V and A represent the volume and the surface of the structure, b is the volume load, t the surface load, and δu an admissible virtual displacement,

The derivation of Eq.(4.16) may be found in many textbooks, e.g. (Zienkiewicz 1977)

In the FE method the structural geometry is subdivided into finite elements and Eq.(4.16) is applied to each elements. Within one element the displacements are approximated by interpolation of the element nodal displacements $\boldsymbol{v}$ as follows:

$$\boldsymbol{u} = \boldsymbol{N}\boldsymbol{v} \tag{4.17}$$

where $\boldsymbol{N}$ is a vector of interpolation functions that satisfy the element boundary conditions.

Then the approximation of strain are:

$$\varepsilon = \Delta\boldsymbol{u} = \Delta\boldsymbol{N}\boldsymbol{v} = \boldsymbol{B}\boldsymbol{v} \tag{4.18}$$

and Eq.(4.16) becomes:

$$\int_V \delta\boldsymbol{v}^T \boldsymbol{B}^T \sigma dV = \int_V \delta\boldsymbol{v}^T \boldsymbol{N}^T \boldsymbol{b} dV + \int_A \delta\boldsymbol{v}^T \boldsymbol{N}^T \boldsymbol{t} dA \tag{4.19}$$

This equation is valid for any admissible virtual displacement δv, and the equation for one element can be written as follows:

$$\int_V \boldsymbol{B}^T \sigma dV = \int_V \boldsymbol{N}^T \boldsymbol{b} dV + \int_A \boldsymbol{N}^T \boldsymbol{t} dA \tag{4.20}$$

The right side of the equation is a vector of element forces consisting of volume and surface forces:

$$\boldsymbol{r} = \int_V \boldsymbol{N}^T \boldsymbol{b} dV + \int_A \boldsymbol{N}^T t dA \tag{4.21}$$

and Eq.(4.20) reads:

$$\int_V \boldsymbol{B}^T \sigma dV = \boldsymbol{r} \tag{4.22}$$

To complete the FE formulation, the constitutive relation has to be applied. As shown in the previous chapter, constitutive relation for aging viscoelastic material is given via creep function (4.23) or relaxation function (4.24).

$$\varepsilon(t) = \int_{t_0}^{t} J(t, t') d\sigma(t') \tag{4.23}$$

$$\sigma(t) = \int_{0}^{t} R(t, t') d\varepsilon(t') \tag{4.24}$$

Due to the fact that the creep and relaxation functions for concrete are functions of two variables, actual time t and age at loading t', analytical exact solution of the integrals (4.23) and (4.24) are not available. Therefore, numerical integration of the constitutive relation must be employed.

4.3.2 Integration of the viscoelasticity constitutive equation

Different methods may be used to solve the basic integral equation. Some of them depend on formulation of the creep (relaxation) function, i. e. creep model, others can be used for any creep (relaxation) function.

4.3.3 Supperposition method

If the creep function is such that the integral (4.23) cannot be solved exactly, it may be replaced by summation of the creep curves (Neville 1983). This method has often been used in combination with the Double Power Low, but it is applicable to any form of the creep function.

In a numerical solution the time of interest is divided into time steps $\Delta t_i = t_i - t_{i-1}$, and the total deformation at time t becomes:

$$\varepsilon(t_r) = \sum_{i=1}^{r} J(t_r, t_i) \Delta\sigma_i \tag{4.25}$$

where $\Delta\sigma_i$ is the stress increment during the time increment Δt_i. Depending on where in the time interval the stress increment is assumed to be applied, different solution methods exist: rectangle rule (central, forward or backward difference methods), trapezoidal rule, Simpson's rule. All these methods are easily programmed, and their accuracy depends on the size and number of time steps. Disadvantage of this method is that the entire stress (strain) history has to be stored, which in the case of large structural systems demands large storage capacity and long computational time. Therefore the superposition method is rarely used in computational analyses today.

4.3.4 Numerical method based on differential formulation

The problem with storing the entire stress history may be avoided if the integral equation is converted to differential equations. Convenience of the differential formulation is that differential equations can be solved step-by-step, which means that the strain state at any time t is defined by the state from the previous step and the change during the last time increment. The summation of the entire strain history at each time step is circumvented.

The drawback of the step-by-step solution methods for differential equations is that the time step should not increase beyond a certain limit because of stability and accuracy requirements. (Bazant 1982) has proposed the recursive algorithm which is stable regardless of the size of time step with only condition that the stress or strain rates and all parameters must be constant during the time step, and may vary by jumps between the steps.

As already mentioned, the relation between stresses and strains can be expressed by means of the relaxation function. For the uniaxial state it follows:

$$\sigma(t) = \int_0^t R(t, t')d\varepsilon(t') \tag{4.26}$$

If the relaxation function is expanded in Dirichlet series:

$$R(t, t') = \sum_{\mu=1}^{N} E_\mu(t')\exp\left[-\frac{(t-t')}{\tau_\mu}\right] \tag{4.27}$$

Eq.(4.26) becomes:

$$\sigma(t) = \sum_{\mu=0}^{n} \int_0^t E_\mu(t')\, e^{-\frac{t-t'}{\tau_\mu}}\, \dot{\varepsilon}\, dt'. \tag{4.28}$$

For time $t+\Delta t$ the stress is:

$$\sigma(t+\Delta t) = \sum_{\mu=0}^{n} \int_0^{(t+\Delta t)} E_\mu(t')\, e^{-\frac{t+\Delta t-t'}{\tau_\mu}}\, \dot{\varepsilon}\, dt' \tag{4.29}$$

The stress increment from time t to time $t+\Delta t$ may be calculated as follows:

$$\Delta\sigma = \sigma(t+\Delta t) - \sigma(t) =$$

$$\sum_{\mu=0}^{n} \int_0^t E_\mu(t') e^{-\frac{t+\Delta t-t'}{\tau_\mu}} \dot{\varepsilon}\, dt' + \sum_{\mu=0}^{n} \int_t^{(t+\Delta t)} E_\mu(t') e^{-\frac{t+\Delta t-t'}{\tau_\mu}} \dot{\varepsilon}\, dt' - \sum_{\mu=0}^{n} \int_0^t E_\mu(t') e^{-\frac{t-t''}{\tau_\mu}} \dot{\varepsilon}\, dt' \quad (4.30)$$

Under assumption about constant strain rate and constant $E_\mu = E_\mu(t^*)$ from t to $t+\Delta t$, the stress increment equals:

$$\Delta\sigma = \sum_{\mu=0}^{n} \left(1 - e^{-\frac{\Delta t}{\tau_\mu}}\right)\left(\frac{E_\mu(t^*)\tau_\mu}{\Delta t}\Delta\varepsilon - \sigma_\mu(t)\right), \quad (4.31)$$

where $\sigma_\mu(t)$ is a state variable:

$$\sigma_\mu(t) = \int_0^t E_\mu(t') e^{-\frac{t-t'}{\tau_\mu}} \dot{\varepsilon}\, dt', \quad (4.32)$$

and during analysis may be calculated by means of a recurrent formula:

$$\sigma_\mu(t+\Delta t) = \int_0^t E_\mu(t') e^{-\frac{t+\Delta t-t'}{\tau_\mu}} \dot{\varepsilon}\, dt' + \int_t^{(t+\Delta t)} E_\mu(t') e^{-\frac{t+\Delta t-t'}{\tau_\mu}} \dot{\varepsilon}\, dt' \approx \quad (4.33)$$

$$e^{-\frac{\Delta t}{\tau_\mu}}\sigma_\mu t + \frac{\tau_\mu E_\mu t^* \Delta\varepsilon}{\Delta t} 1 - e^{-\frac{\Delta t}{\tau_\mu}}$$

Hence, the term describing strain history may be calculated by the state from the previous step and its change during the last time increment, without the storage of the complete stress history.

Physically the Dirichlet series may be interpreted as a Maxwell chain model. E_μ and τ_μ represent age dependent moduli and the relaxation times of individual Maxwell units, respectively.

$$\tau_\mu = \frac{E_\mu}{\eta_\mu} \quad (4.34)$$

where η_μ represents viscosity of the Maxwell dashpot.

An analog formulation may be done for the creep function. If the creep formulation (4.23) is a starting point, constitutive equation must be rearranged such that the stress increment is a function of the strain increment and stress history, the form which is appropriate for the implementation in a displacement based Finite Element Method.

$$\varepsilon(t) = \int_0^t J(t,t')\dot{\sigma}(t')dt' \quad (4.35)$$

The strain increment from t to $t+\Delta t$ equals:

$$\Delta\varepsilon = \varepsilon(t+\Delta t) - \varepsilon(t) = \int_0^t (J(t+\Delta t, t') - J(t, t'))\dot{\sigma}(t')dt' + \int_t^{(t+\Delta t)} J(t+\Delta t, t')\dot{\sigma}(t')dt' \tag{4.36}$$

Assuming that the stress varies linearly over the time increment, i. e. $\dot{\sigma} \approx \frac{\Delta\sigma}{\Delta t}$, and utilizing a generalized mid-point rule ($t \le t^* \le t + \Delta t$), the stress increment becomes:

$$\Delta\sigma = \frac{\Delta\varepsilon - \int_0^t (J(t+\Delta t, t') - J(t, t'))\dot{\sigma}(t')dt'}{\frac{1}{\Delta t}\int_t^{(t+\Delta t)} J(t+\Delta t, t')dt'} \tag{4.37}$$

which can be written as follows:

$$\Delta\sigma = \tilde{E}(t^*)\Delta\varepsilon - \tilde{\sigma}(t) \tag{4.38}$$

with

$$\tilde{E}(t^*) = \frac{1}{\frac{1}{\Delta t}\int_t^{(t+\Delta t)} J(t+\Delta t, t')dt'} \tag{4.39}$$

and

$$\tilde{\sigma}(t) = \tilde{E}(t^*)\int_0^t (J(t+\Delta t, t') - J(t, t'))\dot{\sigma}(t')dt', \tag{4.40}$$

which describes stress history.

The main intention here is to use such a creep function that enables conversion of this integral to a recurrent formula, so the storage of the complete stress history is avoided. The most general form is the Dirichlet series, see e.g. (Bazant 1982):

$$J(t, t') = \sum_{\mu=1}^{N} \frac{1}{E_\mu(t')}\left\{1 - \exp\left[-\frac{(t-t')}{\tau_\mu}\right]\right\} \tag{4.41}$$

This creep function describes a Kelvin chain with E_μ as modulus and τ_μ as the retardation time of the individual chain units.

The analog alghoritm may be applied together with the Kelvin chain. (Bazant 1982) emphasizes that the Dirichlet series expansion should not be regarded as a fundamental law, but only as an approximation to the exact solution of linear aging viscoelasticity used for the purpose of the computational convenience.

Another example of the conversion of the integral creep law to the rate-type creep law is expansion of the Double Power Law creep function (4.42) into a Taylor series:

$$J(t, t') = \frac{1}{E(t')}(1 + qt'^{-d}(t-t')^{p}) \tag{4.42}$$

The part of the DPL creep function $f(t-t') = (t-t')^{p}$ is expanded into a Taylor series around $t\text{-}t' = t_d$.

$$f(t-t') = \sum_{r=0}^{5} h_r(t-t_d)t'^{r} \tag{4.43}$$

where h_r is a function of $t-t_d$, dependent on the power p. The Taylor series converges to the Double Power Law at the interval [0, $2t_d$]. Therefore the development point t_d should be taken halfway the maximum analysis time. Figure 4.1 shows the Taylor series approximation compared with the exact solution. It can be seen that the difference between Double Power Law and its Taylor approximation is largest in the beginning of the time interval, after sudden loading. During the first steps in stress calculation of hardening concrete the E-modulus is very small, and even small stresses may cause considerable strains, since both elastic and creep strain are inversely proportional to the instantaneous E-modulus. The strains are even magnified due to Taylor approximation, what results in the spurious strains in the first period of hardening. These strains influence stresses after long time. The problem may be solved by introducing the t_0 concept Section 3.3.2 and ignoring the stress-dependent strains before t_0.

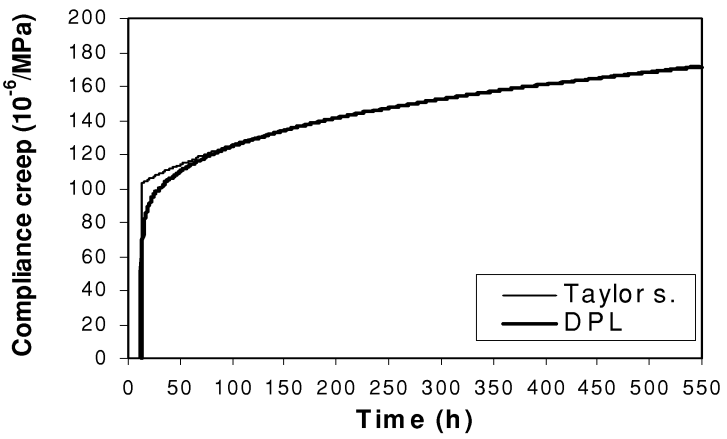

Figure 4.1: Taylor series approximation of the Double Power Low $J(t, t') = \frac{1}{E(t')}(1 + 0.6t'^{-0.3}(t-t')^{0.3})$ at the interval [14h, 550h]

Substitution of (4.41) and (4.43) in (4.39) and (4.40) leads to:

$$\frac{1}{\tilde{E}(t^*)} = \frac{1}{E(t^*)} \cdot \left(1 + \frac{\alpha}{\Delta t} \sum_{r=0}^{5} \frac{(t+\Delta t)^{r-d+1} - t^{r-d+1}}{r-d+1} h_r(t+\Delta t - t_d) \right) \tag{4.44}$$

and

$$\tilde{\sigma}(t) = -\tilde{E}(t^*)\alpha \sum_{r=0}^{5} (h_r(t+\Delta t - t_d) - h_r(t-t_d))\tilde{\varepsilon}_r(t) \tag{4.45}$$

where

$$\tilde{\varepsilon}_r(t) = \int_0^t \frac{1}{E(\tau)} \tau^{r-d} \dot{\sigma} d\tau . \tag{4.46}$$

$\tilde{\varepsilon}_r$ may be calculated during the analysis by means of a recurrent formula as follows:

$$\tilde{\varepsilon}_r(t+\Delta t) = \tilde{\varepsilon}_r(t) + \int_t^{(t+\Delta t)} \frac{1}{E(\tau)} \tau^{r-d} \dot{\sigma} d\tau \approx \tilde{\varepsilon}_r(t) + \frac{\Delta\sigma}{E(t^*)} \cdot \frac{(t+\Delta t)^{r-d+1} - t^{r-d+1}}{r-d+1} \tag{4.47}$$

For more details about procedure see (De Borst, et alia).

Many other methods of solving integral equation (4.23) exist, such as: Effective modulus method, Age-adjusted effective modulus method, Dischinger method, etc., see for instance (Bazant 1982) and (Neville 1983).

It is important to emphasize that the method of superposition should not be confused with the principle of superposition. In some works it has been argued for a differential formulation of creep behaviour because it is better in predicting creep recovery. Both the superposition method and the incremental method are only ways of solving the integral (4.23), which is based on the theory of linearity and principle of superposition. Creep recovery is deviation from the principle of superposition (see condition 2 for linearity, Chapter 3), and should be modelled by a nonlinear theory. More about that will be discussed in the next chapter.

4.4 Finite element discretisation

Since the thermal and mechanical problem are decoupled, the finite element discretisation may be done separately.

The main assumption which has to be satisfied in thermal stress analysis is that element model must permit the same level of complexity for the strain field as for the temperature field. That means that the order of the element in stress analysis has to be of higher order than the element in temperature analysis if the same element mesh is used (Cook 1989). In that way a mismatch between ε and ε_0 in (4.48) is avoided.

$$\varepsilon_0 = \alpha \cdot \Delta T$$

$$\sigma = C(\varepsilon - \varepsilon_0) + \sigma_0 \tag{4.48}$$

If ε and ε_0 are not of the same order, stress oscillations may occur.

Element distribution in temperature-stress analysis for one determined element type depends on geometry, temperature and stress gradient, and where in the structure we are interested in results.

The temperature gradient depends on the total quantity of heat generated, boundary conditions, thermal properties, and discontinuity in geometry and material properties.

The stress gradient depends on temperature distribution, mechanical properties, restraint conditions, discontinuity in geometry and material properties, etc.

Since the stresses are less accurate than displacements and temperatures, stress calculations need finer element mesh than temperature calculations. If the same element model is used in both analysis, stress analysis' requirements are usually decisive.

Chapter 5

Creep

In this Chapter the influence of creep on thermal stresses is investigated. Special attention is paid to the importance of creep in different parts of hardening period. Further, three creep models: Maxwell chain, Double Power Law and Burgers model are compared. On the basis of that comparison both the creep models and creep tests are discussed and some practical recommendation regarding calibration of creep models are given.

5.1 Influence of creep on self-induced stresses

Within the IPACS project a Round Robin calculation has been performed with the aim to map and compare the existing programs for numerical simulation of concrete structure at early ages (IPACS report). Five different programs have been used to simulate temperature and stress development in two examples of hardening concrete structure. Even though all calculations were based on the same set of laboratory test results describing specific concrete properties, the scatter between their results was significant. Creep modelling was identified as one of the most important reasons of disagreement between different programs. The same conclusion was made in (Bosnjak 1997).

Creep is a major factor in the mechanical behaviour of young concrete, and understanding of the creep influence on self-induced stresses is therefore of essential importance in prediction of cracking risk. Modelling of creep at early ages has been a subject of many investigations, but surprisingly few studies about the creep influence on self-induced stresses can be found in literature.

One exception is (Westman 1999), where a comprehensive study of creep influence on cracking risk is given. Stress dependent deformations were divided into three components: instantaneous deformation, short-term creep (creep during the three first days after loading), and long-term creep, and influence of each component on thermal stresses was investigated. Both surface cracking and through cracking were considered. The conclusion was that the short-time creep is the most important part, and that creep at early age has an important role for the development of thermal stresses.

In the present study, the importance of creep in different ages of a structure is investigated. the creep coefficient is varied in different periods of hardening, and calculated stresses compared. To get better understanding of the creep influence on self-induced stresses, different strain components are identified in the TSTM test for various temperature histories and various creep properties. The Double Power Law creep function is used in calculations.

5.1.1 Sensitivity analysis

Stress development in the externally restrained concrete simulated by fully restrained specimen under realistic temperature history is considered.

To make this analysis more simple, neither shrinkage nor cracking is taken into account in calculations and influence of changing temperature on creep is neglected.

Thermal stresses are calculated for a given temperature history shown in Figure 5.1. Then, the creep coefficient is increased by 50% in different periods of hardening: in the heating period, the period with maximal temperature, and the cooling period (arbitrary chosen). Thermal stresses are calculated for different cases and compared with the original calculations, see Figure 5.2 and Figure 5.3.

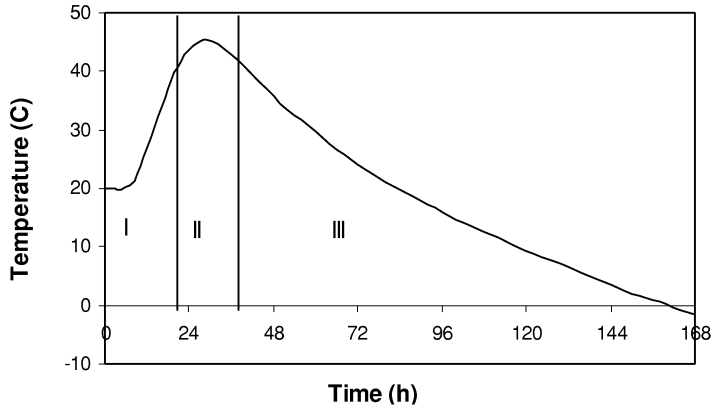

Figure 5.1: Temperature history for externally restrained concrete divided into different periods

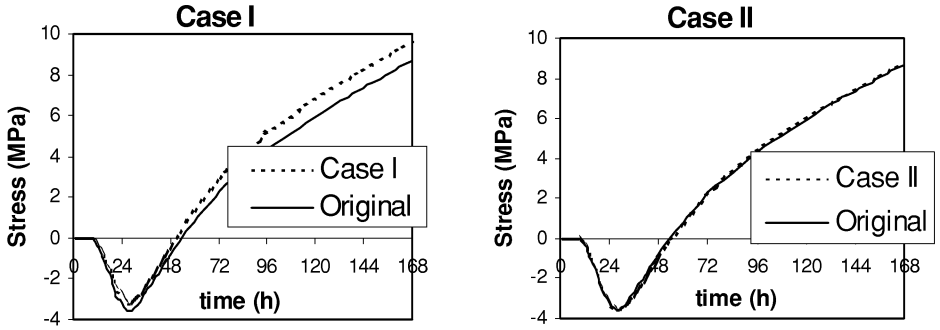

Figure 5.2: Stress development in the externally restrained concrete calculated with 50% increased creep coefficient in different time intervals and compared with the original computations.

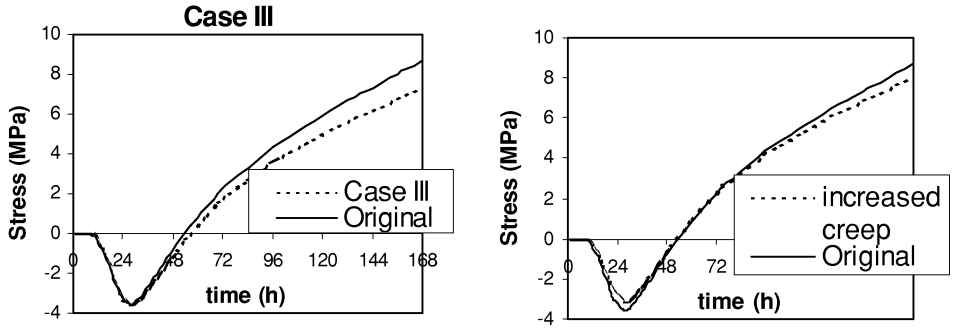

Figure 5.3: Stress development in the externally restrained concrete calculated with 50% increased creep coefficient in different time intervals and compared with the original computations.

From Figure 5.3 it can be seen that higher creep in the early period decreases compression stresses, and consequently, increases tensile stresses. Increased creep in the cooling period decreases tensile stresses to the same extent. 50% increase of the creep coefficient in both cases leads to 10-15% change in thermal stresses. Because of two mutually competing effects, increased creep during the whole period (both heating and cooling phase) does not cause considerable changes in final tensile stresses. To get more insight in this twofold nature of the creep effect on tensile stresses, experimental data of the TSTM are used.

5.1.2 Identification of creep from TSTM test

TSTM test results are very useful for investigation of the influence of some concrete properties on the stress development, and thus, better understanding of young concrete behavior. In the following, test results from (Bjøntegaard 1999) for the BASE concrete are used.

Self-induced stress is measured in the fully restrained hardening specimen exposed to the realistic temperature history in the TSTM as previously discussed in (3.3.4) . Five tests with different temperature histories were performed. To avoid cracking, the full restraint is turned off in two tests after approximately two days, and the deformation of the specimen was measured in the TSTM.

Different strain components from the Eq.(5.1) are identified from the test results and depicted in the Figure 5.4.

$$\Delta\varepsilon_{free} = \Delta\varepsilon_{el} + \Delta\varepsilon_{creep} + \Delta\varepsilon_{th} + \Delta\varepsilon_{ad} \tag{5.1}$$

Free deformation is equal to zero for a fully restrained specimen, otherwise, this strain component was measured in the TSTM. Thermal dilation is calculated by assuming constant value for the thermal dilation coefficient, and the autogenous deformation is determined from the free deformation rig by subtracting the thermal dilation from the total deformation. Elastic strain is determined from the stress measured in the TSTM:

$$\varepsilon_{el} = \frac{\sigma}{E(t)}$$

The E-modulus development was determined from independent tests.

Finally, the creep strain is obtained from the Eq.(5.1) as the only unknown, and includes also transient creep. In the left side of Figure 5.4 stress developments and temperature histories from three TSTM tests are presented. In the right side different strain components are shown.

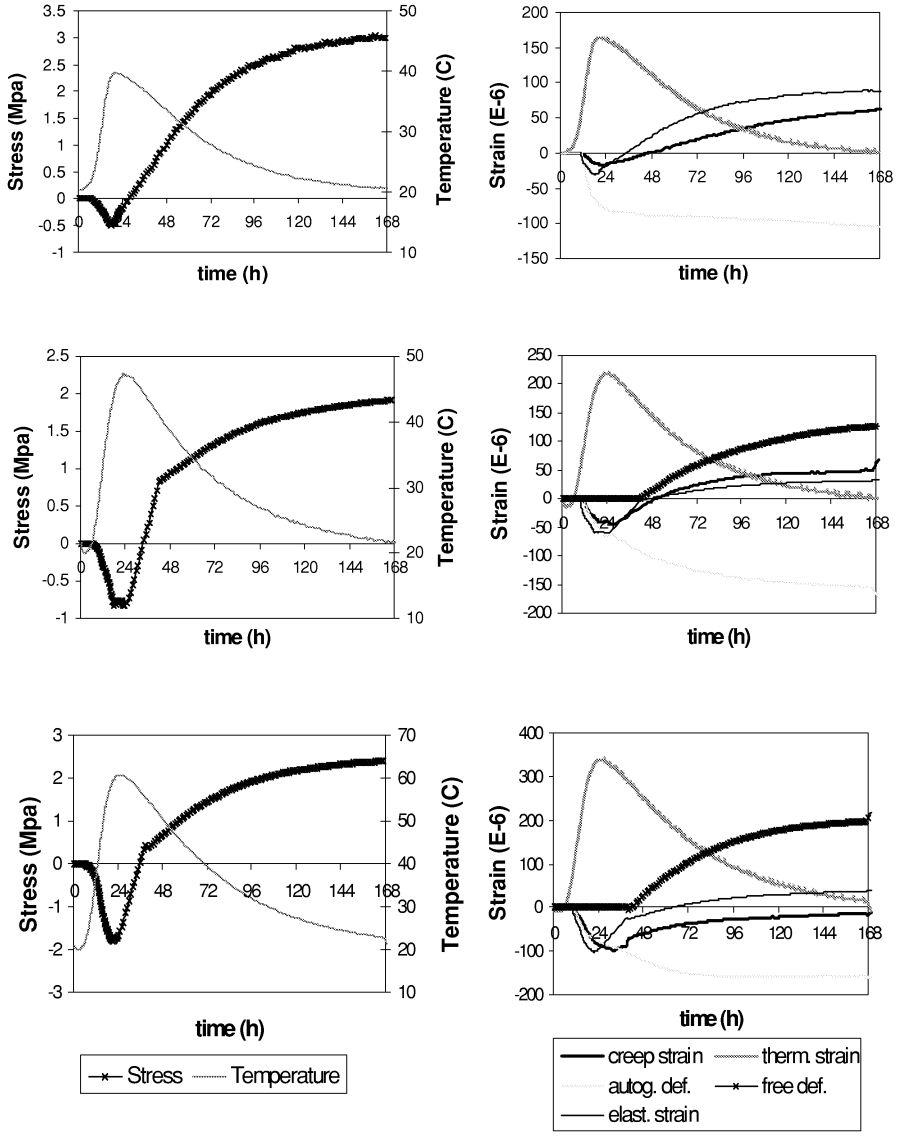

Figure 5.4: Development of stresses and different strain components in hardening concrete exposed to three different temperature histories

The magnitude of the creep strain indicates in which part of the hardening period creep is most important. That seems to vary for different temperature histories. It can be seen that the creep influence on tensile stresses and (cracking risk) is small when the compressive stresses are high, and opposite. The same tendency may be observed in the following analysis. Creep is determined from creep tests in compression and modelled by the Double Power Law. Transient creep is included in calculations according to expression (3.31) . Stress generation is simulated with and without creep and the magnitude of the stresses relaxed because of the creep effect can bee seen in Figure 5.5.

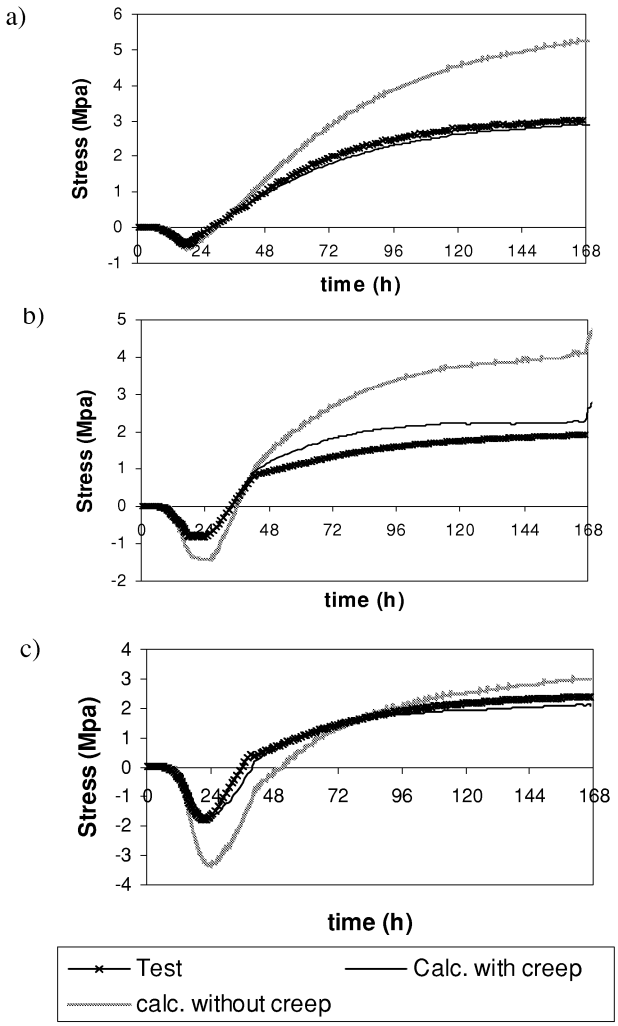

Figure 5.5: Stress development in the TSTM for three temperature histories:
a) $T_{max}=40^0C$, b) $T_{max}=47^0C$, c) $T_{max}=62^0C$, simulated with and without creep and compared to measurements

Numerical values of the relaxed stresses are shown in Table 5.1. It can be seen that creep effect is large: the reduction in stresses due to creep 7 days after casting is about 40-50%. .

	Stresses calculated without creep (MPa)		**Stresses calculated with creep (MPa)**		**Relaxed stresses (%)**	
	compres.	**tension**	**compres.**	**tension**	**compres.**	**tension**
$T_{max}=40^0C$	-0.53	5.25	-0.3	2.89	43.4	44.9
$T_{max}=47^0C$	-1.41	4.09	-0.72	2.28	48.91	44.2
$T_{max}=62^0C$	-3.29	2.98	-1.64	2.1	50.1	29.5

TABLE 5.1: Stresses 7 days after casting calculated with and without creep for different temperature histories

Further, influence of creep on stresses is examined by changing the creep coefficient in two periods of hardening. The first one, early or “compression” period is a period where creep affects compression stresses, so tensile stresses are affected only through the compressive stresses. Second or “tension” period is a period where creep affects tensile stresses directly, whereas compression stresses remain unchanged. By trial-and-error procedure the point which separates these periods is found - that is the time when the stress rate changes sign, i.e. time of the maximal compressive stresses. From the reason of simplicity transient creep is omitted here. Figure 5.6 - Figure 5.8 show stress development for three temperature histories calculated with the original creep coefficient and the creep coefficient decreased by 50% in different periods of calculation. Creep strain and instantaneous strain components are also shown.

It can be seen that a decrease in creep in the first period produces reduced creep strain in that period, and increased creep strain in second period. Change in instantaneous deformation has the same magnitude, but opposite sign. Stresses in compression are increased, whereas tensile stresses are decreased. Creep in the second period influences creep strain in that period directly - decreased creep causes decrease of the creep strain, increase of the instantaneous deformation, and increase of the stresses.

These two effects counteract each other, thus reducing the final creep effect on tensile stresses.

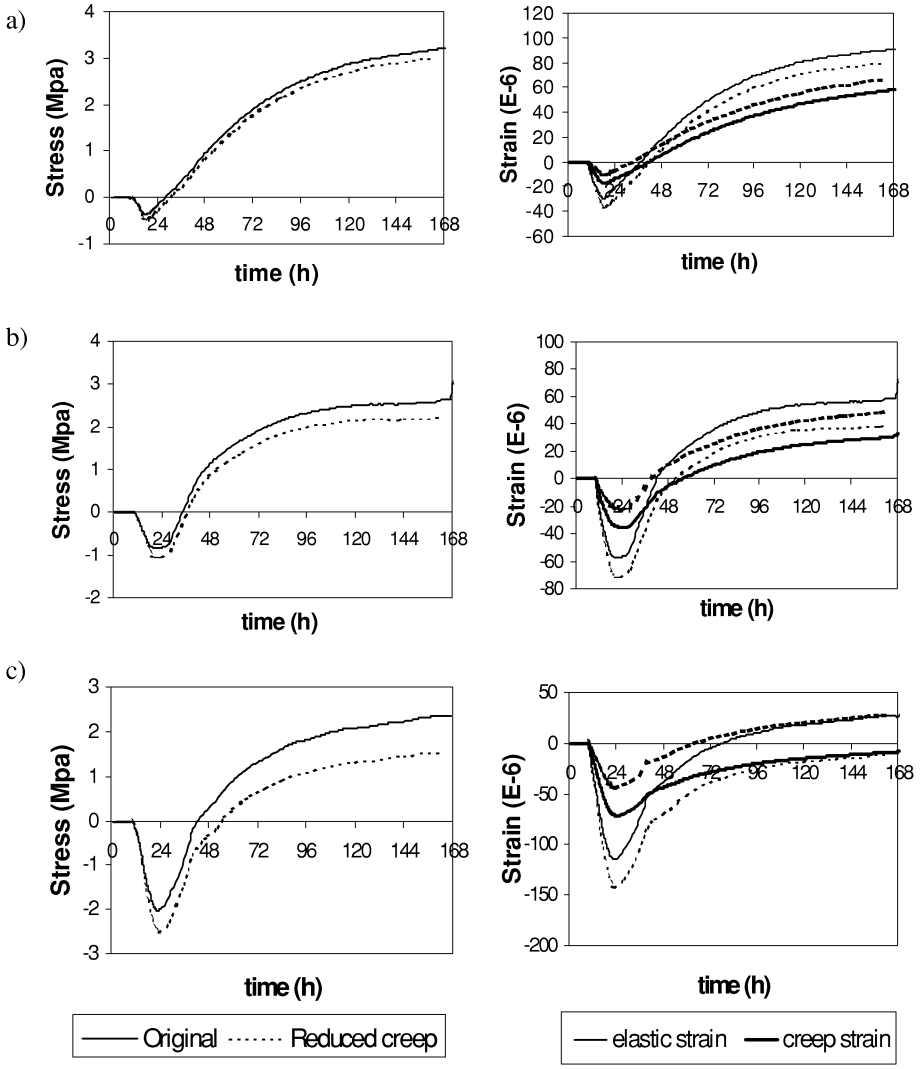

Figure 5.6: Influence of reduced creep coefficient on development of stress, creep strain and elastic strain in the externally restrained concrete. The creep coefficient is reduced by 50% during the first period of hardening. Three temperature histories are considered: a) $T_{max}=40^0C$, b) $T_{max}=47^0C$, c) $T_{max}=62^0C$.

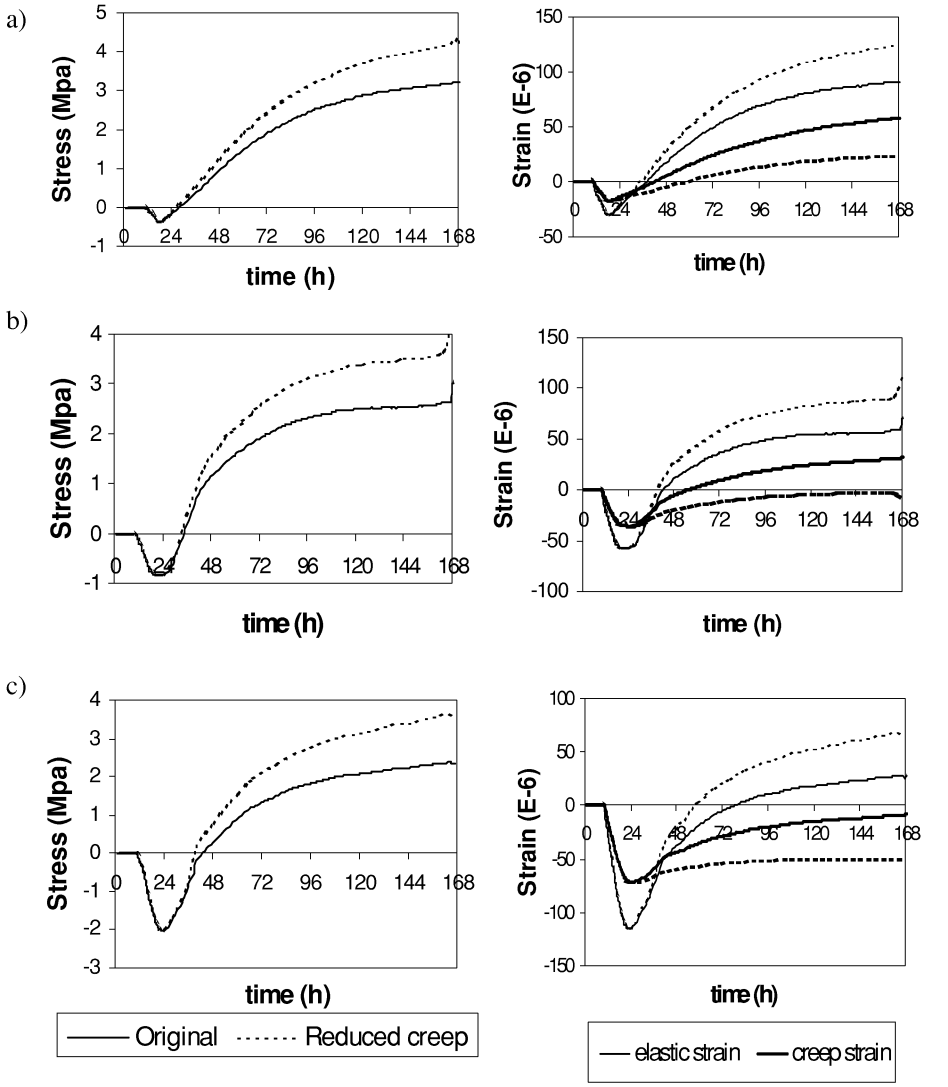

Figure 5.7: Influence of reduced creep coefficient on development of stress, creep strain and elastic strain in the externally restrained concrete. The creep coefficient is reduced by 50% during the second period of hardening. Three temperature histories are considered a) $T_{max}=40^0C$, b) $T_{max}=47^0C$, c) $T_{max}=62^0C$.

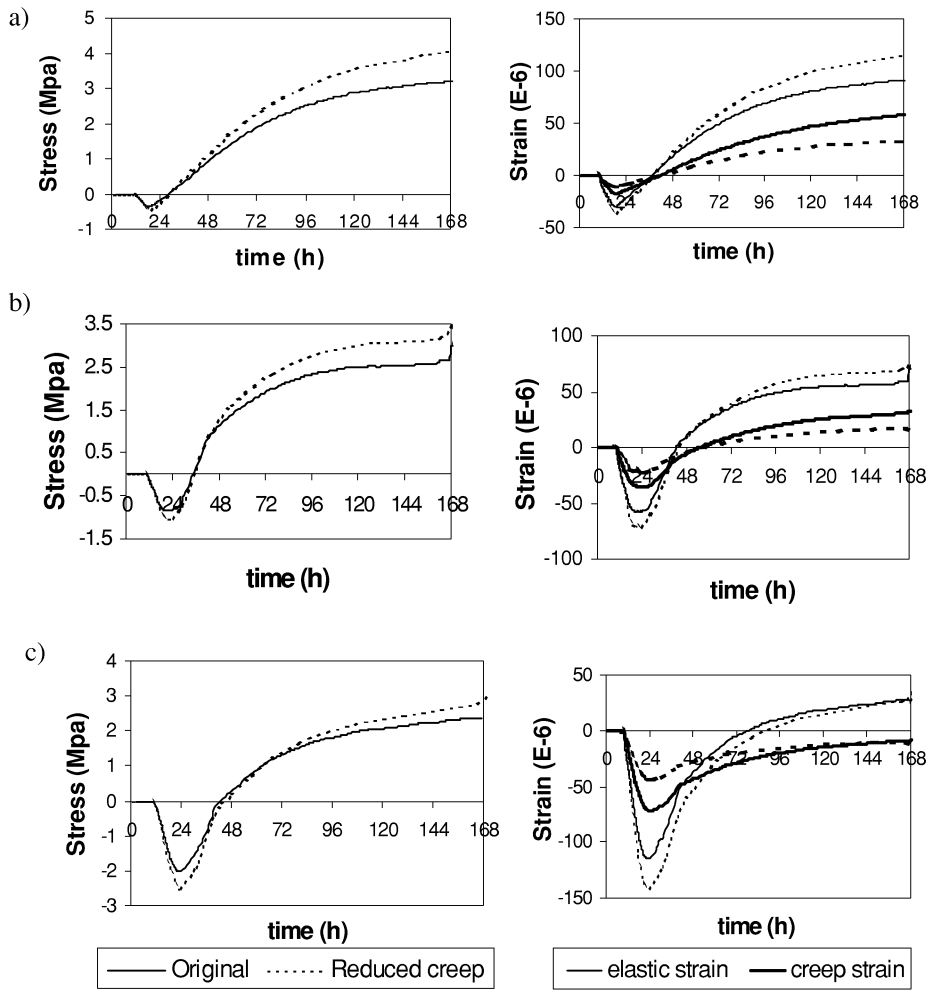

Figure 5.8: Influence of reduced creep coefficient on development of stress, creep strain and elastic strain in the externally restrained concrete. The creep coefficient is reduced by 50% during the whole period of hardening. Three temperature histories are considered a) $T_{max}=40^0C$, b) $T_{max}=47^0C$, c) $T_{max}=62^0C$.

5.1.3 Conclusions

Creep is a very important factor influencing stresses in the order of 40-50% of elastic case. The influence of creep on self-induced stresses is much more clear if hardening period is divided into two parts. The point which separates these periods is the time where the stress increment changes sign. In the case of through cracking, this point corresponds to the point of maximal compressive stresses; in the case of surface cracking, it is the point of

maximal tensile stresses in the surface, and maximal compressive stresses in the core. Creep in the first period of hardening affects stresses in that period directly, and stresses in the second period indirectly. It is important to emphasize that creep in the early period has negative effect on the cracking risk in externally restrained structure: creep reduces compressive stresses, but increases tensile stresses, thus increasing cracking risk. Underestimation of creep in this early period will lead to underestimating of the cracking risk. The opposite is true for internally restrained structures.

To what extent the final stresses are influenced by the creep in the early period is determined by the magnitude of the relaxed stresses in the first period. For a given concrete it depends on many factors: temperature, shrinkage and restraint conditions during the first period. In the case of full restraint, maximal temperature seems to be decisive: high maximal temperature will produce high compressive stresses which will relax much due to creep in the early period, increasing tensile stresses to the same extent. It can be seen in Figure 5.6. In all situations which produce high compressive stresses the effect of creep on cracking risk is diminished.

Creep in the second period affects only tensile stresses, as shown in Figure 5.7. These two effects are thus competing and the final effect is their summation. It is difficult to predict which of them will dominate since that depends of many factors. In some situation creep effects on tensile stresses in the first and in the second period of hardening are of the approximately same magnitude, thus annulling each other. Then significantly different creep properties may give approximately the same tensile stresses, see Figure 5.8-a. When performing sensitivity analysis or comparing different creep models, one must be aware of this twofold nature of creep influence, otherwise wrong conclusions may be made.

In the internally restrained structure with the risk of surface cracking, the creep role is much simpler. Tensile stresses in the surface appear in the first period of hardening and are affected only by the creep in this early period. Creep in the second period of hardening is not relevant for cracking risk.

Because of this complicated influence of creep on the risk of through-cracking, it is difficult to give general rules - creep influence on cracking risk varies from case to case and depends on the concrete situation, i.e. temperature, shrinkage and restraint conditions. In general terms, creep is a very important factor in simulation of hardening, and correct prediction of creep during the **whole** period of hardening is necessary for reliable prediction of cracking risk.

5.2 Comparison of different creep models.

Three models for basic creep, often used in analysis of young concrete, are compared:

1. Double Power Law:

$$J(t,t') = \frac{1}{E(t'_{eq})}[1 + \varphi t'^{-d}(t-t')^{p}] \tag{5.2}$$

2. Maxwell chain:

$$R(t,t') = \sum_{\mu=1}^{N} E_\mu(t_{eq}')\exp\left[-\frac{(t-t')}{\tau_\mu}\right] \tag{5.3}$$

3. Burgers model:

$$J(t,t') = \frac{1}{E_c(t_{eq}')} + \frac{1}{E_1(t_{eq}')}\left\{1-\exp\left[-\frac{(t-t')E_1(t_{eq}')}{\eta_1(t_{eq}')}\right]\right\} + \frac{t-t'}{\eta_2(t_{eq}')} \tag{5.4}$$

Assuming that a Maxwell chain is equivalent to a Kelvin chain, Kelvin chain has not been considered in this comparison.

Models are calibrated to the same test data, and used in the calculation of thermal stresses in externally restrained concrete (see sensitivity analysis).

5.2.1 Calibration of creep models

The Double Power Law is a simple creep function with only three parameters. Therefore their determination is quite easy and without any numerical problems.

The Maxwell chain coefficients may be determined from the experimental relaxation curve. If only creep curves are available, additional efforts should be made to convert creep into relaxation. Because of the large number of degrees of freedom in the model, the approximation is not unique, and mathematical ill-conditioning may occur. It means that small variation in the test data can cause large variations of the parameters. Therefore τ_μ must be chosen in advance. If relaxation times are chosen constant, they can not be spaced more than a decade apart in log (t-t') scale, see (Bazant 1974a). Further, they must cover the entire time of interest [t_{min}, t_{max}]: $\tau_1 \le 3t_{min}$, and $\tau_N \ge 0.5t_{max}$, i.e. the number of units in the Maxwell chain is determined by the time range of interest.

The parameters E_μ may be identified by fitting models to any given creep function. (Bazant 1974a) proposed constant τ_μ and spaced in log (t-t') scale, so the number of units is determined by the time range of interest. The relaxation time of a last unit must be very large (corresponding viscosity = 0).

For the case of thermal stresses in hardening concrete, the time of interest is the first several days after casting, and five chain units are enough for describing creep in that period (τ_1= 0.1 h, τ_2 = 1 h, τ_3 = 10 h, τ_4 = 100 h, τ_5 = 1000 h). Then E_μ, (μ = 1,...,5) may be determined by fitting to the given creep function (or creep data) using a least square procedure.

Some other conditions considering the amount of data, their scatter and smoothing should also be taken care of in fitting (Bazant 1974a). The same procedure is used in program RELAX (Jonasson 1977) that makes it possible to determine Maxwell chain parameters from given test data or from some of the existing creep models. The RELAX program is used in this analysis.

Determination of the parameters for the Burgers model is based on the assumption of division of creep into an irreversible part and a reversible part. To isolate these two creep components, a creep recovery test has to be performed. When a load is applied to a Burgers model, an instantaneous deformation takes place, followed by a time dependent deformation. When a load is removed, an instantaneous recovery takes place, described by the external spring, followed by a time dependent recovery approaching a horizontal line. The period of unloading has to be sufficiently long to allow for the reversible component to be completed. This reversible deformation is described by the Kelvin model, and a remaining deformation, irreversible deformation, is equal to the deformation of the external dashpot. In the Figure 5.9 only the time dependent deformations are shown.

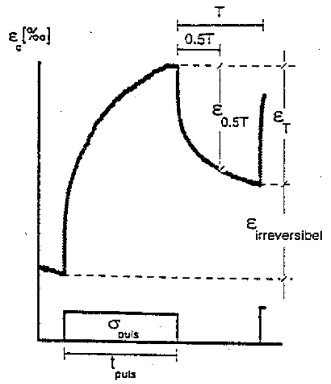

Figure 5.9: Determination of parameters for Burgers model, from (DTI 1996).

The dashpot viscosity is thus determined from the irreversible deformation, whereas the parameters for the Kelvin unit are determined from the reversible component as follows:

$$\varepsilon_{irr} = \frac{\sigma_{puls} \cdot t_{puls}}{\eta_1}, \tag{5.5}$$

$$\eta_1 = \frac{\sigma_{puls} \cdot t_{puls}}{\varepsilon_{irr}} \tag{5.6}$$

Since two parameters from Kelvin unit are unknown, the recoverable strain is measured for two different times: 0.5T and T:

$$\varepsilon_T = \frac{1}{E_2} \cdot \left(1 - e^{-\frac{TE_2}{\eta_2}}\right) \cdot \sigma_{puls} \tag{5.7}$$

$$\varepsilon_{0.5T} = \frac{1}{E_2} \cdot \left(1 - e^{-\frac{TE_2}{2\eta_2}}\right) \cdot \sigma_{puls} \tag{5.8}$$

$$E_2 = \frac{2\varepsilon_{0.5T} - \varepsilon_T}{\varepsilon_{0.5T}^2} \cdot \sigma_{puls} \tag{5.9}$$

$$\eta_2 = -\frac{E_2 T}{\ln\left(1 - \frac{\varepsilon_T \cdot E_2}{\sigma_{puls}}\right)} \tag{5.10}$$

To determine the time development for these parameters, several loading-unloading cycles are performed at different ages. Expression for development of each parameter is then proposed on the basis of these discrete values, see Figure 5.9. For more about procedure, see (DTI 1996) and (Spange 1996).

Since the chosen creep models cannot be fitted to the same type of test, comparison is performed in two parts: first, DPL and Maxwell model are calibrated against a creep test with constant loading and compared, then DPL and Burgers model are calibrated against creep test with alternating loading and compared.

DPL and Maxwell model.

Models are fitted to the creep test from (Westman 1999), see Figure 5.10. Concrete specimens of varying age are subjected to constant loads of 20% of the compressive strength at loading. The strains from external load are determined as the measured strain compensated for load-independent deformation, measured on dummy specimens. More details about test setup is given in (Westman 1999)

The model parameters are given in Appendix 1.

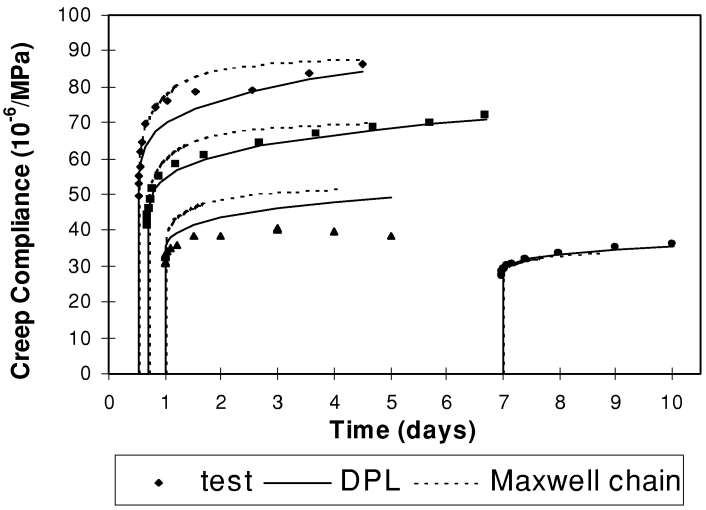

Figure 5.10: Maxwell model and Double Power Law fitted to the experimental data

These models take aging into account in different ways.

In the Maxwell chain the aging effect is expressed with age dependent moduli.

In the Double Power Law model implemented in FE program DIANA, aging is modelled by age dependence of the instantaneous E-modulus. Further, age of loading *t'* is also included in the creep ratio. However, in DIANA *t'* is not replaced by equivalent age, which neglects the influence of aging on creep.

In both models the final value of creep is influenced by aging, whereas the shape of the compliance i.e. rate of the creep is unchanged.

To illustrate the problem, creep curves for Double Power Law and Maxwell chain are plotted at different temperature levels. In the Figure 5.11 creep curves for different loading ages at three constant temperature levels are shown.

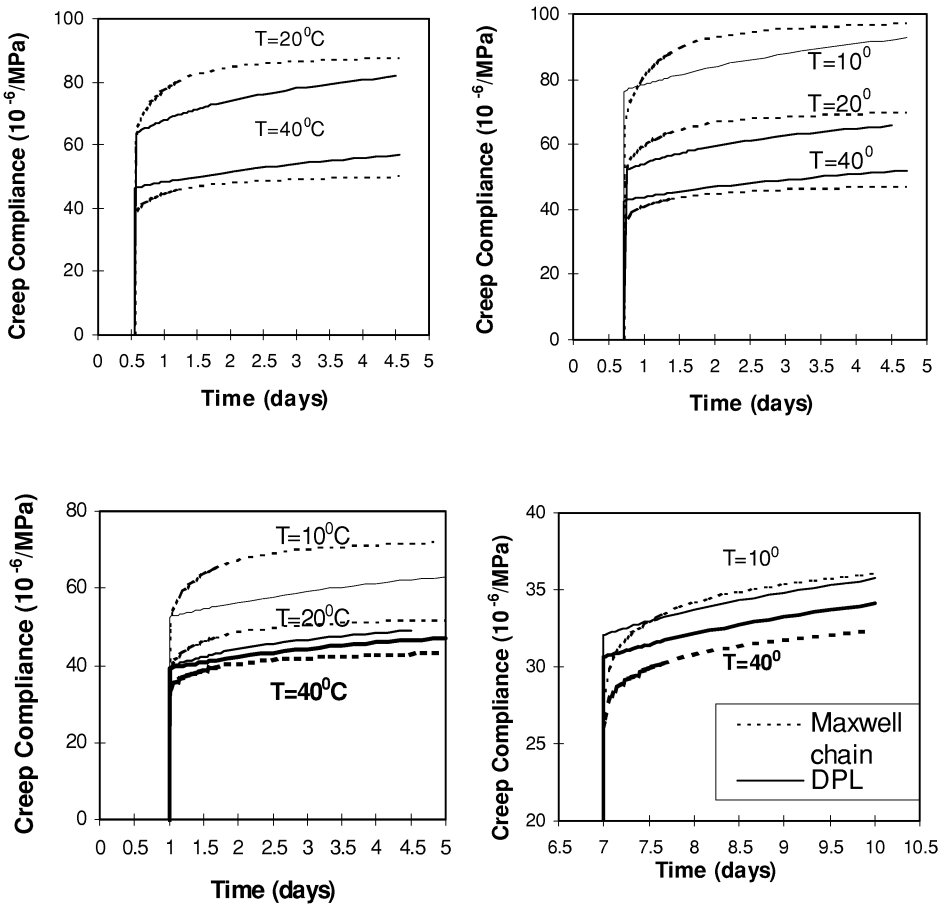

Figure 5.11: Creep curves for Maxwell model and Double Power Law for different temperature levels and different loading ages.

Different aging dependence of two models is evident: fitted at a reference temperature of 20^0C they do not show the same coherence with other loading age. Double Power Law exhibits lower creep than Maxwell chain at temperature T = 10^0C and T = 20^0C, and higher creep at T = 40^0C. The more mature the concrete is, the less is the difference between the two models due to different age at loading.

In order to see how it will influence stresses in a structures, thermal stresses in an externally restrained concrete are calculated using the two creep models. To exclude aging dependence, an additional calculation is performed where the stress development due to an initial strain $\varepsilon_0 = \alpha\Delta T$ is simulated. Considering the mechanical response the temperature is constant, and equal to 20^0C. Temperature history and stress developments are shown in Figure 5.12 and Figure 5.13. It can be seen that stresses calculated with two models agree wery well in both cases.

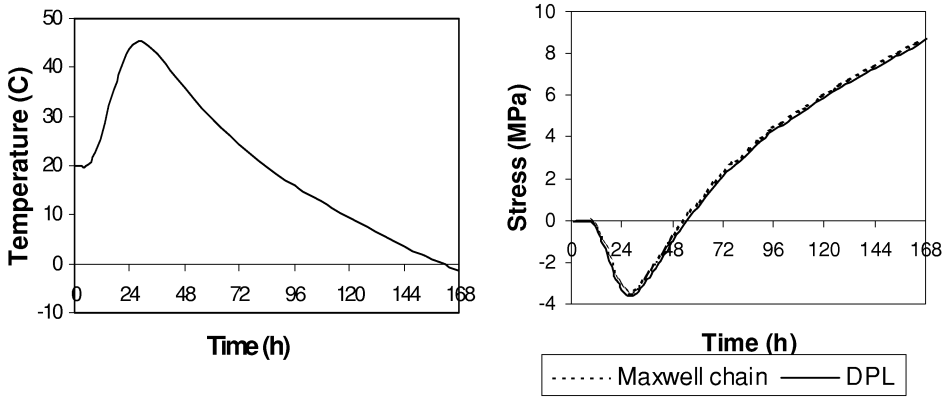

Figure 5.12: Temperature and stress development in externally restrained concrete. Stresses calculated with two different creep models.

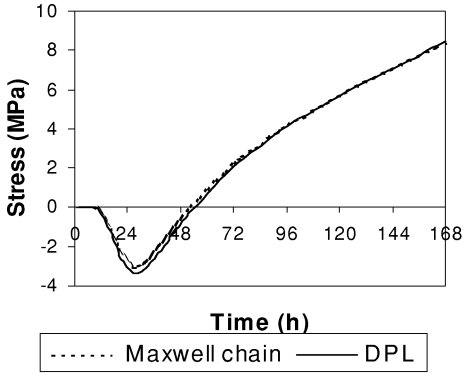

Figure 5.13: Stresses in externally restrained concrete due to initial strain solely

DPL and Burger model.

DPL and Burgers model are fitted to the creep recovery test reported in (Spange 1996). Three concrete specimens are loaded with different loading histories under a constant temperature of 20^0C. The load history for two specimens consists of loading and unloading periods which are short in the beginning of the test and longer as the concrete hardens. The third specimen is under stepwise increasing loading, see Figure 5.14. The load level is chosen as app. 40% of the expected compressive strength. The E-modulus used in fitting is determined from the creep tests. Tests are performed under constant temperature and humidity. The measured concrete strains are compensated for load-independent deformations which are recorded simultaneously on the three unloaded concrete specimens. Detail description of test-setup and testing techniques is given in (Spange 1996).

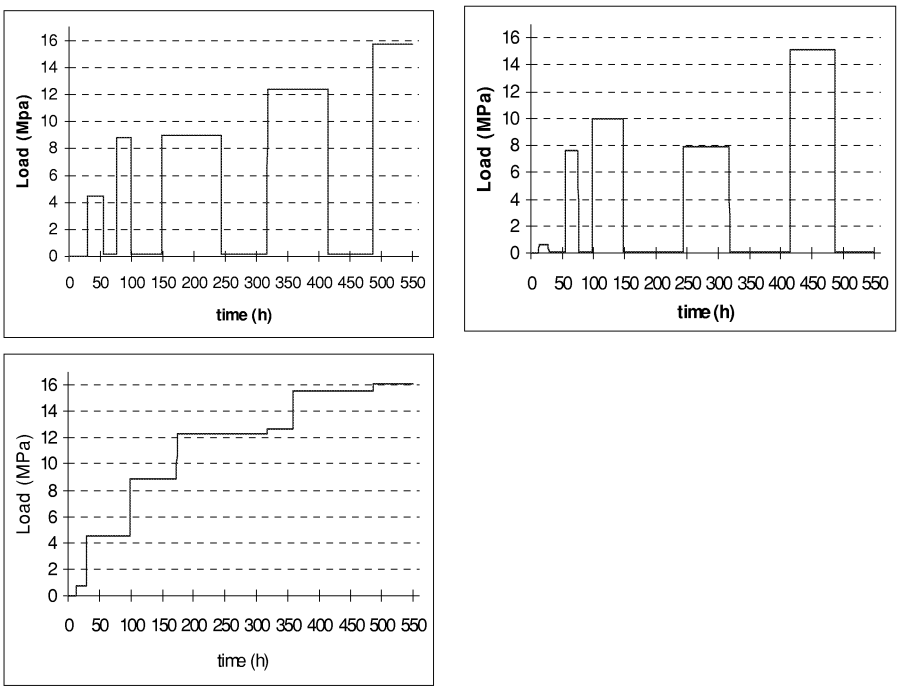

Figure 5.14: Load history

The strains for the Double Power Law are calculated using the principle of superposition, and the parameters are obtained by fitting calculated strains to the experimental ones using the last square method. The same E-modulus is used in connection with both creep models.

The parameters for Burgers model are obtained as described in (DTI 1996) and given in Appendix 1. With the obtained parameters the strains for the actual load history are calculated by solving governing equation (5.11) step by step. Figure 5.15 shows calculated and measured strains for three different loading histories from tests with alternating loading.

$$\dot{\varepsilon}^{creep} = \sum_{\mu=1}^{2} \left(\frac{1}{\eta_\mu} \cdot \sigma - \frac{E_\mu}{\eta_\mu} \cdot \varepsilon^{creep}{}_\mu \right) \tag{5.11}$$

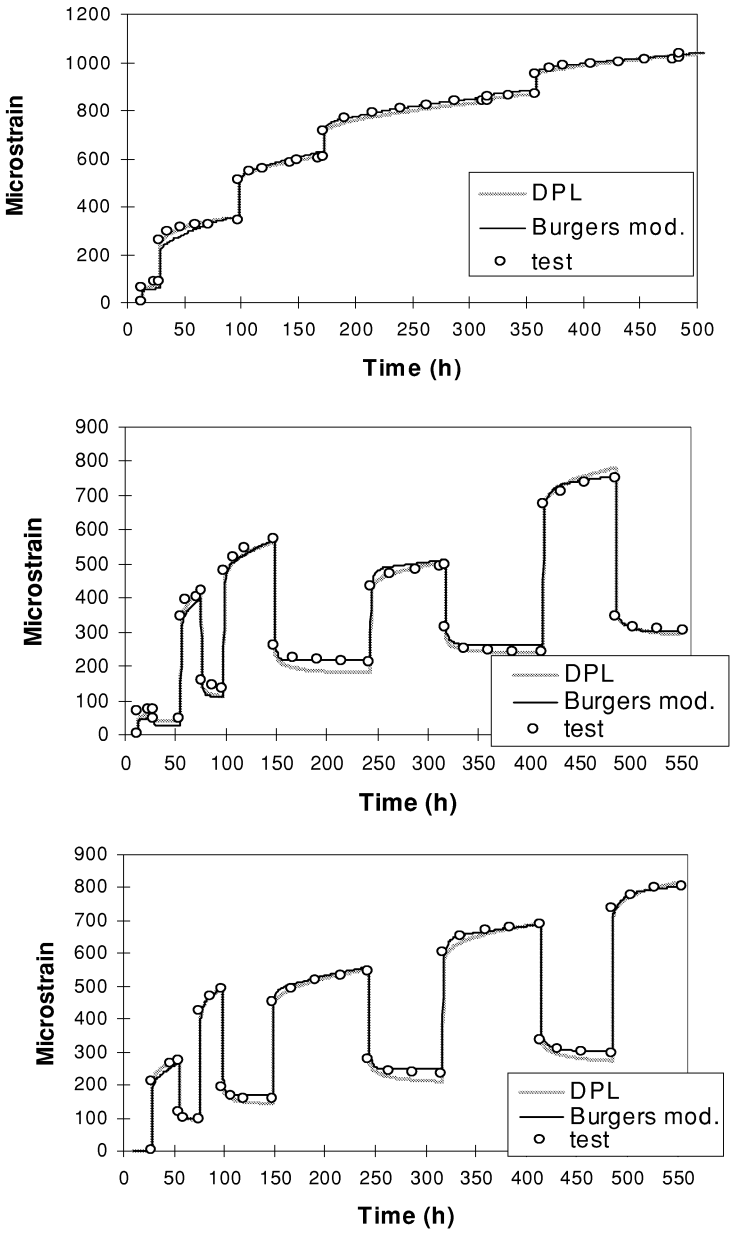

Figure 5.15: Calculated and measured strains for three different loading histories from tests with alternating loading

DPL and Burgers model have different temperature dependence. In Burgers model both moduli and viscosities are made equivalent age dependent without any proportionality between them, which has the consequence of age dependant retardation time in the Kelvin unit, i. e. aging influences the rate of creep. In DPL aging influences the creep coefficient through the instantaneous E-modulus, and the shape of the creep function remains unchanged. That is shown in Figure 5.16

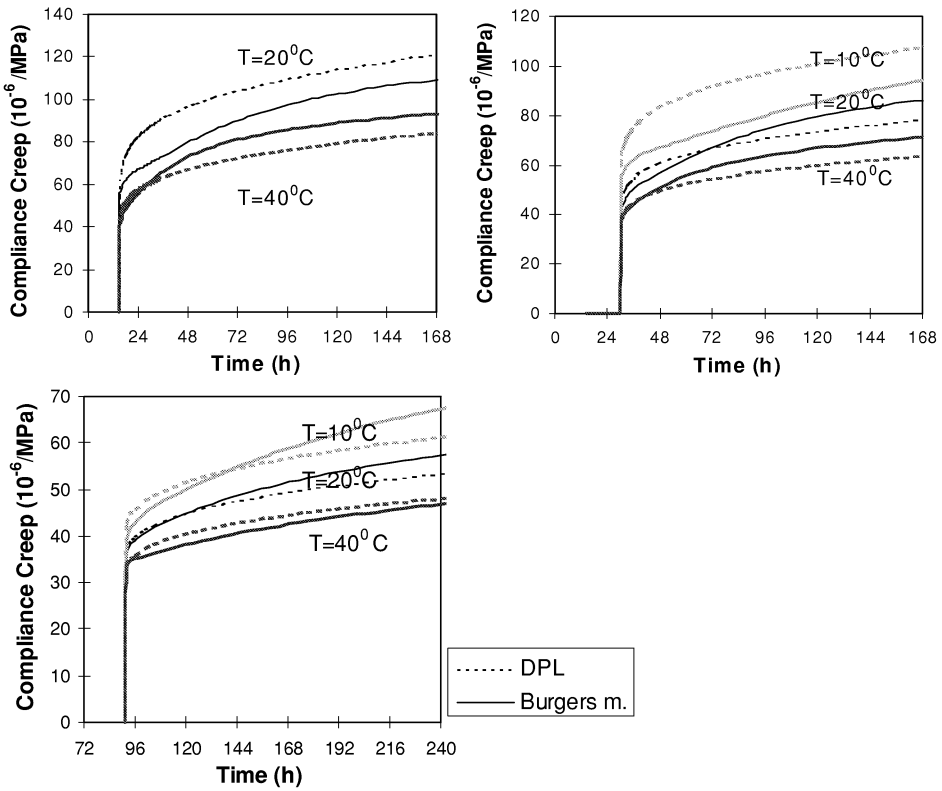

Figure 5.16: Creep functions for DPL and Burgers model for different temperature levels

Again, self-induced stresses are calculated in the structure for prescribed temperature history and initial strain. Results of calculations are presented in Figure 5.17. It can be seen that two models gives different results. The discrepancy between them is not the same in two cases, which means that it can partly be explained by the different temperature dependance of the models.

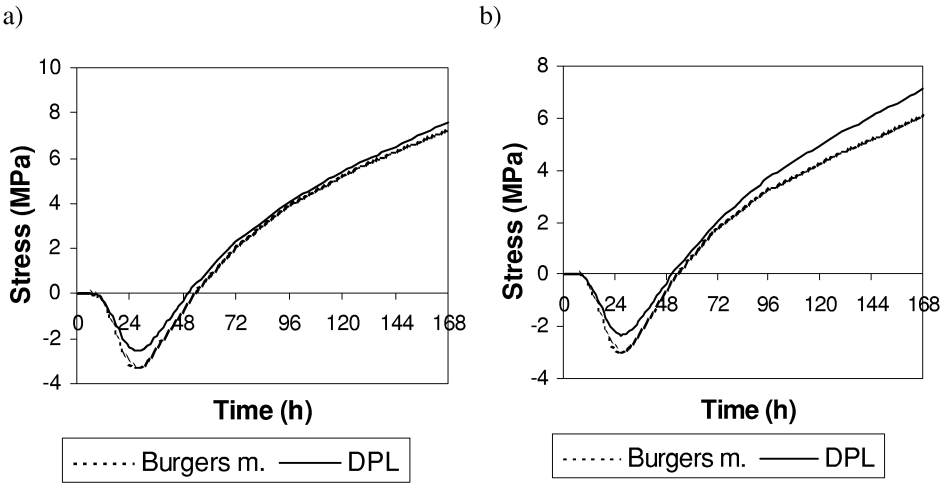

Figure 5.17: Stresses due to: a) temperature b) initial strain, calculated with two different creep models that are fitted to the creep recovery tests

5.2.2 Discussion of the results

As Figure 5.12 and Figure 5.13 show, there is no difference between stresses calculated with DPL and Maxwell model. The different aging effects do not have any significant effect in the structures. The fact that the Maxwell model and the Double Power Law give the same results may be utilized in calibration of the Maxwell model. Fitting of the Maxwell chain requires a considerable amount of test data: the best fit is obtained if creep curves are regularly spaced in logarithmic scale, at least 2 or 3 curves per decade, and if the data cover the time of interest (Bazant 1974a). Otherwise, creep values should be interpolated and extrapolated, which may be a source of errors. On the other hand, the Double Power Law has only three parameters in addition to the instantaneous E-modulus, and their determination is much easier and does not demand such a considerable amount of data as Maxwell chain model. Therefore Maxwell chain may be fitted to the limited test data via the Double Power Law. This is also valid for the Kelvin chain, since the Maxwell and the Kelvin models are equivalent.

The Burgers model and the Double Power Law are fitted to the creep recovery tests with the same accuracy. Nevertheless they do not seem to describe the same creep properties since the calculation results with these two models disagree for the structural example (Figure 5.17). Differences exist in both cases - with and without temperature, indicating that different temperature dependence of the creep models is not the only reason of disagreement. It is reasonable to assume that good agreement between tensile stresses in the analysis with temperature is accidental, since creep models disagree in the first period (see the previous section). Difference between the models becomes evident when the creep curves for different loading times and constant temperature of 20^0C are plotted in Figure 5.18. As can be seen, Burgers model gives less creep in the early period and higher creep after ca 60 hours. That can explain that stresses calculated with Burgers model are

higher in the beginning and lower in the end than stresses calculated with the Double Power Law.

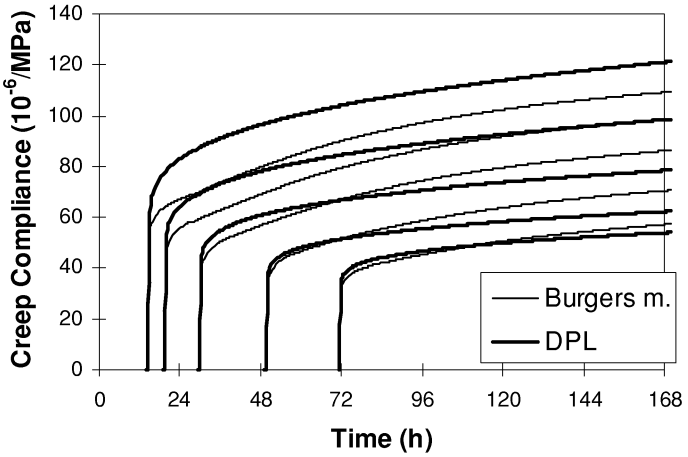

Figure 5.18: Creep curves obtained from the tests with alternating loading.

Models are calibrated to the test results with alternating loading, what has several drawbacks. The main one is that the theory of linearity and the principle of superposition do not apply in this case because of the abruptly load changes (see low-stress nonlinearity). The phenomenon is especially emphasized in the case of creep models that exhibit divergence, such as the Double Power Law. Using the theory of linearity with models that are calibrated against tests where linearity is not valid is, at least, inconsistent. These models fail in representing other concrete behaviour, for instance under constant loading, see Figure 5.18. Besides, this kind of loading is not likely to happen in practice, especially not in concrete structures at early ages.

Further, the short periods of unloading, especially at very early age, do not allow for creep to recover completely, and lead to erroneous observations. In other words, it is not possible to see how creep deformation develops in time, which, in a way, hides disagreement between models and test results. Because of the short periods under load, the instantaneous strain is the major part of the total strain, and the importance of the creep deformation is reduced. That can be seen clearly from Figure 5.19, where only creep deformations from one experiment are printed. Now the differences between models and test are more visible. The other disadvantage with that kind of experiments is that it does not give as clear description of creep properties as Figure 5.18.

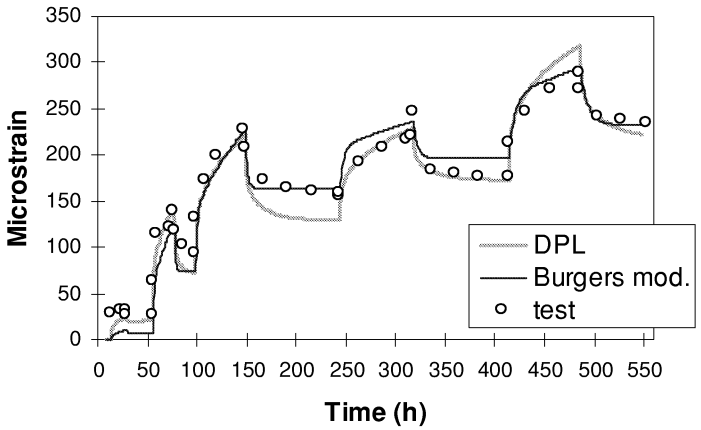

Figure 5.19: Creep deformations (without elastic deformations) from the creep recovery test

Since Burgers model should be calibrated against tests with stepwise loading, it cannot be verified against already existing creep data base, and comparison with other models is very difficult, if not impossible.

5.2.3 Creep test

Previous comparisons have shown that differences between creep models may have its origin in the creep tests the models are calibrated against. This fact raises the question: what kind of test is the most appropriate for creep at early ages?

The most common test for young concrete creep is creep tests with constant stress loaded at different ages, performed at a reference temperature, which completely define the compliance function within the linearity range. The creep model parameters are then determined by minimizing the quadratic sum of the deviations from the test data. Nonlinear effects are modelled by nonlinear models.

A basically different approach is to keep the assumption of linearity, and model nonlinear effects through the creep function, i.e. by fitting it to the test results which are not necessarily linear. Although inconsistent, this approach is tempting: aging viscoelasticity is difficult enough with assumption of linearity, without that assumption it is almost not applicable for engineering practice. When using this approach choice of the creep test should start with the identification of the problem. In the case of young concrete, TSTM test seems to be the most appropriate kind of test.

In TSTM stress generation in hardening concrete may be examined under well defined temperature and restrained conditions in a simple uniaxial stress state. Since the overall behaviour of concrete is investigated, results of such tests present very valuable information for better understanding of young concrete behaviour. The application of the TSTM test may be various (Bernander 1994), (Mangold 1994):

- TSTM test results may be used for checking theoretical numerical models
- the influence of different parameters and concrete constituents on the development of stresses and cracking risk may be investigated
- different concretes may be compared with regard to cracking sensitivity, and on the base of such comparisons concrete mix may be optimized
- test results my be used for determination and modelling of the single concrete parameters.

When using TSTM for determination and calibration of material parameters, one should be aware of the following:

Simulation of stress development in a hardening specimen is an iterative process involving many parameters. The accuracy of computed stresses relies on the accuracy of the modelling and prediction of all relevant factors. Scatter between test results and calculations may have their origin in the statistical errors due to uncertainty in the material parameters, or in the errors in modelling of material parameters and coupling effects, i.e. incapability of the adopted models and theories to describe a complex concrete behaviour at early ages. When one parameter is calibrated by fitting calculations to the measurements, all these errors are attributed to that parameter, and put into its model. Therefore, to make this prediction more reliable, determination of all included parameters may be as accurate as possible.

In the following, TSTM results are used for calibration of the creep model.

Test results from (Bjøntegaard 1999) were used in that purpose. Stresses were calculated according to differential equations (5.1) . The only unknown parameters in the calculations were creep parameters. The meaning was to find a set of creep parameters that is able to fit the calculated stresses with the measurements. Five tests with different temperature histories were used. The creep parameters obtained from one test appeared to be representative only for that particular test and failed in representing stresses in the tests with other temperature histories. The scatter was worst for tests with highest maximal temperature. When the all available tests were used in creep calibration in the same time, obtained creep parameters gave a creep with unrealistically high rate. There was no guaranty that these parameters were able to describe stress generation with arbitrary temperature and restraint conditions. Therefore this idea was abandoned, and creep parameters were found from isothermal creep tests with constant loading.

This attempt and previous comparison have shown drawback of the latest approach: when creep is determined from the creep recovery test or TSTM tests, nonlinearities are included in the compliance function. That creep function is representative only for that particular case of loading, temperature and restraint conditions, and is not able to describe other cases.

When simulating stress generation, all relevant factors including nonlinearities and coupling effects should be considered. In previously described TSTM tests transient creep seems to be most relevant of all possible nonlinearities. Specimens were sealed so that drying shrinkage was prevented and Pickett effect is neglected. High-stress nonlinearity is excluded since measured stresses were below $0.5 \cdot f_t$. Low-stress nonlinearities are also disregarded (see previous chapter).

Transient creep was modelled according to expression (3.31) and included in calculations. Parameters were found by fitting calculated stresses to the measurements. Calculated stresses are shown in Figure 3.3 together with the measured ones.

In author's opinion, the TSTM should be used for calibration very carefully and mainly for modelling of coupling effects or nonlinearities, whereas all material parameters should be determined from independent tests, if possible.

Chapter 6

Support Conditions and Methods for Structural Analysis

Restraint is one of the most essential parameters in calculation of self-induced stresses in hardening concrete structures. In the same time, it is very uncertain factor because it is hard to estimate. In this chapter external restraint from the ground is investigated. The influence from parameters describing geometry of the structure and stiffness of the ground on stresses in hardening structure is examined. Three-dimensional nonlinear analysis are used in that purpose.

Accurate modelling of the support conditions is very difficult, among other things, because it necessitates a large amount of material parameters describing the ground and the bond between the ground and the structure. In this chapter different methods for analysis of hardening structure and interaction of the structure with the ground are presented, discussed and some of them are compared.

Some results from the literature are outlined in the respective sections without any attempt to make a literature review or a state-of -the-art overview.

On basis of these results and discussions, some recommendations for design of concrete structure at early ages, regarding external restraint are given.

6.1 Modelling of structure and support conditions

To obtain a realistic description of the structural behaviour of hardening concrete structure is difficult. To demonstrate complexity of the problem, a wall cast on a foundation is considered.

In the heating phase the wall tends to expand. This expansion is hindered by the previously cast slab and by the friction between the whole structure and the subgrade. As a result, stresses develop in the structure and since the stresses in the top are different from the stresses in the bottom of the wall, the wall has a tendency to rotate upwards (the top of the wall is in tension). In the cooling phase the situation is opposite: contraction is hindered by subgrade and the slab, and the wall tends to rotate downwards (the top of the wall is compressed). The rotation increases pressure on the ground causing additional deformations of the soil and a redistribution of the ground pressure. The ground pressure and the weight of the structure act against rotation, while horizontal frictional forces arising in the contact area between concrete and the ground contribute to the rotation and hinder expansion / contraction. Whether and how much the wall will rotate depends, among others, on two things: how large the lifting stresses are, comparing to the self weight, and how stiff the ground is. Restraint from the slab is transmitted by shear and normal stresses across the construction joint. If the stresses exceed the strength of the concrete in joint, a slip fail-

ure between old and new concrete takes place. Slip reduces the restraint from the slab and the stresses in the wall will significantly decrease.

The most general approach of modelling structure at early ages is 3D FEM analyses with realistic modelling of the ground and the bond between the structure and the ground and between the different parts of structure.

The method is very complex and therefore in practice it is replaced by different simplified methods, such as: three step engineering method, Compensation Plane Method, Compensation Line Method, one-point calculation. In the following different methods are described and discussed briefly, and results from some of them are compared.

6.1.1 Three-dimensional modelling of the structure and the restraint from the ground

3D modelling of the structure involves modelling of the ground and the bond between the structure and the ground. Realistic modelling of the ground is difficult, and requires many parameters which should be determined by laboratory tests and in situ tests. Therefore simplified models are often used in calculations. In (Rostasy 1999) existing and new engineering models for the interaction of the slab with the ground are presented and discussed in detail. For the sake of simplicity, the soil is regarded as an elastic material. This is a conservative assumption for the hardening concrete structure since time dependent soil deformation and relaxation of stresses in the soil are neglected, which results in higher restraint. All mechanical models of interaction of the slab with the ground can be divided into several categories:

- Rigid-plastic or elastoplastic friction models for connection between the slab and soil where the soil is considered to be a rigid body. Consequently, the deformability of soil is disregarded.
- The soil is modelled as an elastic material, presuming rigid bond between soil and slab. Both vertical and horizontal deformability of the soil may be taken into account.
- The soil is assumed to be linear elastic, whereas the bond between slab and soil is described by nonlinear or bilinear models
- Elastic deformation of soil is modelled by elastic springs or interface elements. This model is used in the present work. Elasticity of soil is described by modulus of subgrade reaction, which is defined as:

$$k = \frac{\sigma_n}{s} \tag{6.1}$$

where σ_n is the ground pressure and s the vertical settlement below slab. It can be determined as:

$$k = \frac{E_s}{bf} \tag{6.2}$$

where E_s is the E-modulus of the soil, b is the width of the slab, and f a parameter dependent on the length-width ratio of the slab and the depth-length ratio of the soil layer, see (Rostasy 1999).

It can also be directly determined by experiment (Normaler, Vegbygging 018, p145)

According to (Rostasy 1999), the stiffness modulus method (modelling of soil as elastic half space) is superior to the subgrade reaction method. However, the former one is numerically simpler, and taking into account the uncertainties of both methods and the model parameters, the subgrade reaction method was recommended.

As already mentioned, 3D FEM analyses with realistic modelling of the ground, for instance as described above, is the most general approach of modelling the support conditions of structures at early ages. However, neither that approach is without difficulties: it requires a large amount of data on material properties of the ground and friction between the ground and the structure, which is difficult to determine. In addition, the amount of work required by the 3D analyses is rather time consuming, both regarding processing of input and output data and the computation time. Therefore this method is used only in special cases where the simplified methods can not be used or for verification of those, where 3D analysis results can serve as a exact solution.

6.1.2 The three-step engineering method

The aim of this method is to replace a full 3D model by a simplified model which has the same degree of restraint as the point with maximal cracking risk in the full 3D model. The method consists of three steps. In the first step the temperature and maturity development in the cross-section are calculated by 2D analysis, and the mean E-modulus during the heating and cooling phase are calculated for the hardening concrete. In the second step the restraint factor is found in the point with the highest cracking risk in the structure both for the heating and the cooling phase. For this purpose two linear elastic 3D-, or in some cases 2D analyses of the whole structure are performed. An arbitrary constant temperature load is applied on the hardening concrete and the principal tensile stresses are calculated in the previously mentioned critical point. Restraint factors both for the heating and the cooling phase are found as the ratio between the principal stress from the elastic analyses of the structure and the stress in the case of 100% restraint:

$$R_z = \frac{\sigma_{11}}{\alpha_T \Delta T E_{new}} \tag{6.3}$$

σ_{11} is the principal stress which in most cases is equal to the stress in the structures length direction, α_T is thermal dilation coefficient, ΔT is an arbitrary temperature load, and E_{new} is the elastic modulus of the hardening concrete calculated in the first step. The old adjoining concrete is assumed to have a fully developed elastic modulus in both analyses.

In the third step the simplified model is made, where the hardening concrete structure is replaced by a section of the wall surrounding the point with the highest risk of cracking, whereas the old adjoining structure is represented with a cube which size is determined from:

$$\frac{A_{adj}E_{adj}}{A_{new}E_{new}} = \frac{R_z}{1-R_z} \tag{6.4}$$

Finally, the stress development in the critical point is calculated by means of a time dependent non-linear stress analyses with the simplified model.

To obtain good accuracy of the method, it is important that the temperature histories in the critical points in the simplified and the full model are close.

For more details about the method, see (Kjellman 1999) or (Olofsson 2000).

The method is verified by full 3D analyses of a wall cast on a previously cast foundation in (Kanstad 2000). It was found that the deviation between the engineering method and full 3D analysis is in general less then 10%, see Figure 6.2 and Figure 6.1, which is acceptable having in mind the other uncertainties in the early age cracking problems, for instance in modelling of material properties and external conditions.

The main advantage of this method is that it is as general as full 3D analysis, without any restriction regarding structural geometry. Since the method ends up with a simple model, time consuming 3D time dependent analyses of a full model are avoided. The disadvantages of the method lie in its complexity: first, the point with the maximal stresses in the structure has to be known in advance; second, to determine restraint in a critical point and make the simplified model, the user has to run elastic analysis of the whole structure, which in the general case has to be three-dimensional. Therefore use of this method makes sense mainly in the cases where many analyses have to be performed, for instance to study effect of external factors on risk of cracking. In other words, efforts about making the simplified model are justified if this model should be used many times instead of full 3D model.

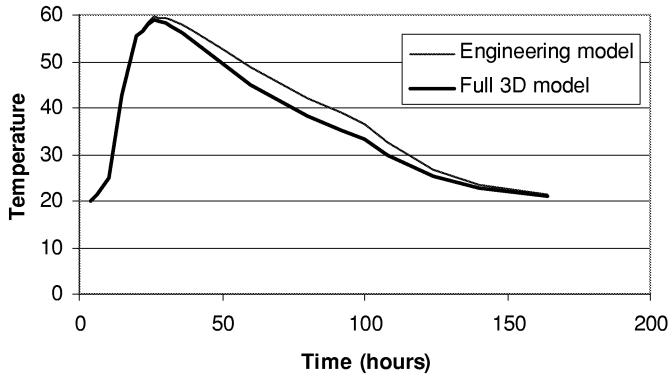

Figure 6.1: Temperature development in the critical position in the hardening wall, calculated by Engineering method and full 3D analysis, from (Kanstad 2000)

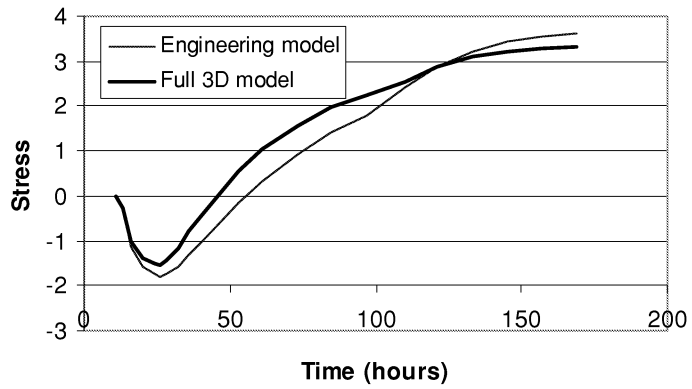

Figure 6.2: Stress development in the critical position in the hardening wall calculated by Engineering method and full 3D analysis, from (Kanstad 2000)

6.1.3 Compensation Line Method (1D)

In this method the structure is approximated as a beam subdivided into discrete layers with different temperature histories. The beam is allowed to translate and rotate in one direction due to temperature changes and shrinkage, and it is assumed that plane cross sections remain plane. The free deformations - translation and curvature in one plane are calculated by means of the equations of equilibrium for the compensation line:

$$\sum X = 0 \Rightarrow \int \sigma \, dA = 0$$

$$\sum M = 0 \Rightarrow \int \sigma \, y \, dA = 0 \tag{6.5}$$

where σ are the self-induced stresses, and y is the distance from the centre of gravity.

The final incremental strain developed during Δt in one layer on the distance y from the centre of gravity will be:

$$\Delta\varepsilon = \Delta\varepsilon^{tr} + \Delta\varepsilon^{rot} = \Delta\varepsilon^{tr} + \Delta\kappa \cdot y \tag{6.6}$$

where $\Delta\varepsilon^{tr}$ is longitudinal deformation, and $\Delta\kappa$ is curvature, assuming free translation and rotation. External restraint may be taken into account by restraint factors, so residual incremental strain will be:

$$\Delta\varepsilon = (1 - k_T)\Delta\varepsilon^{tr} + (1 - k_R)\Delta\kappa \cdot y \tag{6.7}$$

where k_T is axial restraint factor, and k_R is rotational restraint factor. For zero external restraint ($k_T = 0$, $k_R = 0$) the section may translate and rotate freely. Full restraint ($k_T = 1$, $k_R = 1$) means that translation and rotation are not possible.

The method is described among others in (Emborg 1989) and (Rostasy 1994).

6.1.4 Compensation Plane Method (2D)

The method can be described as the 2D generalization of the Compensation Line Method: the cross-section is divided into elements, and rotation is allowed in two directions. The temperature (maturity) distribution in the cross-section may be calculated by means of 2D analysis, whereas the strains in the out-of-plane direction are calculated using the assumption that plane sections remain plane:

$$\Delta\varepsilon = \Delta\varepsilon^{tr} + \Delta\kappa_x \cdot y + \Delta\kappa_y \cdot x \tag{6.8}$$

where $\Delta\varepsilon^{tr}$, $\Delta\kappa_x$ and $\Delta\kappa_y$ may be obtained from the equations of equilibrium for the compensation plane:

$$\sum X = 0 \Rightarrow \int \sigma \, dA = 0 \tag{6.9}$$

$$\sum M_x = 0 \Rightarrow \int \sigma y \, dA = 0$$

$$\sum M_y = 0 \Rightarrow \int \sigma x \, dA = 0.$$

The method is described by (Emborg 1994a), (Rostasy 1994) and (Pedersen 1994)

The advantage of the plane section method comparing to 3D analysis is obvious. The number of the unknowns is strongly reduced. If the Compensation Plane Method is formulated in the simplest way, the number of unknowns is only 3: one translation and two curvatures. Both computational time and the time spent on the modelling and survey of the results is considerably reduced. The disadvantage is that method is accurate only for long structures with uniform cross-section and boundary conditions in the longitudinal direction, i e when the temperature distribution and the stress component in the longitudinal direction do not change from one cross-section to another except near to the ends.

For structures with lower length-to-height ratio the assumption about plane sections does not apply. The stresses in these structures are generally lower than determined under the assumption of plane sections, a fact which can be handled by reducing the restraint over the height. For that purpose the resilience factor is introduced (see the next method).

The second shortcoming of the Plane section method is that external restraint factors should be known, otherwise stresses may be estimated only in the extreme cases of the restraint conditions: the structure is allowed to rotate and translate freely ($k_R = 0$, $k_T = 0$), the structure is completely restrained against rotation and translation ($k_R = 1$ $k_T = 1$), or combination of free rotation and restraint translation and opposite. This is also the basic assumptions of some special-purpose programs for hardening concrete structures (4C-Temp & Stress). Translational restraint is difficult to model, and it is usually assumed to be zero, i e the horizontal restraining forces are neglected. The structure's ability to curve is considered to be dependent of the length-to-height ratio and the stiffness of the ground

(Andersen 1997). The influence of these factors on the stresses in the structure will be investigated in the Section 6.2.1 .

The same restrictions about structural geometry are valid for the Compensation Line Method. The method is even more simple: the structure is subdivided into layers, and constant temperature is assumed in each layer, meaning that temperature is allowed to vary only in one direction - over the height of the structure. The method is one-dimensional and is accurate for the structure extended in two directions, i.e. plates.

6.1.5 One-point calculation

One point calculation is the most simple method for stress calculation in hardening concrete structure. The restraint factor in decisive point must be known, and then, the stress increment can be calculated as:

$$\Delta\sigma = E_c(\Delta\varepsilon - \Delta\varepsilon_T - \Delta\varepsilon_{AD}) \cdot \psi \cdot \gamma_R, \tag{6.10}$$

where E_c is modulus of elasticity which may include high-stress nonlinearity, $\Delta\varepsilon_T$ is thermal strain increment, $\Delta\varepsilon_{AD}$ is autogenous deformation, ψ is relaxation and γ_R is restraint factor. The simplicity of the method is obvious. The problem is that the structural restraint factor in decisive point must be known in advance. Degree of restraint in one structure depends on many factors such as: stiffness of the soil, quality of bond between the structure and the ground, dimensions and geometry of the structure, stiffness of the restraining structure, length and nature of the joint, etc. In (Nilsson 2000) methods for determination of the restraint factors were developed both for plane-section analysis and non plane-section analysis. The assumption about plane sections may be applied for long structures with length-to-height ratio above five. For shorter structures deviations from the plane-section analysis was modelled by means of resilience factor. The resilience factor k_{res} was estimated from 3D FEM analyses as the restraint factor in a structure which is prevented to translate and rotate. k_{res} depends on the length-to-height ratio of the section and varies over the height of the structure. The restraint factors describing influence of the ground stiffness were found from the analysis of beam founded on elastic materials. Three different cases were studied: structures totally resting on the ground, structures resting on the ground at one single point and structures partly resting on the ground, i.e. with the lifting ends. Influence of the joint was included by means of the slip failure factor, which prediction was based on field experience.

6.2 Influence of the support conditions and length of the structure on stresses in hardening concrete structure

Influence of the support conditions on the size and distribution of stresses in young concrete was investigated in (Andersen 1995). The structure's ability to curve was studied since it was recognized as the main factor affecting the stress distribution and the stress level. In that purpose elastically supported beams with different length and flexural stiffness were investigated for different values of the modulus of subgrade reaction. The beams were assumed to be loaded by an externally applied moment. The ratio of the moment at the centre of the beam to the applied moment was used as an indicator of the curvature of the beam. Ratio close to one indicates free curvature, ratio close to zero indi-

cates no curvature. It was shown that the increasing modulus of subgrade reaction and increasing beam length reduced the curvature of the beam. The stiffness of the ground has a smaller effect on the curvature and stress level than the length of the structure.

Influence of the stiffness of the ground on the restraint stresses is also investigated in (Pettersson 1998) where concrete slabs resting on the ground exposed to imposed strains from temperature or shrinkage were considered. The concrete was regarded as linear elastic and the restraint stresses were calculated with a two-dimensional FE-model where the contact surface was simulated with non-linear contact elements, taking into account both horizontal and vertical movements. The temperature changes regarded here were due to climatic conditions; hydration heat was not considered, i. e. the concrete was supposed to be hardened. Influence from parameters describing geometry, ground restraint and imposed deformations on restraint stresses were investigated in detail. It was shown that influence of all parameters interfere, and that influence of one parameter can not be regarded independently. Thus, according to Pettersson, influence of the vertical ground stiffness on the restraint stresses depends on the length of the slab: increased ground stiffness gives increasing stresses in short slabs, whereas stresses in long slabs are almost independent of ground stiffness. Another interesting conclusion is that in the case of temperature gradient over the cross-section increasing length of the structure first gives a fast increase of the maximum stress, and after a certain length the maximum stress is almost constant. In the case of uniform temperature change over the cross-section, an increase of the length gives higher restraint stresses. It was assumed that the conclusions would remain unchanged if the nonlinear behaviour of concrete was taken into account.

6.2.1 Finite element analysis investigation

Literature dealing with restraint in hardening concrete structures is mainly based on simplified methods or linear elastic FE analyses with simple models, assuming that the same conclusions would be valid also in case of more realistic modelling of non-linear behaviour of concrete. In the next section, the influence of the structural geometry and ground stiffness on magnitude and distribution of the stresses in hardening structures is investigated by means of the three-dimensional nonlinear FE analyses. In that way the number of simplifications and assumptions, which are possible sources of errors are reduced, and the structure is modelled as realistic as possible. This approach gives the possibility to predict both the level and the distribution of each stress- and strain component in the structure in different cases of restraint conditions.

A typical example of a concrete structure at early ages with the risk of through-cracking is considered: a wall cast on previously cast foundation. The deformability of the ground is modelled by the modulus of subgrade reaction in the vertical direction, which describes the relation between normal stresses and relative displacement, and the modulus of subgrade reaction in horizontal direction describing the relation between the tangential stresses and relative horizontal displacements between the structure and the ground. Influence of each component on restraint stresses is examined separately.

Influence of the length of the structure and the vertical ground stiffness on the self-induced stresses .

Two walls with different length-to-height ratios are considered. The cross sections of the walls are identical, see Figure 6.8, and the length is: 15m (L/H=2.6), and 30m (L/H=5.2). Different restraint conditions for the walls are applied:

- the walls are allowed to rotate freely, friction between the foundation and the ground is neglected
- the walls are prevented to rotate, friction between the foundation and the ground is neglected
- the deformability of the ground is described by the modulus of the subgrade reaction both in the horizontal and vertical direction. In the vertical direction so-called "no tension" bedding was applied with constant value for the modulus of subgrade reaction k_v = 60MN/m^3 in compression, and k_v = 0 in tension. In the horizontal direction a rather low value for the modulus of the subgrade reaction is used, k_h = 10 MN/m^3, to reduce influence of the friction on the stresses (Pettersson 1998). In that way, mainly the effect of the vertical ground stiffness is considered. Influence of the horizontal restraining forces will be investigated in the subsequent section.

Figure 6.3 presents stress distribution over the height of the wall 7 days after casting for different restraint conditions.

The same results are presented in different way in Figure 6.4, where the stress distributions for the two walls are directly compared to illustrate the importance of the structure's length.

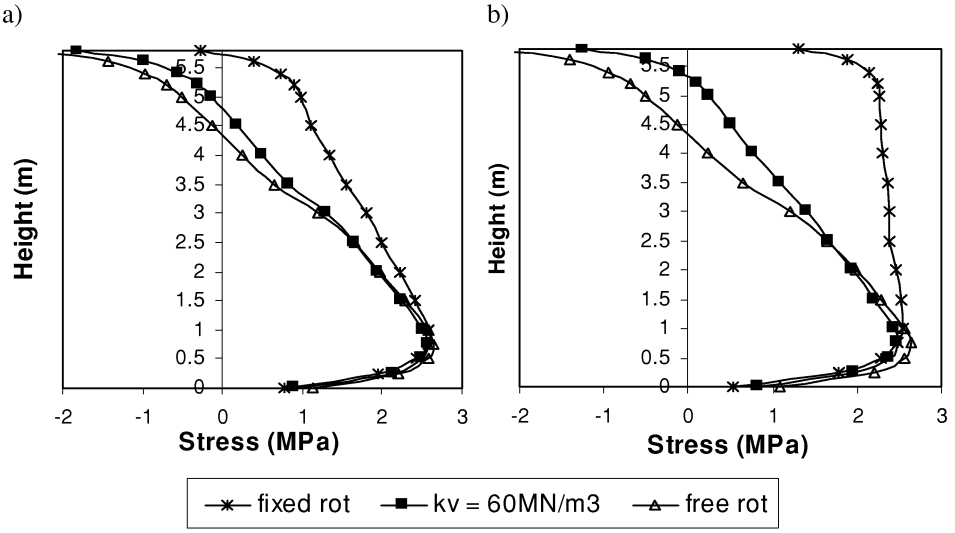

Figure 6.3: Distribution of the stresses in the longitudinal direction over the height 7 days after casting for different restraint conditions a) short wall (L/H = 2.6), b) long wall (L/H = 5.2)

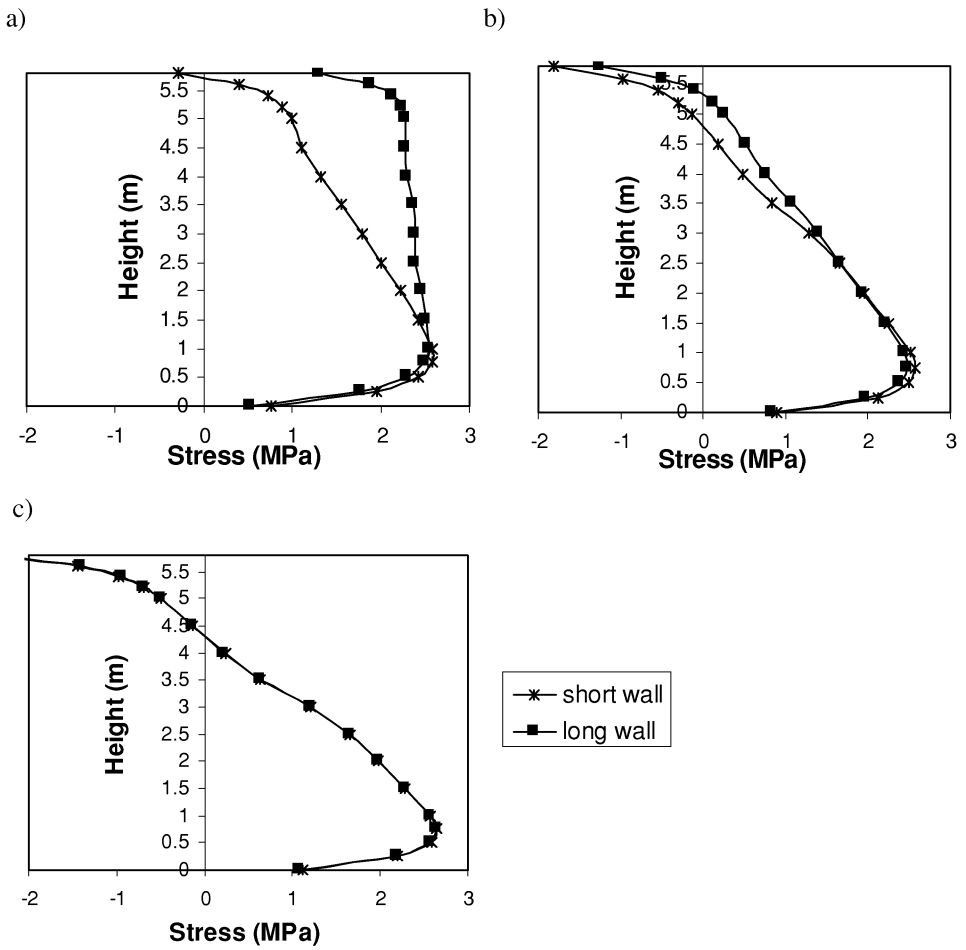

Figure 6.4: Distribution of the stresses in the longitudinal direction over the height 7 days after casting for two walls with different length a) fixed rotation, b) ground stiffness k_v = 60MN/m^3, k_h = 10MN/m^3 c) free rotation

It can be seen that the vertical ground stiffness affects the distribution of the stresses over the height: the size of the maximum stress in the bottom of the wall remains almost unchanged, whereas the size of the stresses in the top are different. It can be also seen that the influence of the wall's length and ground stiffness interfere and can not be considered independently. The stiffer the ground is, the more important the length is. In the case of free rotation, the stresses in the fifteen-meter and thirty-meter long walls are identical. For no-tension bedding with k_v = 60 MN/m^3 the difference between two walls appears: the size of the maximal stress in the bottom of the wall are not affected, but the stresses in the top are changed. In the case of fixed rotation, difference becomes remarkable. To which extent an increase of the length affects the stress distribution in the wall depends on the support conditions. The zone with large tensile stresses is higher in the long wall. In prac-

tice that means that the short wall will have nearly the same cracking risk as the long wall, but fewer crack will appear and they will be shorter than in the long wall.

From Figure 6.4b it can be seen that the behaviour of the wall is close to the free rotation for both lengths, even though it is founded on a relatively stiff ground (k_v = 60 MN/m^3). To behave like the rotation is fixed, the wall should be much longer than 30 m. The vertical ground stiffness in this example has a small effect on the structure's ability to curve.

Influence of the friction between the ground and the structure on restraint stresses.

For concrete structures resting on ground horizontal restraining forces due to friction arise in the contact area. In (Pettersson 1998) experimental results from friction tests are reported. Frictional forces are given as a non-linear function of the displacements. The best approximation is a bilinear curve, given by the modulus of subgrade reaction in the tangential direction and the friction coefficient, see Figure 6.5.

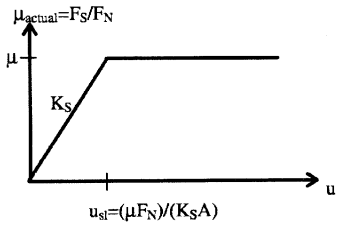

Figure 6.5: Simplified friction curve, from (Pettersson 1998)

The parameters are not only influenced by the ground material, but also by the load level, and reasonable values vary from 0.5 to 3 for the coefficient of friction, and from 5 to 85MN/m^3 for the modulus of subgrade reaction.

In this analysis, the friction is described by only one parameter, modulus of subgrade reaction in horizontal direction k_h (k_h = Ks), which is a conservative assumption. This modulus describes the relation between the tangential stress and the relative tangential displacement between the structure and the ground.

To investigate the influence of the friction on the stresses in the structure, three values are used:

- k_h = 10 MN/m^3, describing low friction between the structure and the ground,
- k_h = 60 MN/m^3, the value which may be used for crushed aggregate
- k_h = 200 MN/m^3, to simulate very high friction

The stresses are calculated for two walls with 15 m and 30m length. Different values for k_h do not cause considerable changes in stresses for the short wall. However, the stresses in the long wall are significantly influenced. In Figure 6.6 the distribution of the stresses over

the cross-section height in the middle of the long wall 7 days after casting are presented. In Figure 6.7 the stress development in the lower part and in the top of the wall are shown.

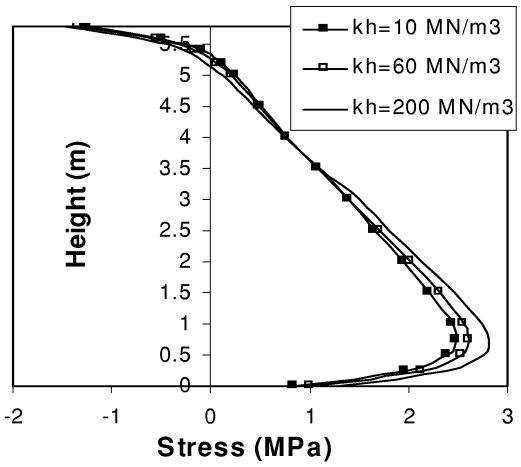

Figure 6.6: Distribution of the stresses in the longitudinal direction over the height 7 days after casting for the 30 meter long wall for different values of the friction between the structure and the ground

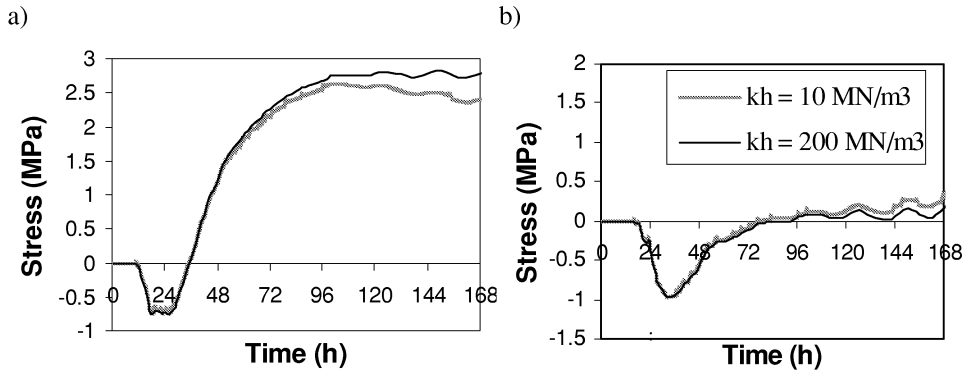

Figure 6.7: Stress development a) 0.5 m from the foundation, b) 1 m from the top for the wall calculated with two different values for modulus of subgrade reaction in horizontal direction

Since the horizontal frictional forces work similarly as eccentrically applied external loads, they affect the stresses in the whole cross section. In this specific case change of modulus of subgrade reaction in horizontal direction from 10 MN/m^3 to 200 MN/m^3 causes change in maximal stresses of approximately 15%. Stresses in the top of the wall are less affected. Friction is more important for long than for short structures.

6.3 Comparisons of different methods

In the following, different calculation methods are used in the simulation of strain/stress development in the wall cast on the previously cast foundation. The cross section of the wall is shown in Figure 6.8.

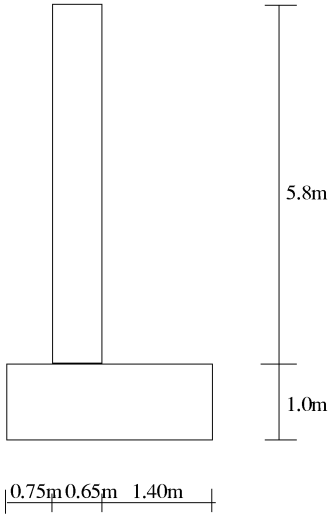

Figure 6.8: Cross section of the wall

Two FE models are used in the simulation (Figure 6.9):

- full 3D model (because of the symmetry only one half of the wall in the length direction has been modelled)
- simplified model – a "slice" of the structure with unit thickness. The basic assumption for the simplified model is that the wall can be treated like an infinitely long structure with constant temperature and constant principal stresses in the longitudinal direction. In this case the plane bending principle for deformations is valid, meaning that FE analysis with this model will give the same results as the Compensation Plane Method.

Practical modelling of the plane section constraint in DIANA is possible by means of user specified linear dependencies between nodal displacements. If rotation of the structure is prevented, the only freedom of movement is translation, which can be modelled by prescribing equal displacements in the out-of plane direction for all nodes in one plane. Plane-section rotation is modelled by means of linear proportion between nodal displacements in the out-of plane direction.

Two analyses with the simplified model have been performed:

1. Fixed rotation around horizontal axis in the cross-section
2. Free rotation around horizontal axis in the cross-section

The horizontal restraining forces due to friction between foundation and subgrade are neglected.

To find out to which extent the simplification about plane cross-sections influences stress and strain results in the structure, full 3D analyses have been performed for the two wall's lengths: 15 m and 30 m. The same restraint conditions have been used as in the previous analyses, i.e.: free and fixed rotation around horizontal axis in the cross section. Horizontal frictional forces have been neglected. The self-weight has been taken into account. The results of the calculations are presented in Figure 6.10.

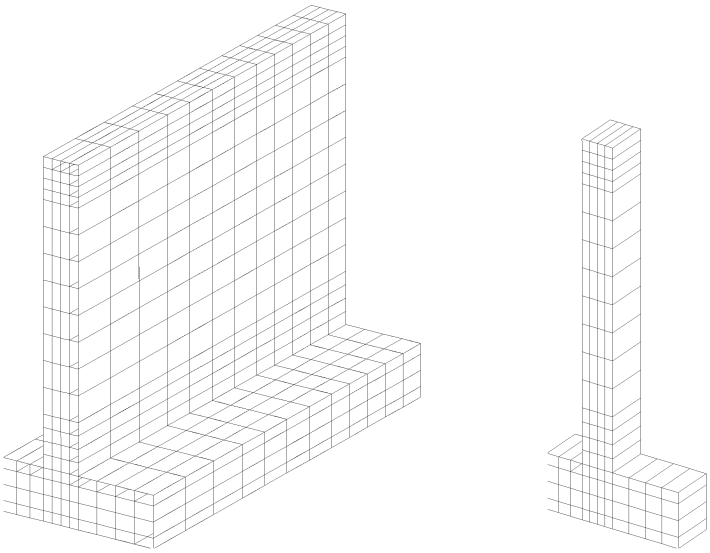

Figure 6.9: Finite element models

Figure 6.10 shows the distribution of the stresses over the height 7 days after casting for two cases of free rotation and fixed rotation around the horizontal axis in the cross section plane. It can be seen that stresses calculated by two methods completely overlap for both the short and long wall in the case of free rotation. In the case of fixed rotation two methods give different results. The fact that the deviation of the plane-sections analysis from the full 3D analysis, so-called resilience, is different for different restraint conditions, makes it difficult to combine resilience with $2\frac{1}{2}$D analysis, as proposed in (Emborg, 1989). Here the resilience was estimated by 3D FEM analyses of a structure prevented to both translate and rotate, and superposed with translational and rotational strain determined by the plane-sections analysis. The main prerequisite for this approach is that resilience is independent on the external restraint conditions. According to these results, this is not correct.

Further, it can be seen that these two methods give similar results for the long wall. For the short wall, the difference between $2\frac{1}{2}$D analysis and 3D analysis in the case of fixed rota-

tion increases with the distance from the foundation, which means that the tensile stresses in the bottom are less influenced by the choice of method than the stresses in the top of the wall.

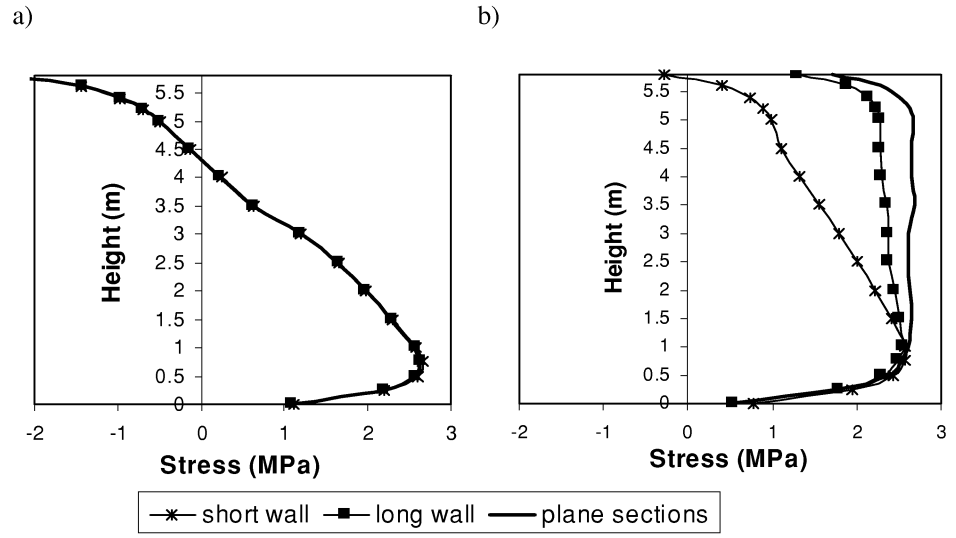

Figure 6.10: Stress distribution over the height of two walls with different length (15 m and 30 m) 7 days after casting calculated by 3D analysis and Compensation Plane Method. Two different restraint conditions are assumed: a) free rotation, b) fixed rotation

A similar comparison is done for another structure with different flexural stiffness - a wall founded on a slab. The cross-section of the wall is shown in the Figure 6.11 and FE models in Figure 6.12. Length of the wall is 15 m and because of symmetry, only one half of the structure in longitudinal direction and one half of the slab is modelled. The main difference between this and previous structure is the slab width.

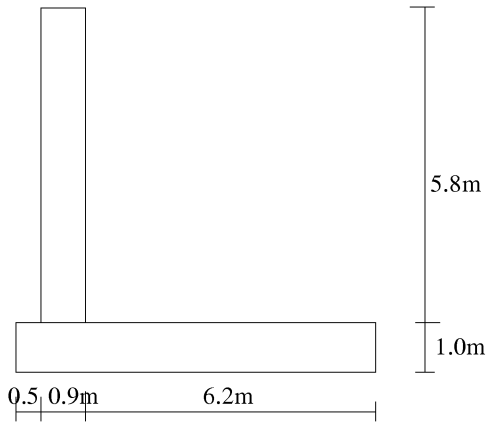

Figure 6.11: Cross section of the wall founded on the slab

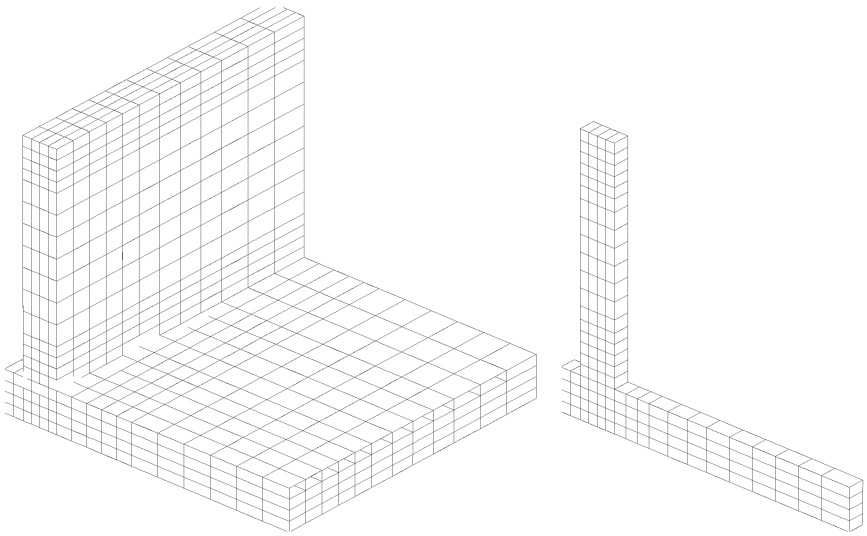

Figure 6.12: Finite element models used in calculations

Stress and strain developments calculated by two methods in two points in the middle of the wall are shown in the Figure 6.13-Figure 6.14. Two different support conditions are assumed in both methods: free rotation and fixed rotation around horizontal axis in cross-section plane.

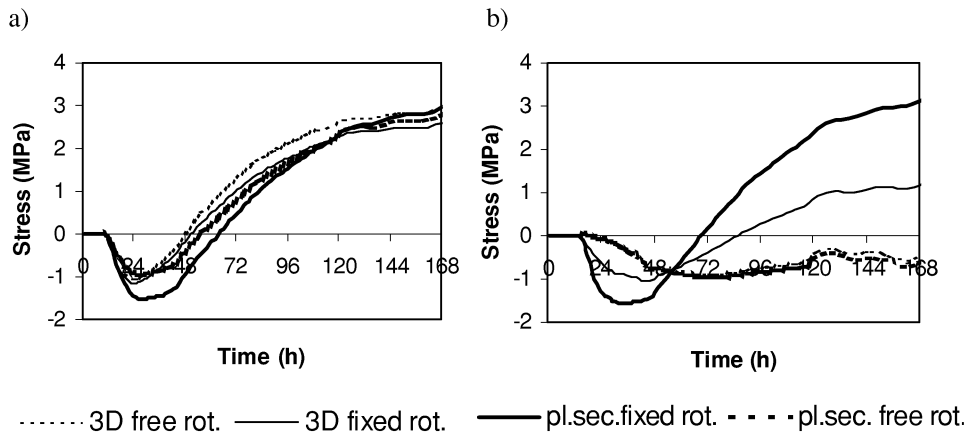

Figure 6.13: Stress development in the middle of the wall calculated by 3D analysis and Compensation Plane Method assuming free rotation and suppressed rotation around horizontal axis in the cross section. Stresses in two points are shown: a) 1 m from the foundation, b) 1m from the top

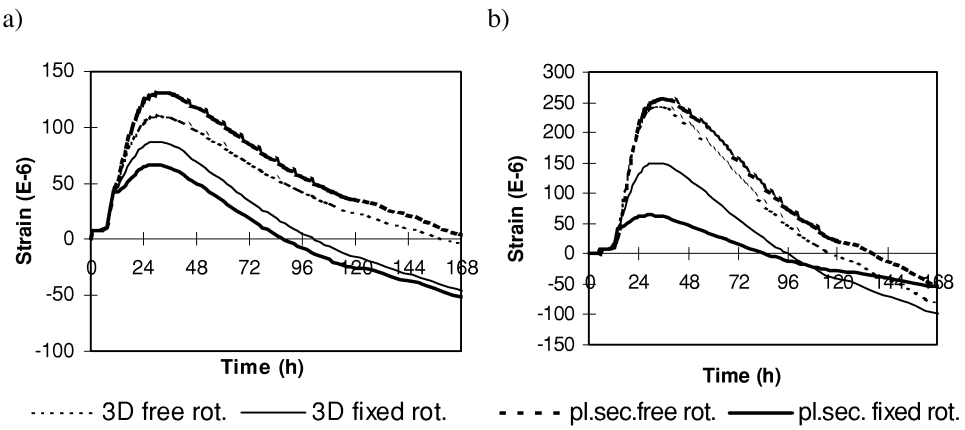

Figure 6.14: Strain development in the middle of the wall calculated by 3D analysis and Compensation Plane Method assuming free rotation and suppressed rotation around horizontal axis in the cross section. Strains are depicted in two points: a) 1 m from the foundation, b) 1m from the top

In this case the differences between Compensation Plane Method and 3D analysis are more significant for both cases of the external restraint conditions. Still, it is more pronounced for the case with fixed rotation.

When the Compensation Plane Method is used two extreme cases of structural behaviour are simulated: free and fixed rotation around the x-axis. All real situations are placed somewhere between these two cases, depending of the ground stiffness and the structure's

length. The structure's ability to curve is important only for the stresses in the upper part of the wall. Maximum stresses in the bottom remain almost unchanged.

In the subsequent analysis stresses in the wall founded on the stiff ground ($k_v = k_h = 60$ MN/m^3) are calculated by 3D analysis are compared with the stresses calculated by Compensation Plane Method for free and fixed rotation. The cross section of the wall is given in Figure 6.8, and two different lengths are used: 15 m and 30 m. Figure 6.15 presents stress developments calculated in the middle of the wall in different points. Corresponding deformations are shown in the Figure 6.16.

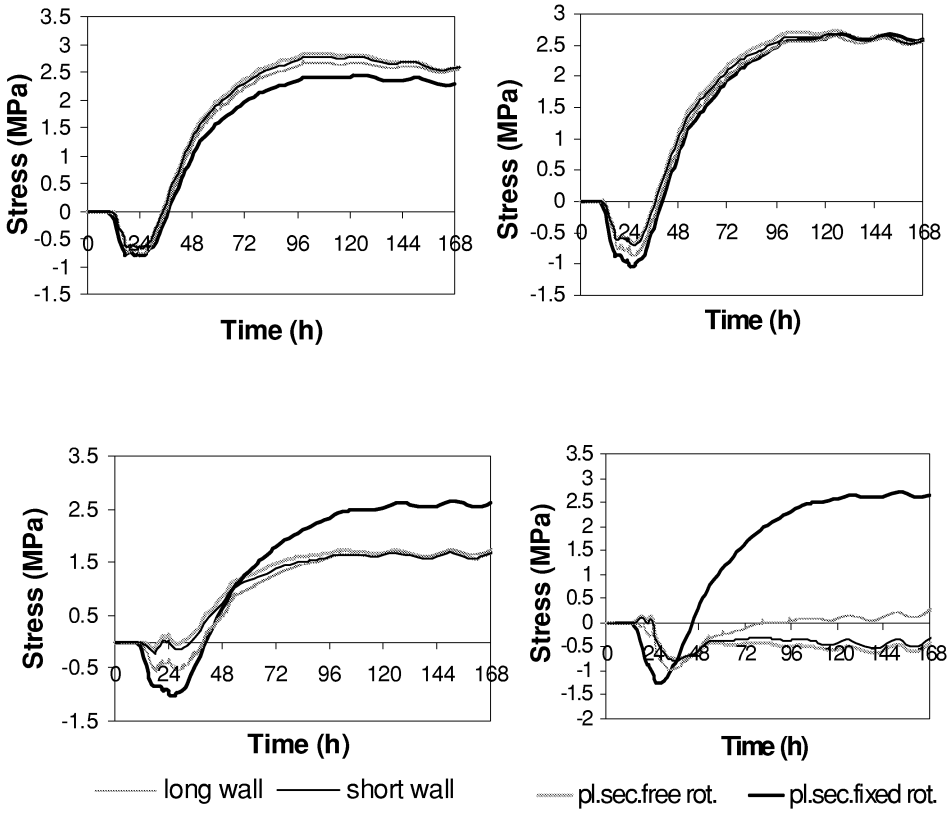

Figure 6.15: Stress development in the middle of the wall calculated by 3D analysis and Compensation Plane Method. Four points are considered: a) 0.5 m from the foundation, b) 1m from the foundation, c) 2.5 m from the foundation and d) 0.8 m from the top of the wall.

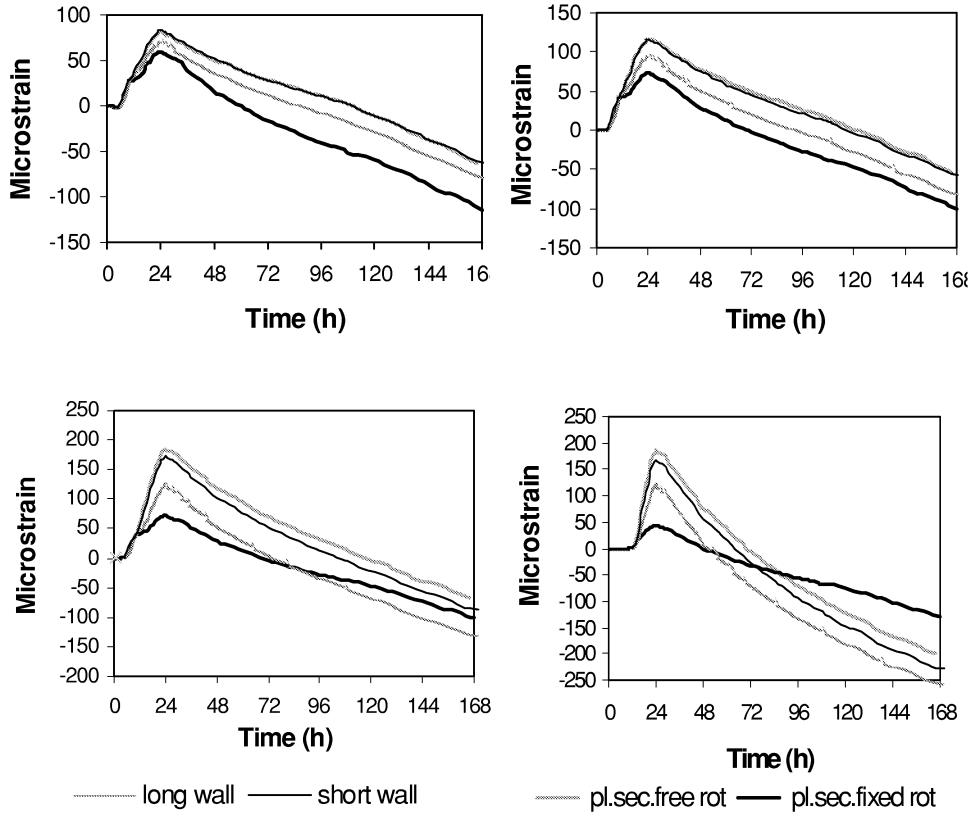

Figure 6.16: Strain development in the middle of the wall calculated by 3D analysis and Compensation Plane Method. Four points are considered: a) 0.5 m from the foundation, b) 1m from the foundation, c) 2.5 m from the foundation and d) 0.8 m from the top of the wall.

It can bee seen that both the short and long wall may reasonable accurately be calculated by the Compensation Plane Method with assumption of free rotation even though they are founded on stiff ground. In he previous sections it is shown that the high ground stiffness and large length suppress the curvature. The stiffness of the ground has less importance on the structure's ability to curve than length of the structure.

From these results it follows that the Compensation Plane Method and the full 3D analysis gives similar results for long structure ($L/H>5$). For short structure ($L/H<5$) the deviation between two methods is strongly dependent on the restraint conditions. In the case of free rotation the difference between two methods is small. In the case of fixed rotation the Compensation Plane Method predicts lower strains and, consequently, higher stresses than 3D analysis giving thus conservative results.

Further, the difference seems to be more pronounced for the structure with high ratio between stiffnesses of the hardening part and restraining part, for instance wall founded on the slab.

Stresses in the bottom of the wall are not much influenced by the choice of method, in contrary to the stresses in the top.

6.4 Design recommendations

Deviation between Compensation Plane Method and 3D analysis depends on the support conditions and length of the structure. In this study the structures with the length-to height ratio between 2.6 and 5.2 are investigated. For long structure (L/H = 5.2) two methods agree very well, for short structures deviation between two methods is large in the case of fixed rotation.

In some special purpose programs for hardening structures where the Compensation Plane Method is used, stresses can be estimated only in two extreme cases of structural behaviour: free and fixed rotation about horizontal axis in cross-section plane. In that case an assumption about structural behaviour should be made. Structure's ability to curve affects the stress distribution, whereas the size of maximal stress remains almost unchanged. Whether the structure will curve and how much it is difficult to know in advance. When the vertical ground stiffness is modelled by means of the modulus of subgrade reaction, stiffness of the ground has a small influence on the stresses and the structure's ability to curve. For short structures ($L/H < 5$) free curvature may be assumed regardless of the ground stiffness. Consequently, completely fixed rotation should be assumed if the structure is anchored in the very stiff ground or in cases with extremely high length-to-height ratio.

Friction between the structure and the ground has also a small influence on the stresses for walls with the dimensions as studied in this section. Therefore, in the case of sand or crushed aggregate as a subgrade (k_h = 5-85 MN/m^3) friction may be neglected for the design process.

Chapter 7

Field Test

In this chapter temperature and strain development are determined for two sections of a real structure, the Maridal culvert in Oslo. A comprehensive laboratory test program was performed at NTNU to identify material parameters. Both thermal and mechanical properties were tested. Material models were checked in the TSTM for three different realistic temperature histories. Within the Brite-Euram project IPACS a large field instrumentation programme has been carried out to measure temperature and strain development in the culvert. 3D analyses of the foundations and walls in two of the instrumented sections of this structure were performed with DIANA and calculated results are compared to measurements.

7.1 General about the field test

The Maridal culvert is a part of the Ring road around Oslo, seeFigure 7.1 . The total length of approxiately 340 m has been cast in sections of 15 m length.

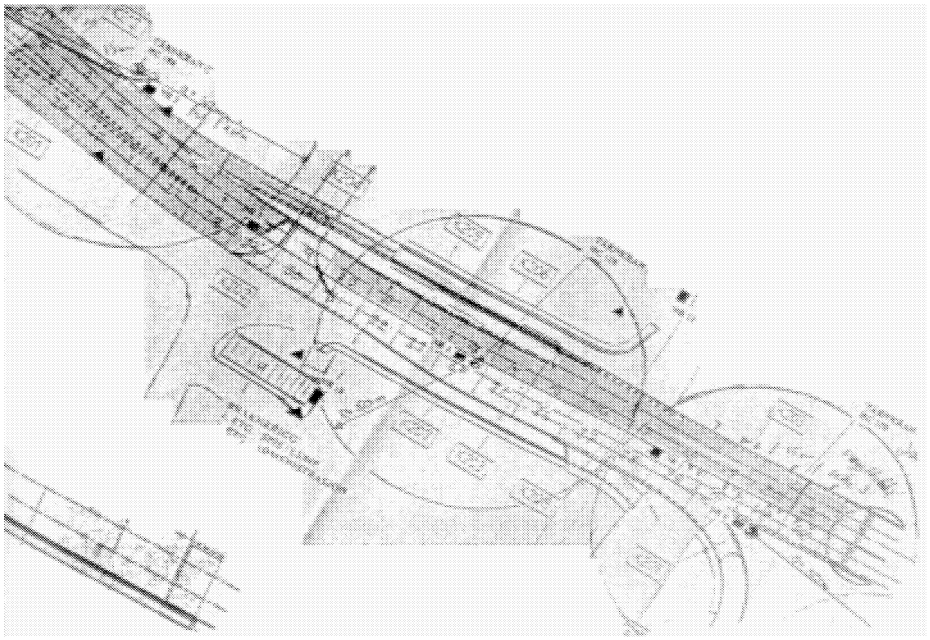

Figure 7.1: Plan view of the Maridal Culvert

Depending on how the walls of the culvert are founded two types of sections may be distinguished: one with the bottom slab under the whole cross-section, and one with strip foundation (Figure 7.2).

a)

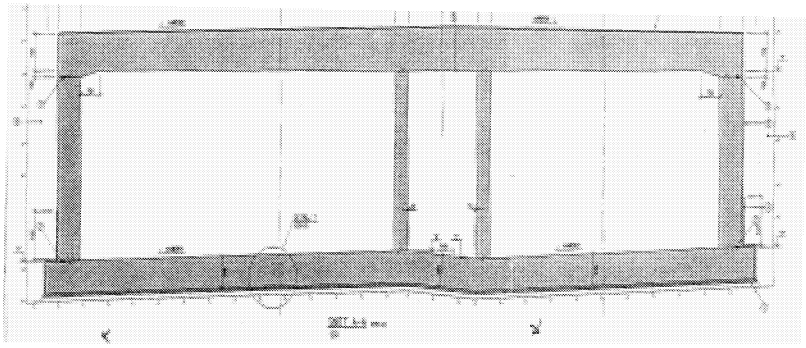

b)

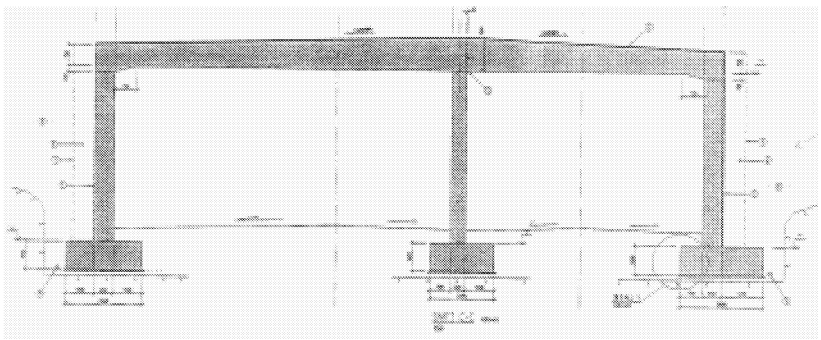

Figure 7.2: Two typical sections of the Maridal culvert a) Section 2 b) Section 42

Three sections, including four walls, three slabs and two foundations, have been instrumented with strain gauges and temperature sensors, and temperature and strains in the structure have been recorded from the casting. Instrumentation was carried out by the Norwegian IPACS partners: Selmer, Directorate of roads, and NTNU. The results are reported in (Heimdal, 1999) and (Heimdal, 2000).
Two walls, one founded on the slab (Section 2) and one with strip foundation (Section 42), have been analysed in this study. The walls were heavily instrumented. Since measurements will be compared with the calculations, the procedure and the results are presented and discussed here.

7.2 Instrumentation

7.2.1 Different measuring methods

Four different types of strain gauges have been used in instrumentation: strain gauges welded to the reinforcement bars type TML AWC-8B, strain gauges glued to the rein-

forcement bars type TML WFLA-6-11, NGI Geonor vibrating wire type P-300, and Geokon vibrating wire type VCE-4200

Strain gauges TML AWC-8B

This type of sensor is welded to the reinforcing bars prior to concrete casting. The reinforcement strains are monitored as a change in the electrical resistance of a metal thread.

The measuring length is 8 mm. To achieve reliable results, it is necessary with two symmetrically located gauges on one bar in each measuring points.

Glued strain gauges TML WFLA-6-11

This type of sensor has to be glued to the reinforcement bar. Working principle is the same as for welded strain gauges. The measuring length is 6 mm, and also here two gauges in each measuring point are recommended.

NGI Geonor vibrating wire type P-300

This gauge is designed by the Norwegian Geotechnical Institute and Geonor. Welded to the reinforcement bar, it monitors strains in the reinforcement. Because it is made of steel with higher strength than the reinforcement steel, it also operates after yielding of the reinforcement. P-300 monitors the average strain over the length of 470 mm.

Geokon vibrating wire type VCE-4200

The sensor is designed for direct embedment in the concrete. The steel wire is tensioned between two end blocks. The strain in the concrete moves the end blocks causing a change in the tension of the wire. This is registered as a change in the resonant frequency of vibration. The measuring length is 153 mm. This strain gauge sensor incorporates a temperature sensor, which supplies data for temperature compensation.

All four types of gauges monitor temperature compensated strains, and to get the total, true strains, the temperature strain of the strain gauge itself must be added:

$$\varepsilon_{true} = \varepsilon_{tempcom} + \alpha_T \Delta T \tag{7.1}$$

To check out the value for thermal dilation coefficient stated by the producer, the strain gauges were calibrated in the laboratory.

7.2.2 Calibration tests in laboratory

Two types of the strain gauges were calibrated: welded strain gauges and Geokon vibrating wire strain gauges. They were used to measure strains in the hardening concrete specimen exposed to the realistic temperature histories. The thermal dilation coefficients for the strain gauges were found by comparing these strains to the strains measured by the permanent instrumentation system in the TSTM and in the free deformation rig. The concrete was the same as used in the Maridal culvert.

Calibration of welded strain gauges.

The strain gauges were welded to the reinforcement bar in the concrete specimens in the TSTM and free deformation rig. In the TSTM specimen two reinforcement bars were used

to take eccentricity of the specimen into account. Two gauges were used in each point to compensate for possible variations due to local bending effects.

To simulate the situation on a construction site, the gauges were connected to the registration unit by 11m long cables that were cooled down to 7^0C for a period of time to investigate the effect of variations in the cable temperature on measurements. The ambient temperature was approximately constant.

The TSTM specimen was fully restrained, i e the total deformation was zero. The total strain in the free deformation rig was measured by a LVDT system.

With the thermal dilation coefficient of the strain gauges α_t = 10.5 E-6 good agreement with the permanent instrumentation system was achieved, see Figure 7.3. This value differs from the value stated by the producer, which is α_t = 12 E-6.

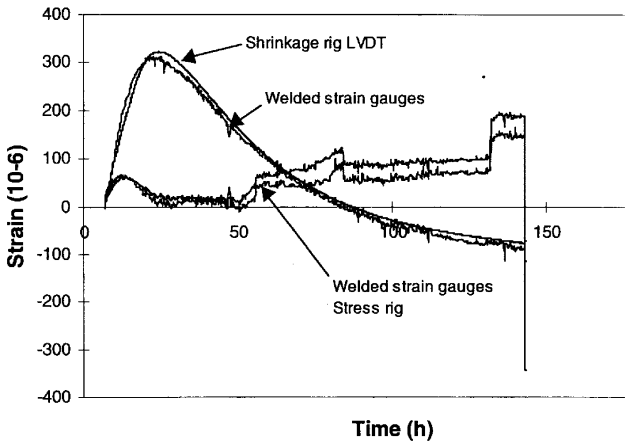

Figure 7.3: True strains measured by welded strain gauges and LVDT in the free deformation rig and TSTM. The true strains for welded strain gauges are determined by assuming α_T = 10.5E-6 (from Heimdal 1999)

Calibration of the Geokon vibrating wire strain gauges

The Geokon vibrating wire VCE-4200 was directly embedded in the concrete specimen in the free deformation rig. Good agreement between the strain gauges and the LVDT system is achieved when the thermal coefficient is set to 11.2E-6, see Figure 7.4. According to the producer thermal dilation coefficient for Geokon vibrating wire strain gauges is α_t = 12.2E-6.

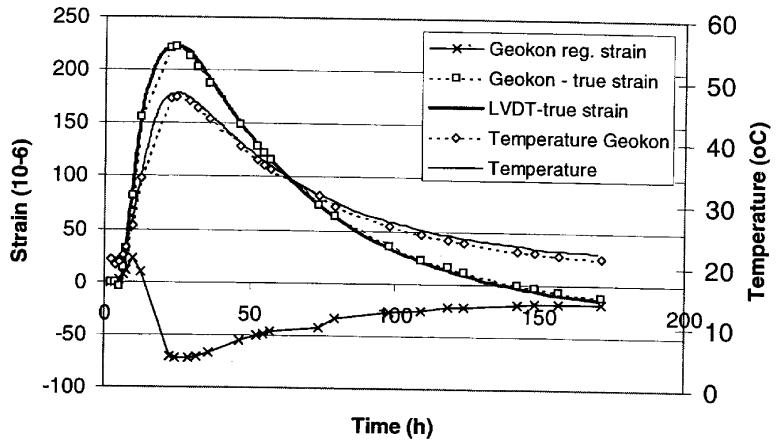

Figure 7.4: True strains measured by Geokon vibrating wire strain gauges and LVDT in the free deformation rig. The true strains for Geokon strain gauges are determined by assuming α_T = 11.2E-6 (from Heimdal 1999)

7.2.3 Field test results

Section 2

Section 2 has a bottom slab under the whole width of the culvert, see Figure 7.2. Foundation slab, outer wall and top slab were instrumented. All four gauge types were used in the wall, whereas the foundation and the top slab were instrumented with Geokon vibrating wires only. The main objective of the instrumentation was to investigate the correlation between the different types of gauges, and to study how the strains vary along the structures.

The positions of the gauges in the wall and the foundation are shown in Figure 7.5. All gauges were located in the mid plane of the wall.

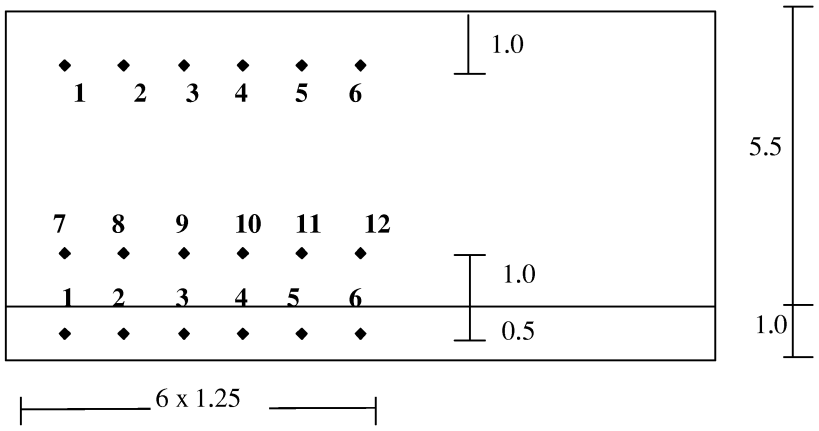

Figure 7.5: Location of the strain gauges in the wall and foundation in section 2.

Strain gauges used in the wall, according to Figure 7.5 are:

Position 6 and 12: All four types of the strain gauges

Position 5 and 11: Only Geokon vibrating wire

Position 4 and 10: Glued and welded strain gauges

Position 1, 2, 3, 7, 8 and 9: Geokon vibrating wire, glued and welded strain gauges

The temperatures were measured by thermistors incorporated in the Geokon vibrating wire gauges, and results of measurements are shown in Figure 7.6 and Figure 7.7.

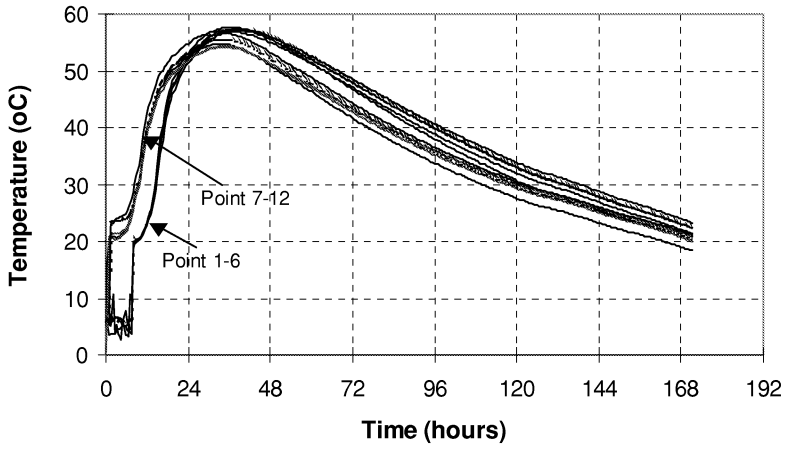

Figure 7.6: Recorded temperature development in the wall

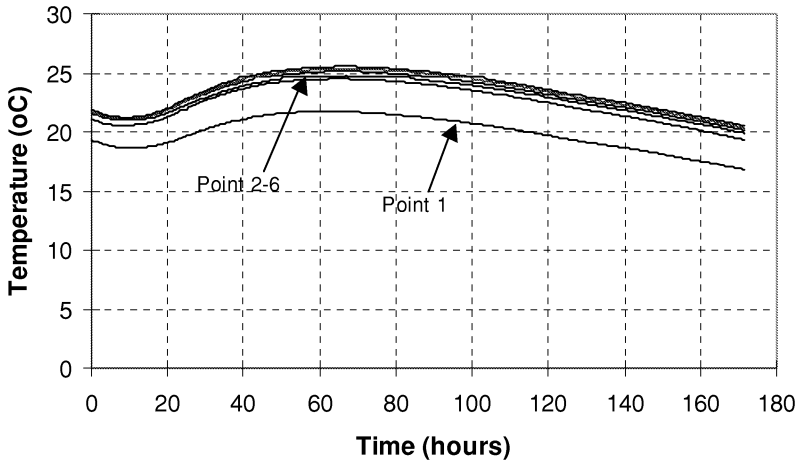

Figure 7.7: Recorded temperature development in the foundation slab

It can be seen that the temperature variation along the wall is very small - temperature difference between the mid-section and the section 1.25 m from the end is approximately 3^0C. Also the casting history can be seen from Figure 7.6 where the time difference between starting temperature in the bottom and in the top of the wall is about 7 hours.

Figure 7.8 presents the true strains in point 6 for the four different types of strain gauges. The strains are set to zero 14 hours after casting start i. e. six hours after strain gauges had come into contact with concrete. For the NGI strain gauges no data were available before 22 hours after casting start. To be able to include this type of gauges in the comparison, data were zeroed in that way that the first recorded value was equal to the welded strain gauges value. The new, corrected thermal dilation coefficients were used in comparison: $\alpha_T = 11.2 \times 10^{-6}$ for Geokon vibrating wire, $\alpha_T = 10.5 \times 10^{-6}$ for welded strain gauges, $\alpha_T = 12 \times 10^{-6}$ for glued gauges and NGI strain gauges. The glued strain gauges results differ from the other types gauges results significantly. The welded strain gauges and the Geokon vibrating wire strain gauges agree within $\pm 50 \times 10^{-6}$.

According to (Heimdal 1999), the main reason for the deviation between the different measuring methods is strain incompatibilities between reinforcement and concrete first hours after casting. Geokon vibrating wires, glued and welded strain gauges monitor strains in the reinforcement, which may differ from concrete strains due to slip between concrete and reinforcement.

The walls in section 18 has also been instrumented with all four types of gauges in order to explore the correlation between them. In this case also the glued strain gauges had a large deviation from the other ones, whereas a good correlation has been found between the welded strain gauges and the Geokon vibrating wire strain gauges. Since the Geokon

vibrating wire strain gauge is inexpensive, simple to handle and install, it was decided to continue instrumentation with this type of instrument.

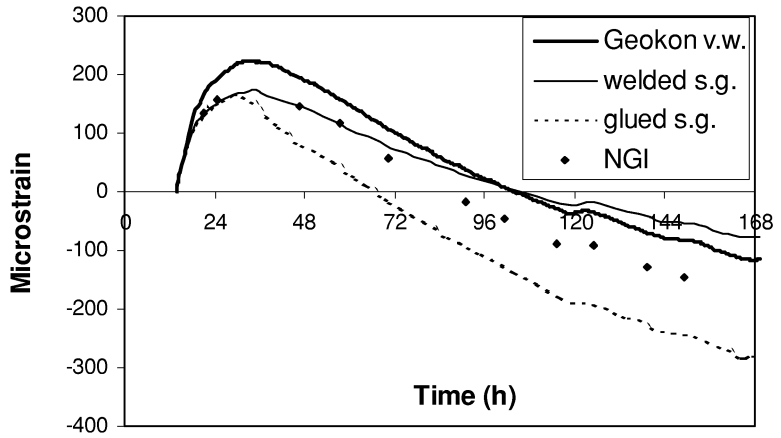

Figure 7.8: True strains in point 6 (top of the wall) recorded with four different types of strain gauges

In Figure 7.9 the true strains in the wall and the foundation slab registered by Geokon vibrating wires are presented. The strains are set to zero 6 hours after the gauges came into contact with concrete.

a)

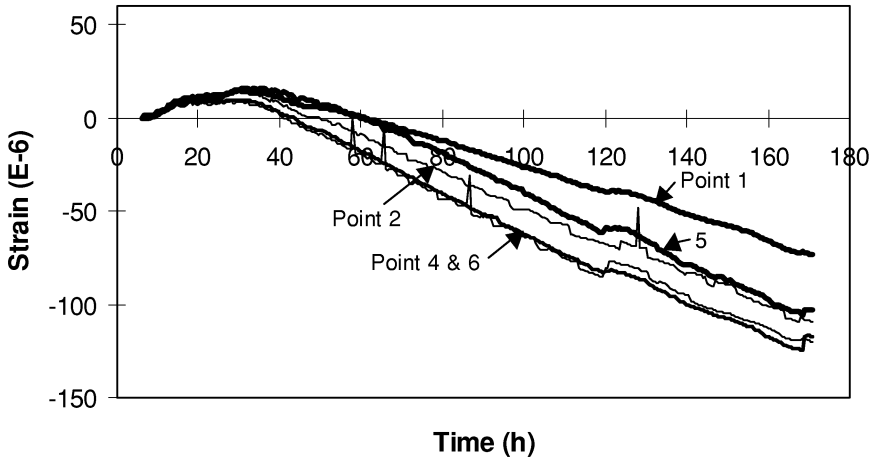

b)

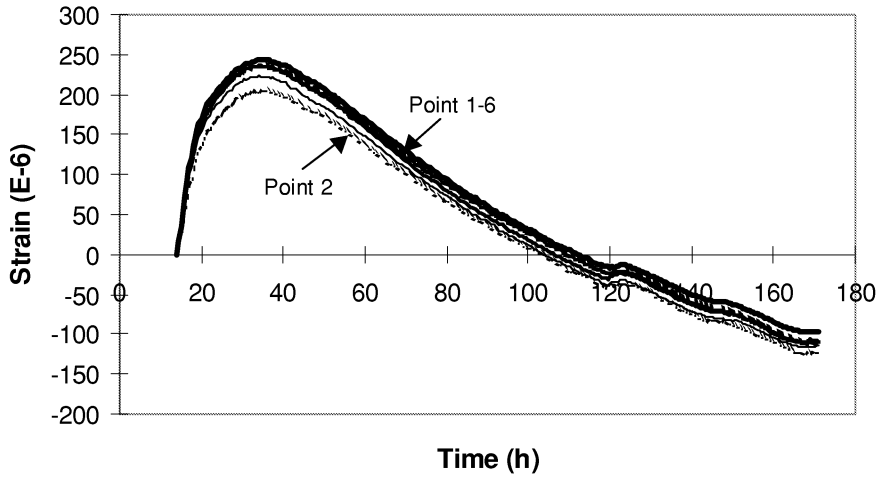

c)

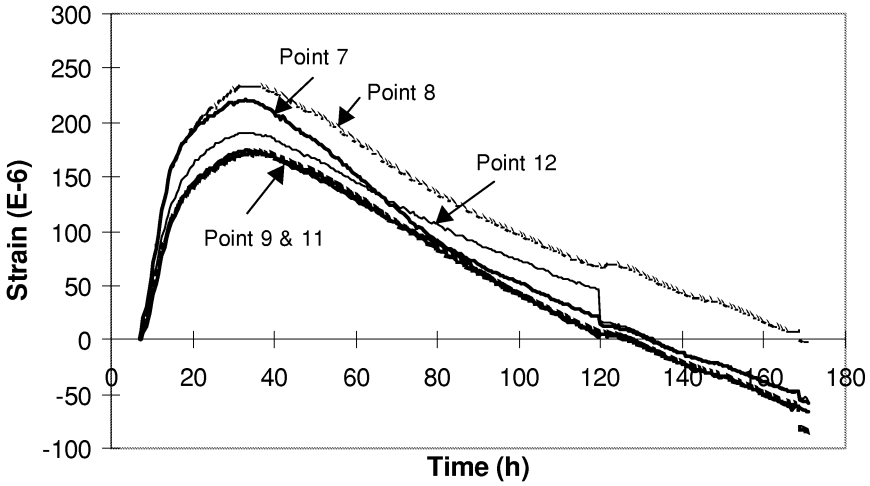

Figure 7.9: True strains recorded by Geokon's vibrating wires in a) the foundation slab, b) the top of the wall, c) the bottom of the wall

As Figure 7.9 shows, there is a small difference between strain development in different points in the top of the wall. On the contrary, there is a larger variation between the strains in the bottom. The strains are largest in point 7 and 8, which are closest to the wall's end. The cracks appeared in the wall, but the crack pattern was not observed for this section.

Section 42

The section 42 has a strip foundation under the walls and the cross-section is shown in the Figure 7.10.

The main objectives were to investigate the strain variation across the height of the structure at different distances from the end, and the possible slip in the joint. Section was instrumented only with Geokon vibrating wires, and the positions of the gauges are given in the figure. Since the foundation was cast several weeks before the wall, the concrete was hardened at the instrumentation time. The strains in the foundation were measured by the extensiometer, but for some reasons, recording gave unreliable results. Therefore they are not included in comparison, and it is difficult to identify the possible slip in the joint.

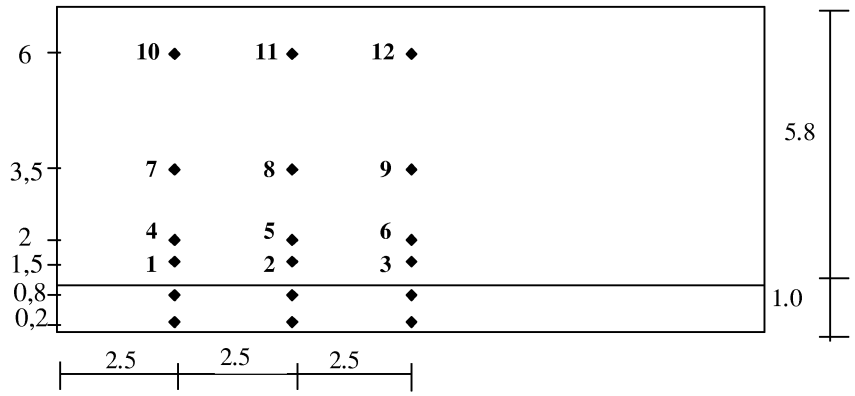

Figure 7.10: Locations of the strain gauges in the middle plane of the wall

The temperatures were measured by the built-in thermistor temperature sensors in the strain gauges and shown in the Figure 7.11.

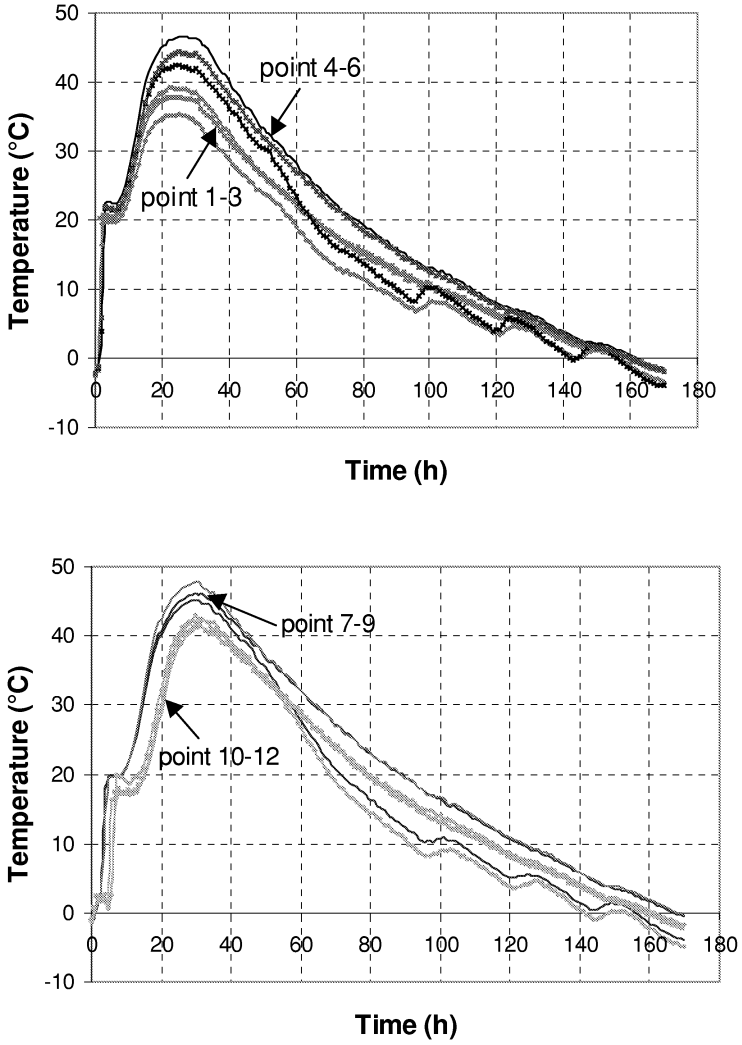

Figure 7.11: Temperature development in the wall, section 42

The time difference in casting between the bottom and the top of the wall is in this case about 5 hours.

Figure 7.12 shows the true strains in the wall of the section 42. As it can be seen, some difficulties were experienced in the recording, and results in point 3, point 12, and partly in point 6 were lost.

The crack pattern in the wall is shown in Figure 7.13. The cracks were observed from the floor, which is 40 cm over the bottom of the wall.

a)

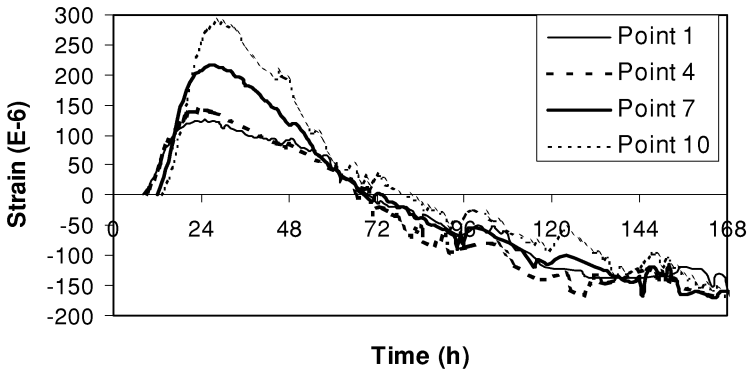

b)

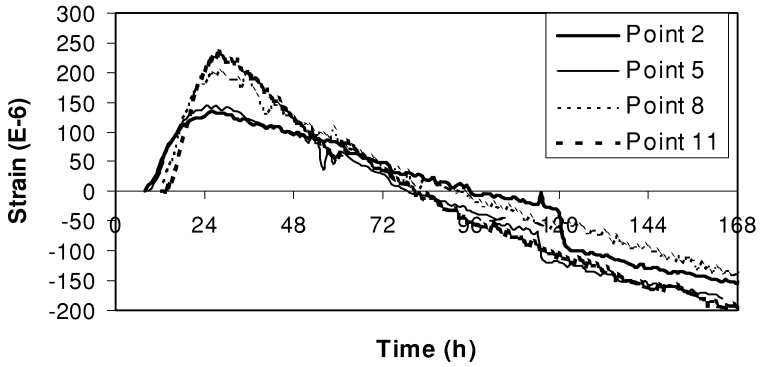

c)

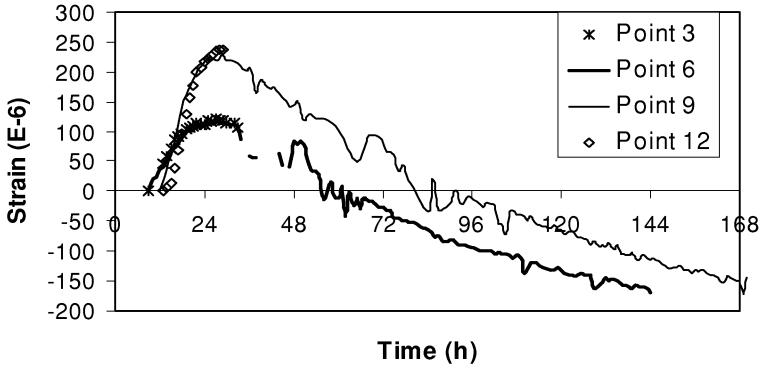

Figure 7.12: True strains in the wall a) 2.5 m from the end, b) 5 m from the end, c) middle of the wall

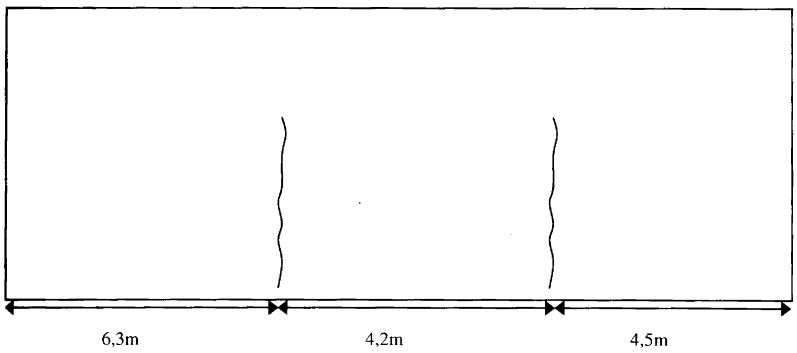

Figure 7.13: The crack pattern in the Section 42 , from (Thomassen 1999)

7.3 Concrete properties

The mix design of the concrete used in the Maridal culvert is given in Table 7.1.

Material	**Content [kg/m^3]**
Cement, OPC Type CEM I 52.5	350
Silica fume	18
Plasticizer, Sika BV 40	4.0
Superplastiziser, Sikament 92	3.0
Aer, Sika AER	0.7
Svelvik Sand 0-8 mm	953
Svelvik Gravel 8-14 mm	206
Svelvik Gravel 14-24 mm	658
Total water content	154.4
Water/binder-ratio	0.40

TABLE 7.1: Mix design for the Maridal concrete

A comprehensive laboratory test program has been performed at NTNU to identify input parameters for the numerical calculation. Both thermal and mechanical properties have been tested and test program and results are described below.

7.3.1 Thermal properties

Within the NOR-IPACS project a Round-Robin test program on activation energy and heat release of the Maridal concrete was carried out. The main goal was to test the reproducibility of the experimental results determined in different laboratories. Five participants were involved: Selmer, Elkem, Norcem, NTNU, and SVV, and different test set-ups were used. A detailed description of the procedures is given in (Helland 2000)

First, activation energy parameters have been found from the compressive strength tests at different hardening temperatures. The Norwegian Code (NS 3656) prescribes isothermal testing at three temperature levels: 5, 20, and 50^0C. The results from the isothermal strength tests were plotted against equivalent time. Then, activation energy parameters were found by fitting results at the level of 40% of maximal strength, see Figure 7.14. Activation energy is modelled according to expression(3.6).

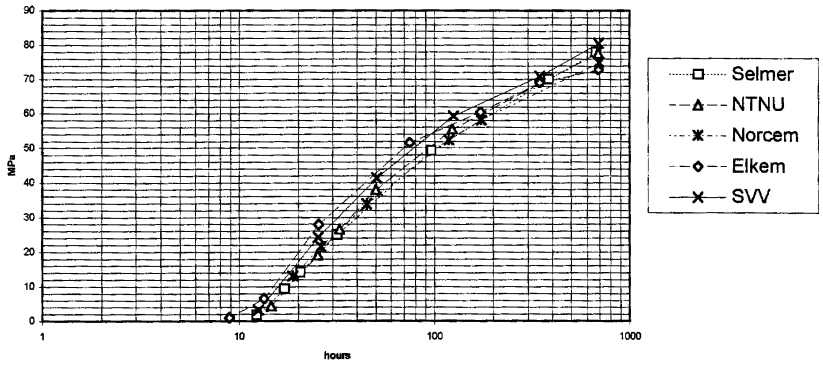

Figure 7.14: Strength development versus maturity, determination of the activation energy parameters, from (Helland 2000)

In addition to these standardized tests, the strength development was determined on test specimens exposed to realistic temperature history. This was done to investigate whether the activation energy parameters determined from the isothermal tests also can be used to describe the effect of the realistic temperature history. Temperature histories are shown in Figure 7.15.

In this approach, model parameters for strength development have been found first from the isothermal tests on 20^0C. Then, activation energy parameters have been determined by fitting strength development from the tests with realistic temperature histories to the model, using the least squares method, see Figure 7.16.

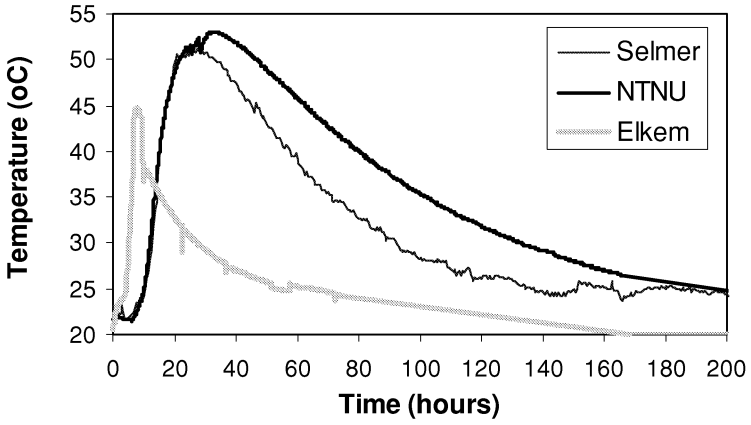

Figure 7.15: Temperature history for semi-adiabatic strength development

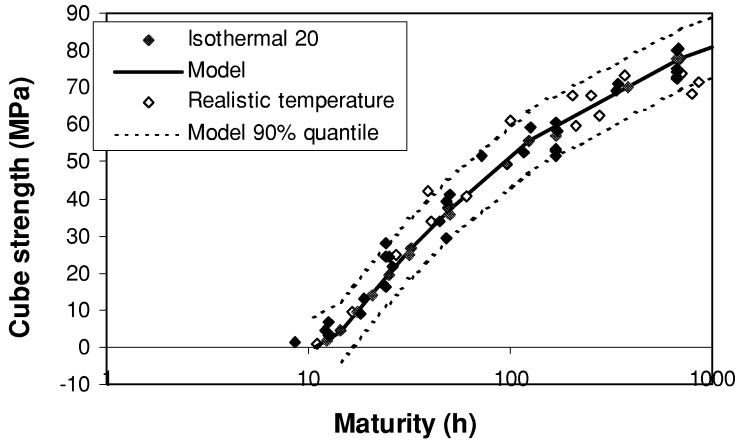

Figure 7.16: Compressive strength development, model and experimental results

The results from both methods are shown in Table 7.2. As it can be seen, there is no significant difference between these two methods, and results according to the NS3656 will be used in calculations.

	NTNU	SELMER	ELKEM	SVV	NORCEM	Average
NS3656	E_a=26867 E_b=987	E_a=26177 E_b=892	E_a=26332 E_b=1518	E_a=23046 E_b=1483	E_a=25528 E_b=1100	E_a=25588 E_b=1196
Realistic temper.	E_a=26613	E_a=26480	E_a=25491			E_a=26195

TABLE 7.2: Activation Energy parameters

The activation energy parameters are also used for the determination of the hydration heat parameters. The Freiesleben-Hansen heat function (3.11) is used in the temperature analysis and the model parameters are determined from the semi-adiabatic test. Measured concrete temperatures are converted to produced heat by compensating for the heat loss from the insulated concrete to the surroundings. The heat loss may be determined in two ways:

1. By use of a measured value of the cooling ratio
2. By calculating the cooling ratio under the assumption of negligible heat production during a certain time interval. In this test the criterion was: average dQ/dt < 0.1 kJ/kg h between 150 and 200 maturity hours, see (Smeplass 2000).

Results of both methods are presented in Table 7.3. The mean values of the isothermal heat calculated in two ways are plotted in the Figure 7.17.

The difference between two methods is negligible.

	NORCEM	**NTNU**	**Selmer**	**SVV**	**Elkem**	**Average**
Calculated cooling ratio						
Q_∞	296	352	382	356	406	353
τ	13.29	17.84	16.33	16.31	16.65	16
α	1.74	1.44	1.46	1.5	1.32	1.51
Measured cooling ratio						
Q_∞	339	349	381	322	345	347
τ	14.57	18.04	16.38	14.98	14.94	15.88
α	1.4	1.44	1.45	1.91	1.68	1.56

TABLE 7.3: Hydration heat development parameters

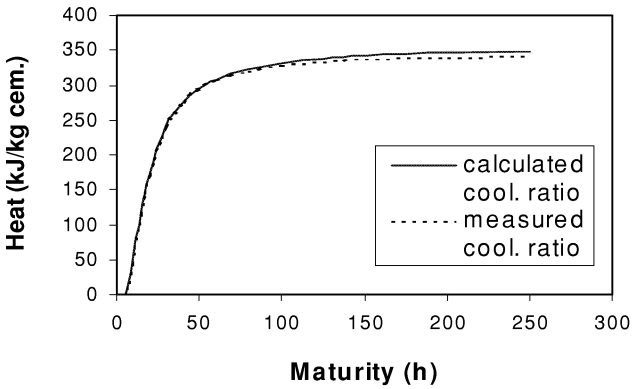

Figure 7.17: Mean values of the isothermal heat development calculated by two different methods (calculated and measured cooling ratio)

The deviations in the results from the different partners can be explained by variations in concrete mix, mixing procedure, and test set-up.

The isothermal heat development obtained by using calculated cooling ratio is presented in Figure 7.18 together with the mean value and the 90% quantile (Q_{90}= Q_{mean} ± 1.38 x st.dev.).

The curve which represents the mean value of the hydration heat development will in subsequent sections be used as input to the temperature calculations of the culvert.

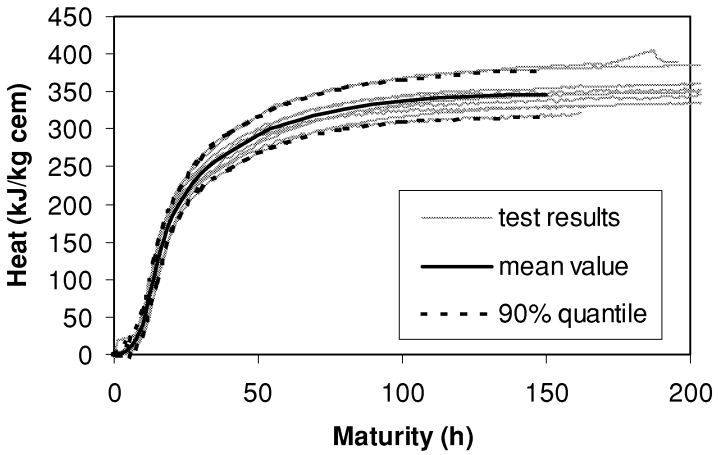

Figure 7.18: Hydration heat development, experimental results

The other concrete thermal properties used in the calculations are: thermal conductivity: 2.2 J/ms^{0}C, and heat capacity: 1100 J/kg^{0}C

7.3.2 Mechanical properties

E-modulus and strength development

The modified version of the CEB-FIP MC1990 equation (7.2) is used to describe the development of the compressive strength, tensile strength, and modulus of elasticity:

$$f_c(t_e) = f_c(28) \cdot \exp\left[s \cdot \left(1 - \sqrt{\frac{28}{t_e - t_0}}\right)\right]$$

$$f_t(t_e) = f_t(28) \cdot \left\{\exp\left[s \cdot \left(1 - \sqrt{\frac{28}{t_e - t_0}}\right)\right]\right\}^{n_t}$$

$$E_c(t_e) = E_c(28) \cdot \left\{\exp\left[s \cdot \left(1 - \sqrt{\frac{28}{t_e - t_0}}\right)\right]\right\}^{n_E} \tag{7.2}$$

The parameters s and t_0 are common for all three properties, and were determined from the compressive strength tests, whereas parameters n_t and n_E were determined from the tensile strength and E-modulus tests, respectively.

A large amount of data for the compressive strength exists, due to the previously described Round-Robin test for activation energy and other tests performed on the "in situ concrete" and in the laboratory at NTNU (Figure 7.19).

The tensile strength has been determined indirectly from tensile splitting tests. In (Kanstad 1999) the following relations between uniaxial tensile and splitting strength of cylinders or cubes were found, applying linear regression analysis on a large amount of data:

100x200 mm cylinders:

$$f_t = 0.7 \cdot f_{ts} + 0.87 \tag{7.3}$$

100 mm cubes:

$$f_t = 0.76 \cdot f_{ts} + 0.20 \tag{7.4}$$

where f_{ts} is the splitting strength and f_t is the uniaxial tensile strength.

Test results from the splitting tests are transferred to the uniaxial tensile strength, and the model parameters are found by curve fitting.

E-modulus tests in compression were also carried out in the laboratory at NTNU. The procedure is described in (Kanstad 1999), where it was assumed that E-modulus in compression is equal to E-modulus in tension.

Figure 7.20 and Figure 7.21 present test results for tensile strength and E-modulus versus time.

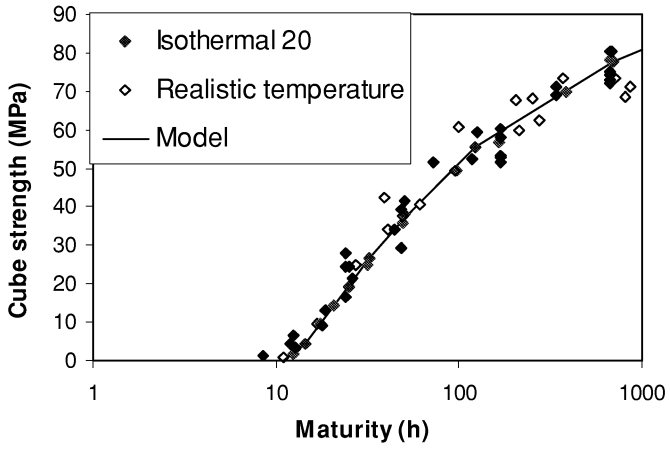

Figure 7.19: Compressive strength development, model and experimental data, data from (Helland 2000)

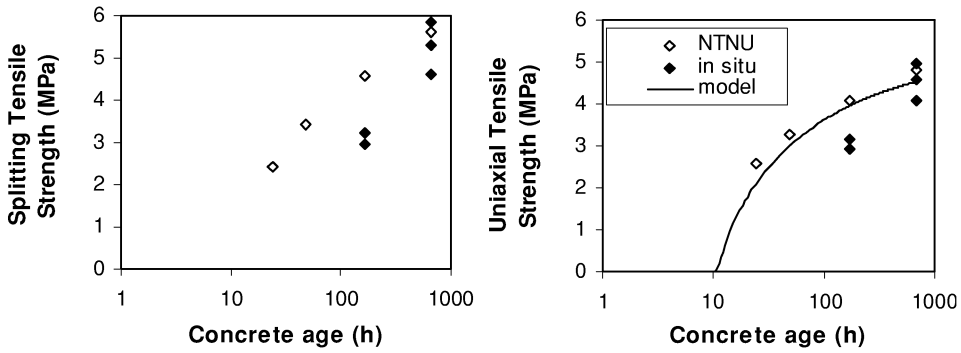

Figure 7.20: Tensile strength development, model and experimental data, from (Kanstad 1999a). Each marks represents 2-6 specimens.

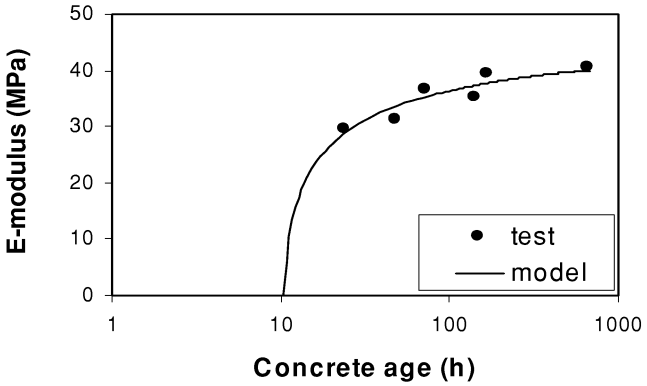

Figure 7.21: E-modulus development, model and experimental data

The following model parameters were determined:
$f_c(28)$ = 75.8 MPa, t_0 = 10, s = 0.210,
$E_c(28)$ = 40005 MPa, n_E = 0.278,
$f_t(28)$ = 5.23 MPa, n_t = 0.624

Creep
Double Power Law creep model is used in numerical simulations:

$$J(t,t') = \frac{1}{E(\tau)}(1 + \varphi_0 \cdot \tau^{-d}(t-\tau)^p) \tag{7.5}$$

Whereas the E-modulus was determined from the mechanical test programme, the creep model parameters φ_0, p, and d were determined from creep tests in compression. Cylinders with a diameter of 150 mm, and a length of 300 mm were cured at 20^0C before loading. The specimens were sealed to prevent drying shrinkage. Two specimens were loaded at the same time, and accompanied by one dummy specimen to compensate for autogenous shrinkage. A more detailed test procedure is given in (Atrushi 2000). In Figure 7.22 it is seen that the model is in reasonable agreement with experimental results when the creep parameters: φ_0 = 0.9, $d = p$ = 0.32 are used.

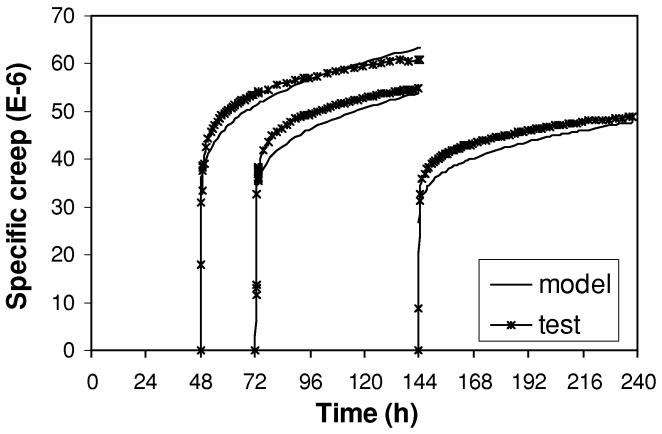

Figure 7.22: Creep curves for different loading times, model and experimental results

TSTM tests

In order to test the material models and the solution method, TSTM experiments have been performed in the laboratory (Bjøntegaard 1999). Three tests with different temperature histories have been carried out. Temperature histories measured in the middle of the wall in section 2 and section 42 have been used in two of them (Figure 7.23-a. and Figure 7.23c., respectively. The temperature history used in the third test (Figure 7.23-b.) is representative for the BASE concrete which has similar thermal properties as the Maridal concrete.

To avoid cracking the 100% restraint was turned off after two days, and a more realistic stress history of a partly restrained structures was obtained. The free deformation after this time was recorded in test, and used in the subsequent calculation.

In parallel with the TSTM test, the total free deformation was measured in the free deformation rig for the same temperature history.

Assuming constant value for the thermal dilation coefficient, α_T = 8.0E-6 $/^0$C, the autogenous deformation can be determined from the shrinkage-rig by subtracting the thermal dilation from the total deformation. The simplification about constant α_T does not introduce any significant error in the calculations as far as the sum of thermal strain and autogenous deformation is correct for temperature histories similar to the tested ones.

Total deformation from the shrinkage rig and free deformation from the stress rig are presented in the Figure 7.24.

a)

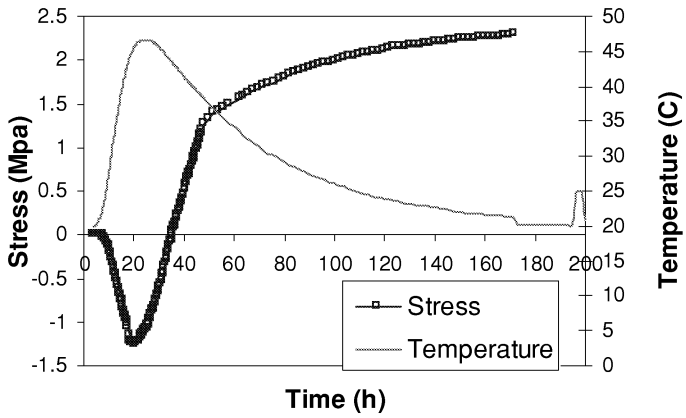

b)

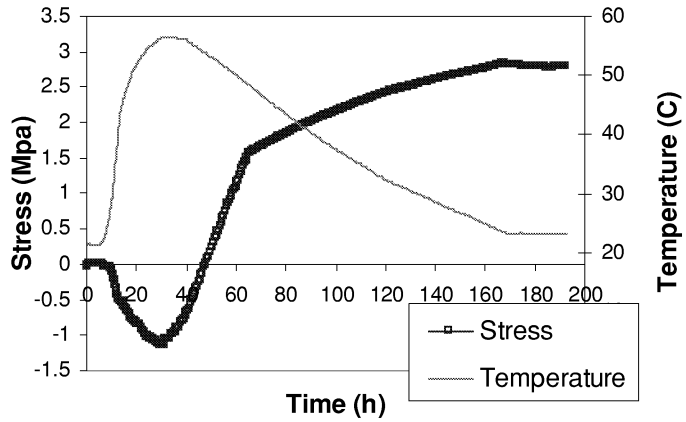

c)

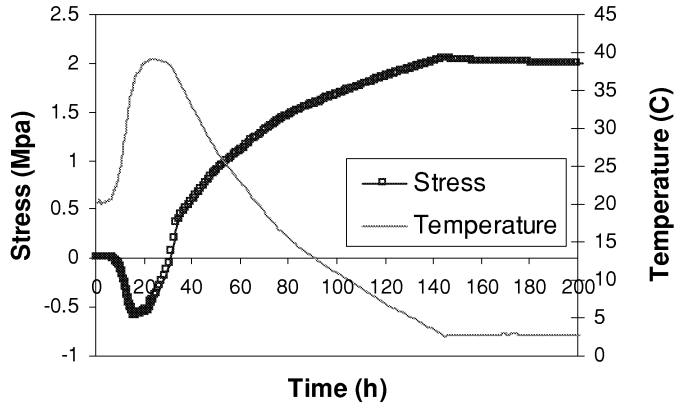

Figure 7.23: Imposed temperature and measured stresses in TSTM

a)

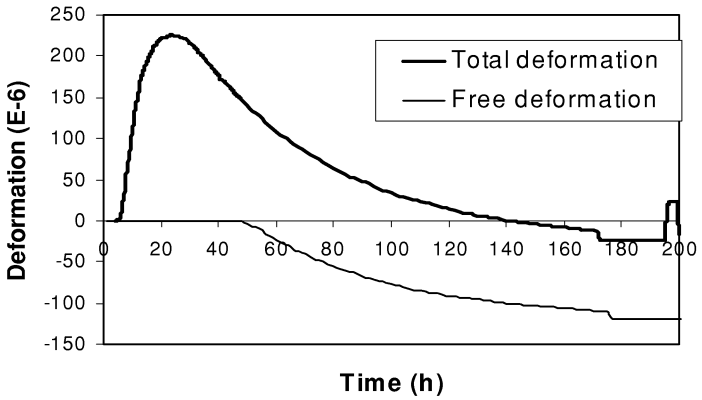

b)

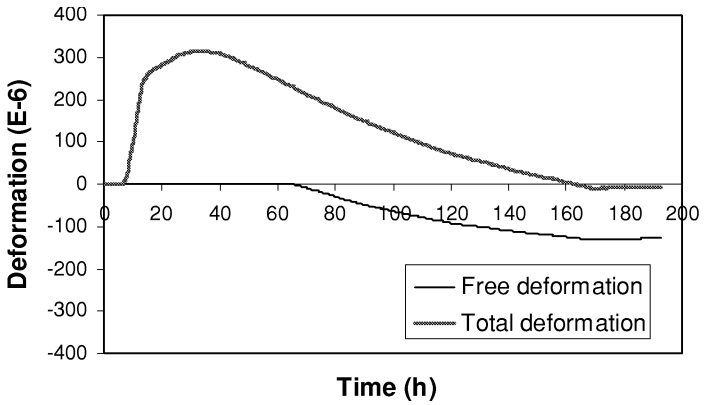

c)

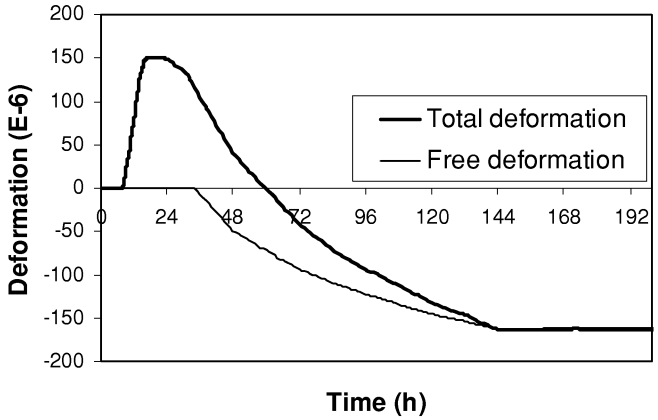

Figure 7.24: Measured total deformations and free deformations for different temperature histories a) $T_{max} = 47^0C$, b) $T_{max} = 56^0C$, c) $T_{max} = 39^0C$

The stresses are calculated as previously described in Section 4.3.4 . The first intention was to obtain the creep model parameters from the TSTM tests, but this approach failed from the reasons described in Chapter 5. Therefore the creep model parameters have been found from isothermal creep tests in compression. The transient creep term (3.31) is included in calculations and the parameters are found from the TSTM tests by fitting calculated stresses to the measurements. The results are compared to the experimental data in Figure 7.25.

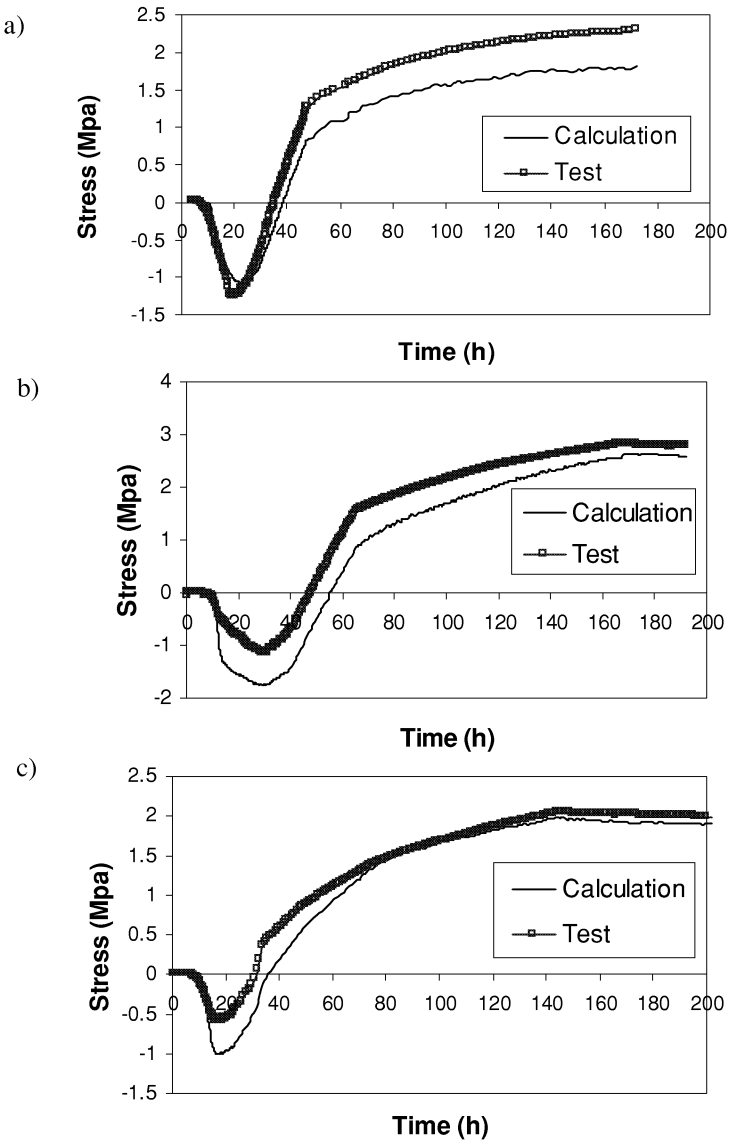

Figure 7.25: Stress development in concrete specimen in TSTM, experimental data and numerical simulations a) $T_{max} = 47^0$C, b) $T_{max} = 56^0$C, c) $T_{max} = 39^0$C

Discussion of results

Figure 7.25 shows measured and calculated stresses of partly restrained concrete for different temperature histories. In general the numerical results are lower than the measured results. Discrepancy between calculations and measurements seems to be generated from the beginning of the stress development. At the time when the 100% restraint was turned off, the calculated stresses were approximately 0.5 MPa lower than the measured stresses in all three tests. After one week the differences between calculated and measured tensile stresses are: 0.44MPa (19%) for the test with $T_{max} = 47^0C$, 0.28MPa (10%) for the test with $T_{max} = 56^0C$, and 0.09 MPa (4%) for the test with $T_{max} = 39^0C$. The difference is largest for the test with $T_{max} = 56^0C$.

Generally, discrepancies between calculations and measurements are larger than in the case of the BASE concrete, see Figure 3.3. The two concretes are quite similar with w/b = 0.4, 5% silica fume and the same cement type. The Maridal concrete, however, has about 15% higher stiffness than the BASE concrete mainly because aggregate type, content, and grading are different: the maximum aggregate size for the BASE concrete is 16 mm, while for Maridal concrete it is 24 mm. The higher aggregate content makes the Maridal concrete more difficult to work with in laboratory tests then the BASE concrete.

On the other hand, the reliability of the TSTM test results for the Maridal concrete with maximum temperature $T_{max} = 56^0C$ may be questioned, since the stress development does not seem to be logical when compared to the test with $T_{max} = 47^0C$. Due to the higher maximal temperature ($T_{max} = 56^0C$), free deformation ($\varepsilon_T + \varepsilon_{AD}$) measured on the unrestrained specimen is significantly larger than the free deformation for $T_{max} = 47^0C$, see Figure 7.24. In spite of that fact, the compressive stress developed in the TSTM with full restraint is lower than compressive stress for $T_{max} = 47^0C$. There is no logical explanation for that at the present time. Since the test results for $T_{max} = 47^0C$ are in good correspondence with the test results for the BASE concrete with the same temperature history (Bjontegaard, 1999), there is no reason to distrust these results. Therefore a new attempt to calibrate transient creep parameter ρ was done, this time without the test with $T_{max} = 56^0C$. Surprisingly, the parameter did not change ($\rho = 0.36$).

The discrepancy between calculations and measurements in two other tests does not follow the same trend: in the test with $T_{max} = 47^0C$ the agreement between calculations and measurements is good in the compression phase, and poor in the tension phase. The opposite is truth for the test with $T_{max} = 39^0C$, which makes it difficult to identify reasons for the disagreement between numerical and experimental results.

7.4 Numerical simulation

7.4.1 Section 42

Figure 7.26 shows the cross-section of the wall in section 42. The length between the joints is 15 m.

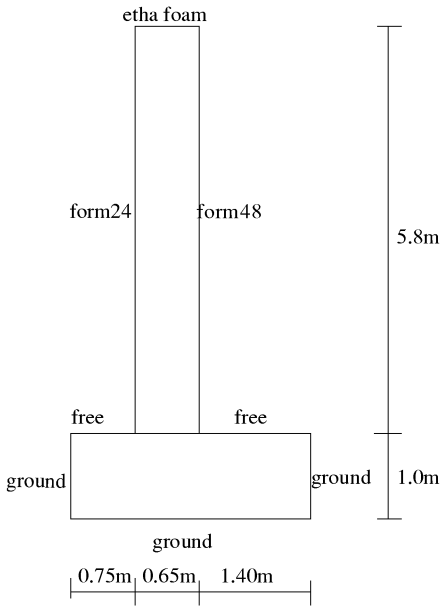

Figure 7.26: Cross section of the wall in section 42

The actual external conditions on the construction site are used for the temperature calculations. The formwork, plywood with 21 mm thickness, was removed from one side of the wall 24 hours after casting and from the other side after 48 hours. The top of the wall was covered by the insulation Etha foam with10mm thickness. The wind velocity is assumed to vary from 0 to 2 m/s, which gives the following convectivities for the concrete surface:

Wind velocity 4 m/s + formwork, convectivity = 0.00404 kJ/m^{2}s^{0}C

Wind velocity 2 m/s + formwork, convectivity = 0.00361 kJ/m^{2}s^{0}C

Wind velocity 4 m/s + insulation, convectivity = 0.0036 kJ/m^{2}s^{0}C

Wind velocity 2 m/s + insulation, convectivity = 0.0031 kJ/m^{2}s^{0}C

Wind velocity 0 m/s + insulation, convectivity = 0.0023 kJ/m^{2}s^{0}C

Wind velocity 4 m/s + free surface, convectivity = 0.0211 kJ/m^{2}s^{0}C

Wind velocity 2 m/s + free surface, convectivity = 0.0133 kJ/m^{2}s^{0}C

Wind velocity 0 m/s + free surface, convectivity = 0.0055 kJ/m^{2}s^{0}C

Concrete towards ground, convectivity = 0.139 kJ/m^{2}s^{0}C

The air temperature was recorded, and the fresh concrete temperature planned to be 20^{0}C. The foundation was cast several weeks before the wall, and the concrete in the foundation assumes to be hardened when the wall is cast. The section was cast on a 20 cm thick compacted gravel layer, and 5 cm thick blinding of concrete.

To describe the effect of the casting history, the wall is modelled in two phases with 4 hours' time difference.

Figure 7.27 shows the element model used in the analysis. Because of the symmetry only one half of the wall is modelled

.

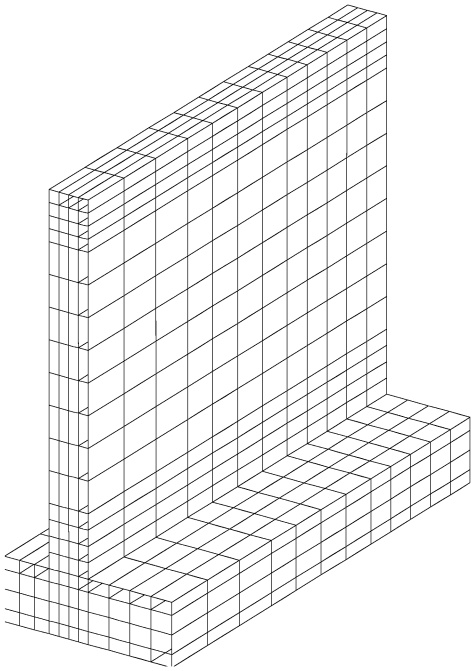

Figure 7.27: FE model for the wall in section 42

7.4.2 Section 2

The wall is founded on the slab, see Figure 7.28.

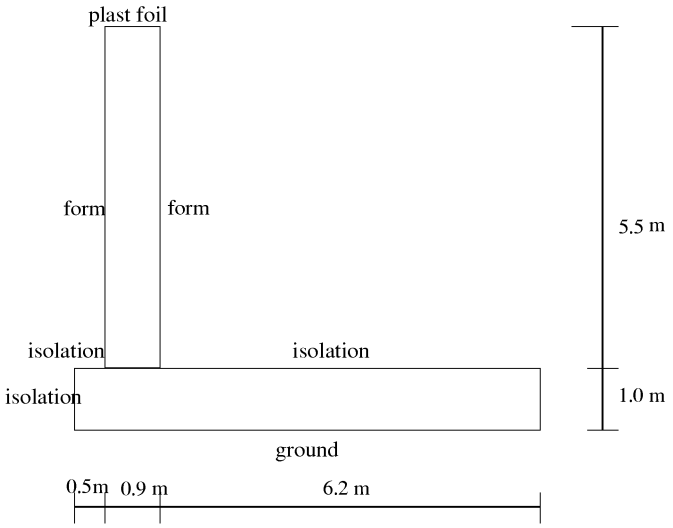

Figure 7.28: Cross section of the wall in section 2

For this section the formwork, plywood with 21 mm thickness, was removed after one week. The top of the wall is covered by plastic foil. The foundation slab was cast one week before the wall, and covered by the insulation Etha foam with 10 mm thickness to preserve hydration heat. When the wall was cast the slab temperature was about 20^0C. The wind velocity varied from 0 to 1 m/s, which gives the following convectivities:

Wind velocity 0 m/s + formwork, convectivity = 0.0026 kJ/m^{2}s^{0}C

Wind velocity 1 m/s + formwork, convectivity = 0.0033 kJ/m^{2}s^{0}C

Wind velocity 0 m/s + insulation, convectivity = 0.0023 kJ/m^{2}s^{0}C

Wind velocity 1 m/s + insulation, convectivity = 0.0028 kJ/m^{2}s^{0}C

Wind velocity 0 m/s + plastic foil, convectivity = 0.0048 kJ/m^{2}s^{0}C

Wind velocity 1 m/s + plastic foil, convectivity = 0.0076 kJ/m^{2}s^{0}C

Also for this section the air temperature was recorded and given in (Heimdal 1999), and the fresh concrete temperature was planned to be 20^0C.

This section is also modelled in two phases with 4 hours' time difference, and FE model is shown in Figure 7.29.

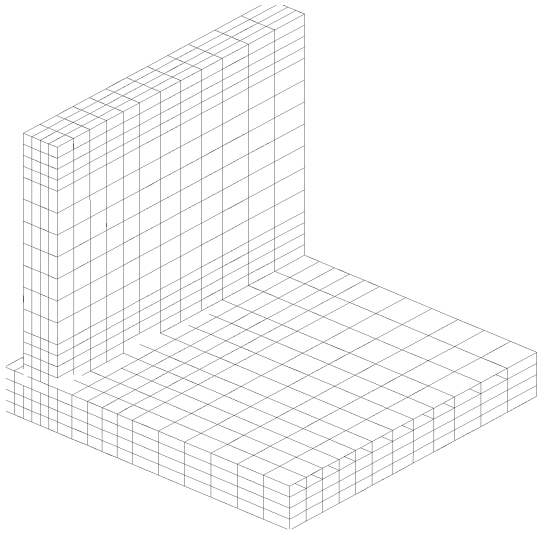

Figure 7.29: FE model for wall in section2

7.4.3 Temperature calculation

The temperature calculation is performed with a mean value of input data for the hydration heat development obtained from the Round-Robin test program, as described in Section 7.3.1 . The results for section 42 are shown in Figure 7.30, and for section 2 in Figure 7.31.

As it can be seen, the agreement between calculated and measured temperature in section 42 varies from the complete overlapping (point 6), to the difference of about 4^0C (point 3 and point 12). In the wall from section 2 calculated results agree very well with the observations. In the slab the difference between calculated and measured temperature is less than 3^0C.

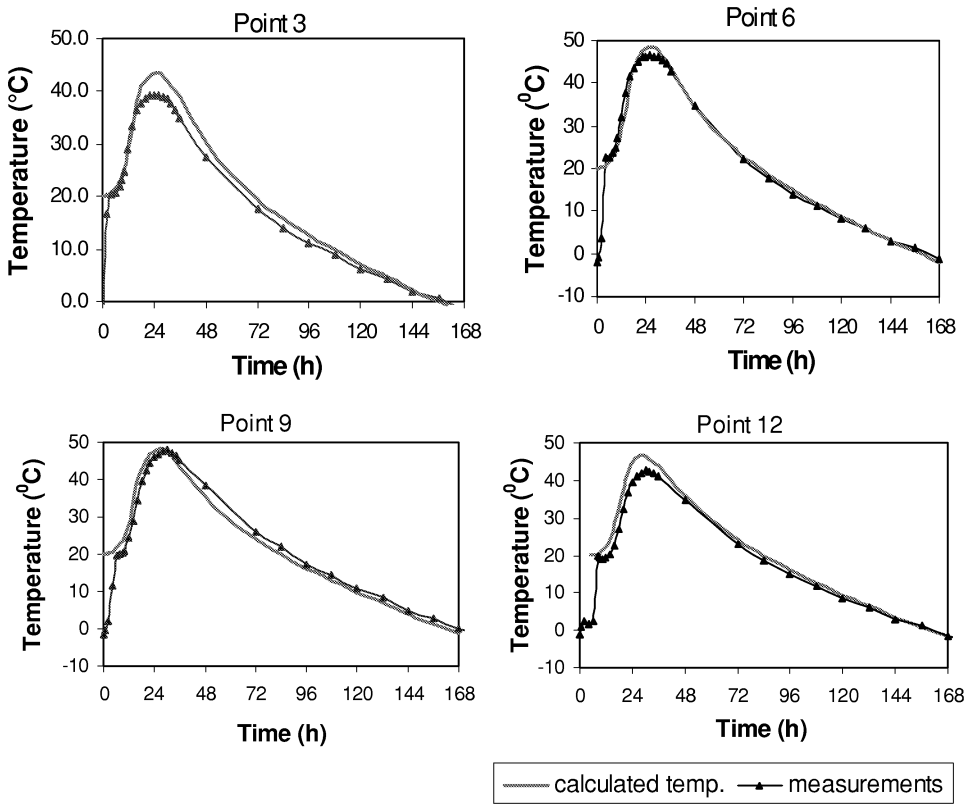

Figure 7.30: Calculated and measured temperatures in the middle of the wall in Section 42

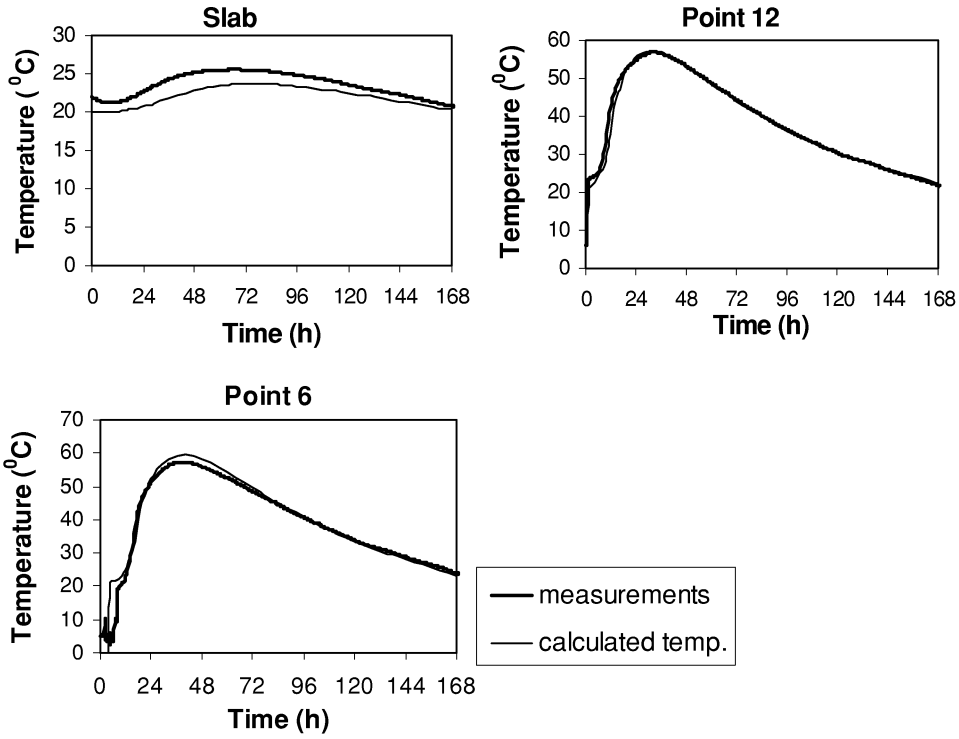

Figure 7.31: Calculated and measured temperatures in the middle of the wall in Sec. 2

7.4.4 Stress calculation

The same element model is used in both the temperature and stress calculation. To avoid spatially oscillation of stresses, the element used in stress analysis must have an order higher interpolation polynomial than the element in temperature analysis (see Chapter 4). Therefore quadratically interpolated elements with symmetrically spaced mid nodes are used in the stress analysis. The finite element calculation is carried out in 81 steps, starting with a step of 1 h up which increases to 4 h in the end. A Newton-Raphson iteration procedure is used with an energy norm as a convergence criterion set equal to 10^{-4}.

It is assumed that the E-modulus is 0 during the first 10 hours (equivalent time) after casting, Eq.(7.2). It means that the strains in this period result only from temperature changes (autogenous deformation is also 0 during this time) and that they are independent of restraint conditions.

In a numerical analysis it is not possible to have zero stiffness, and in stead of zero, a small value is used (the default value in DIANA is E_{min} =0.01 E_{28}). Together with the Double Power Law it results in spurious strains in the first hours after casting, and influences the stresses after long time, see Section 4.3.4 . The problem is solved by ignoring the thermal

strains in this period by setting $\alpha_T = 0$. After finishing the calculation the results are corrected manually, and the strains in the first 10 hours (when E = 0) are set equal to:

$$\varepsilon = \varepsilon_T = \alpha \Delta T \tag{7.6}$$

The equivalent time t_0, where the concrete starts developing measurable E-modulus, and consequently stresses, varies from point to point in a real structure due to local temperature variations. This cannot be taken into account in the present approach where the stresses in the whole structure are assumed to be zero before t_0. However, the consequences of using one t_0 for the whole structure are not significant, because in the first period of hardening, the temperature (and equivalent time) variation is not considerable throughout the structure. In the case when the structure is modelled in more phases, each phase has its own t_0.

Modelling of the restraint from the ground.

In this analysis the subgrade reaction modulus method is used to model the deformability of the ground.

In our case with rather stiff subgrade, the chosen value for the modulus of subgrade reaction is k_v = 60 MN/m^3 (Normaler, Vegbygging 018). If the vertical settlements of the structure are in compression, the k-value is constant. If the structure lifts up, $k_v = 0$, so-called "no tension" bedding.

The horizontal restraining forces from the ground are caused by friction between the ground and the foundation. For the sake of simplicity, the horizontal forces in the contact area between the structure and the ground are described by the modulus of subgrade reaction in the tangential direction. The value of 60 MN/m^3 is used in calculations (Petterson 1998).

Practical modelling of the subgrade stiffness is done by means of interface elements. These elements are quadratically interpolated, see Figure 7.32. The "lower" nodes, ground nodes, are fixed in all directions, and the "upper" nodes are common nodes for the structure and the interface element. The constitutive model for the interface element is shown in the Figure 7.32.

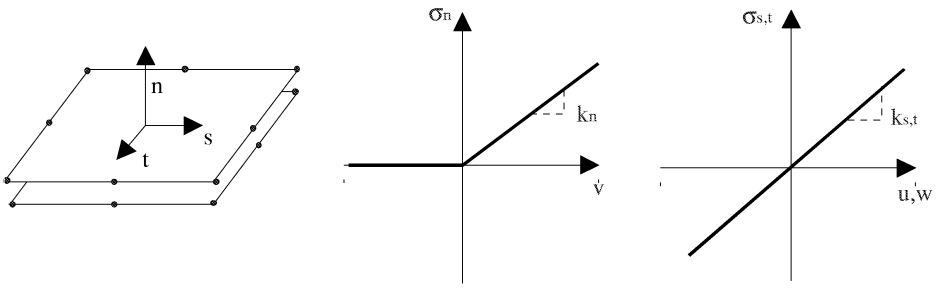

Figure 7.32: Interface element, constitutive model

A lumped integration schema for the interface elements is used since exact Gaus integration may lead to oscillations in the case of a large difference between the stiffness of the interface elements and the stiffness of the structure.

Calculation results for Section 42.

In simulation of stress and strain development it is assumed that no stresses can be generated before t_0 = 10 h, and that strains before this time originate from the temperature only. The same assumption is used for measured strains when they are compared to the simulation results, and measured strains are zeroed in a way that they are approximately equal to the calculated strains at the time $t = t_0$. In that way a mismatch between calculations and measurements in the first period of hardening is avoided.

As mentioned in Section 7.2.3 , the results of measurements in point 3, 12, and partly in point 6 are lacking. From Figure 7.12 it can be seen that there is no large variation in the strains in the longitudinal direction. Therefore the results from point 2, 5 and 11 are used instead in comparison.

In Figure 7.33 measured and calculated strain developments in the middle of the wall are presented. Corresponding stresses are shown in Figure 7.34.

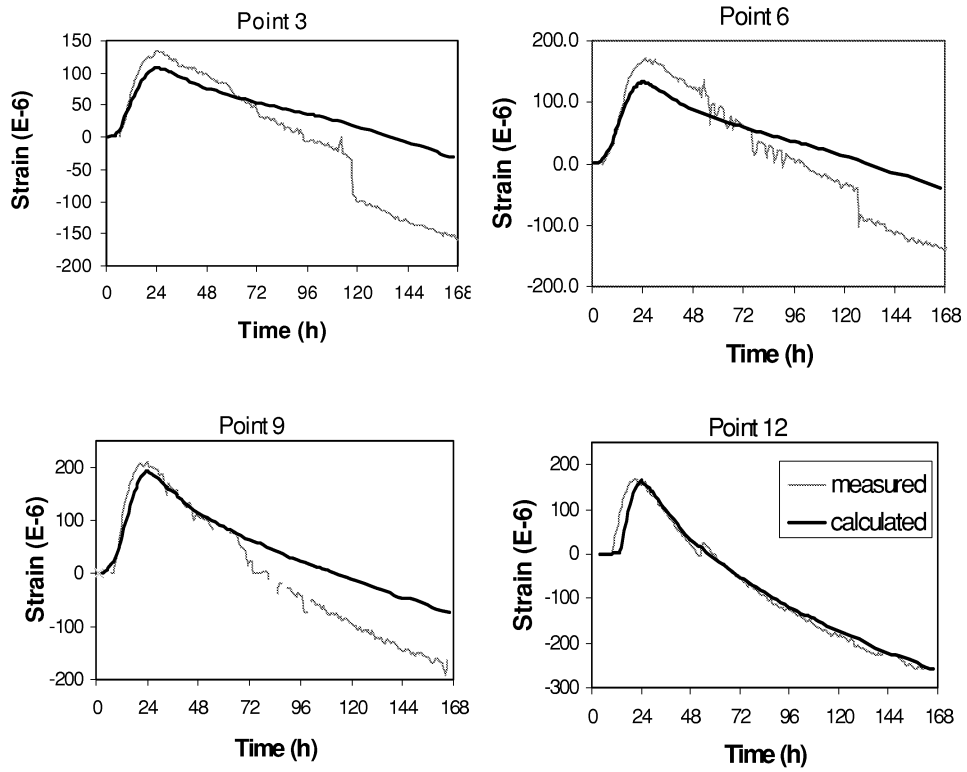

Figure 7.33: Calculated and measured strain development in the middle of the wall in Section 42

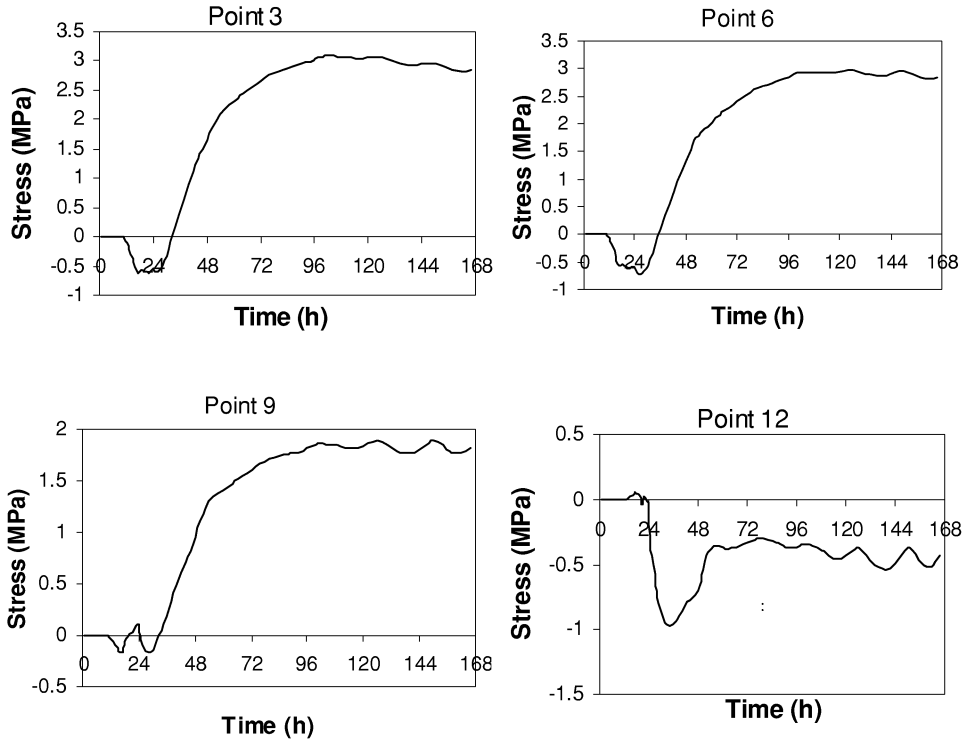

Figure 7.34: Calculated stress development in the middle of the wall in Section 42

The maximum tensile stress in the wall is in point 3. To estimate the through-cracking risk, the effective tensile strength development is calculated in this point, (see Section 2.4.4), and the crack ratio is:

$$\eta_{cr} = \frac{\sigma}{f_{cte}}$$

The cracking risk in the structure in different points of time is depicted in Figure 7.35. It can be seen that maximum cracking risk is 0.93.

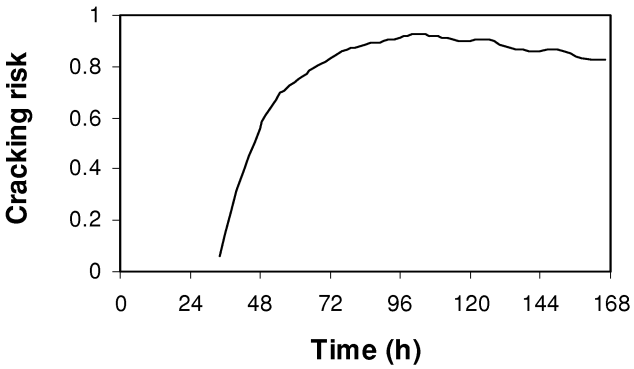

Figure 7.35: Cracking risk in the wall versus time

Calculation results for Section 2.

Calculated strain developments in the middle of the wall are presented in Figure 7.36 and Figure 7.37 together with the measurements. Stresses are shown in Figure 7.38. The measured strains are zeroed in the same way as for Section 42.

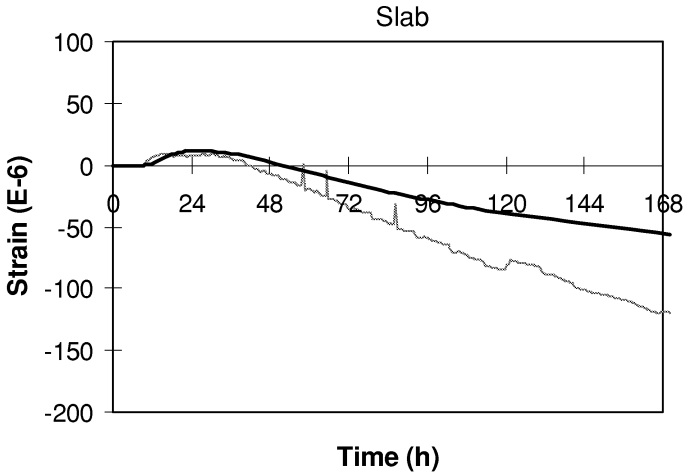

Figure 7.36: Measured and calculated strain development in the slab in section 2

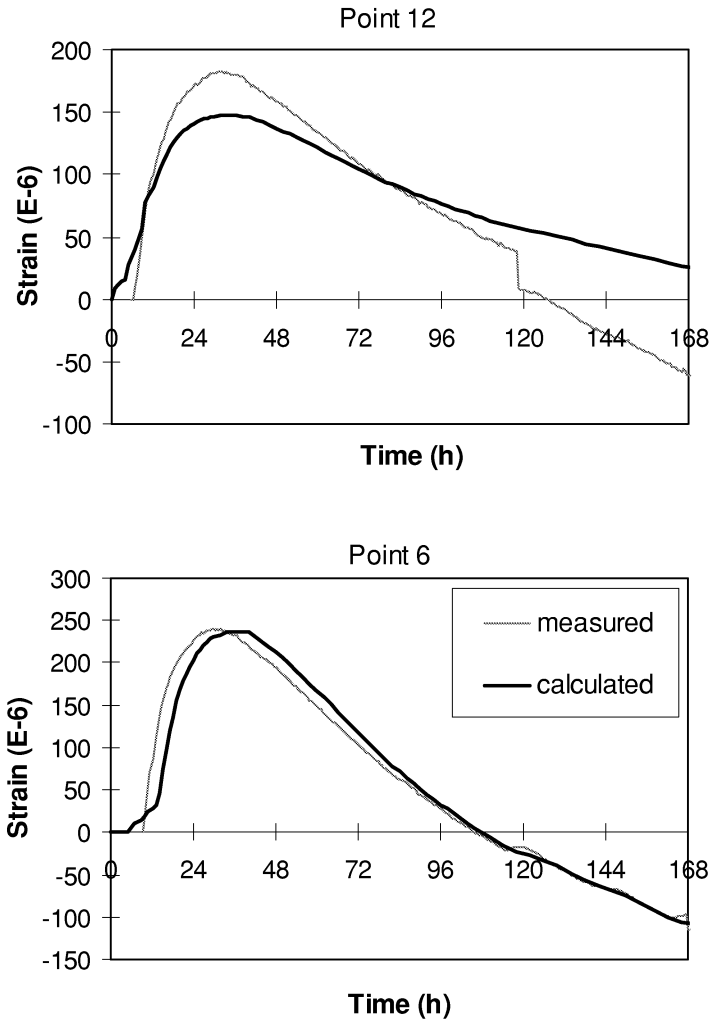

Figure 7.37: Measured and calculated strain development in the middle of the wall in section 2

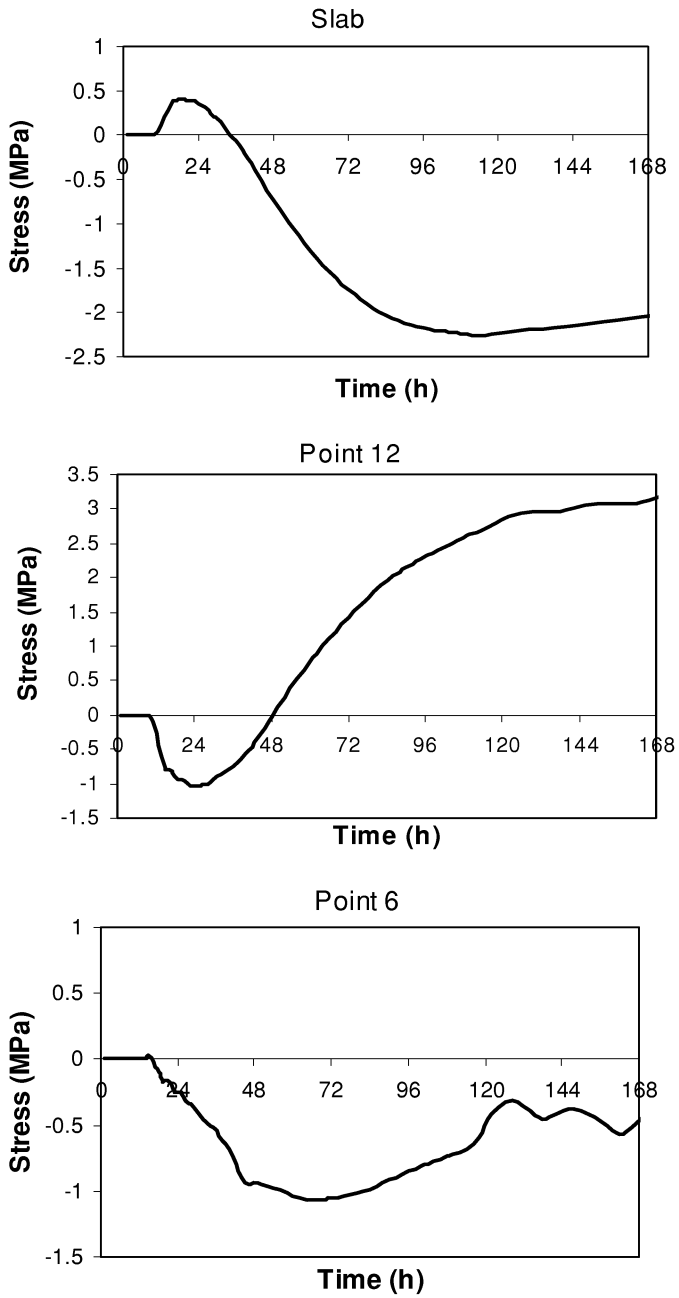

Figure 7.38: Stress development in the middle of the wall in section 2

Figure 7.39 shows the cracking risk in the wall during the hardening. Also in this section the maximum value is 0.92.

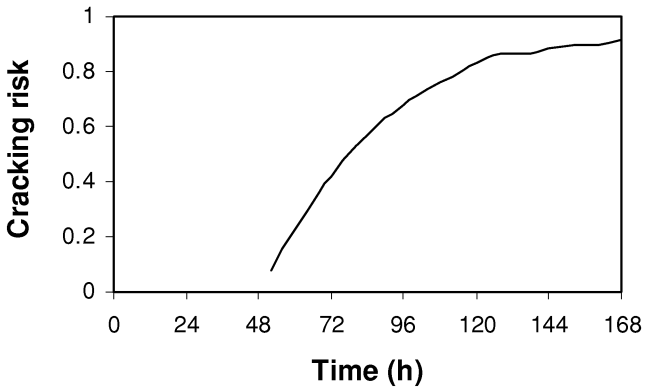

Figure 7.39: Cracking risk in the wall in Section 42

7.4.5 Discussion of the results

The calculated temperatures in the middle of the wall in Section 2 agree very well with the measurements. For Section 42 the agreement is not as good and the deviation between calculated and measured temperatures is largest for the point close to the foundation (cc 4^0C). The reasons for the disagreement may be numerous: different initial temperatures due to variations in fresh concrete temperature and casting history, unknown wind velocity, differences between properties of the concrete in situ and in laboratory, etc. It is general experience that is difficult to obtain lower deviation between measured and calculated temperatures than $\pm 5^0 C$.

When calculated strains are compared to the measurements in both sections some general observations are made:

The calculated strains are smaller in magnitude than the measured ones, both in compression and in tension.

The strains in the upper part of the wall agree well with the measurements. The deviation between calculations and measurements is larger for the strains in the bottom of the wall. When the "jump" in measurements, which probably represents a crack is neglected, the deviation comes to $\pm 50 \times 10^{-6}$.

There are many reasons for the deviations between calculated and measured strains. One of them is the deviation between the calculated and measured temperatures. As already mentioned, in Section 42 this deviation is about 4^0C in point 3 and point 12. To examine the influence of this difference, a new analysis is performed where the very good agreement between measured and calculated temperatures is obtained in all points in the middle of the wall, see Figure 7.40

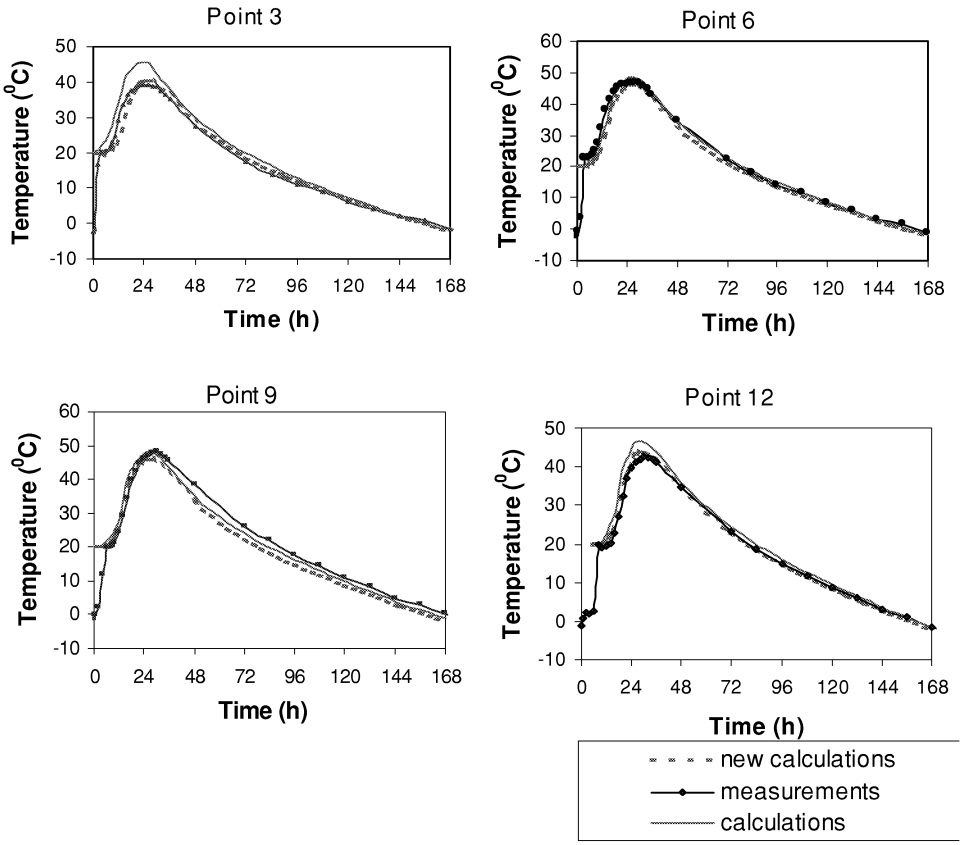

Figure 7.40: Temperature development in the middle of the wall in Section 42 calculated with two different sets of input data

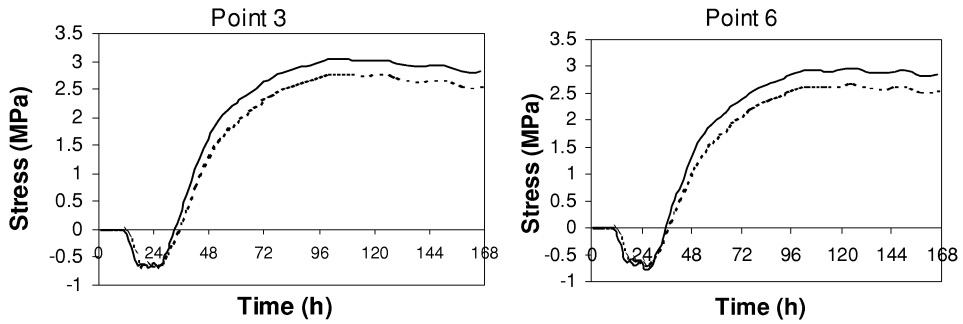

Figure 7.41: Stresses in the bottom of the wall in Section 42 for two different temperature histories

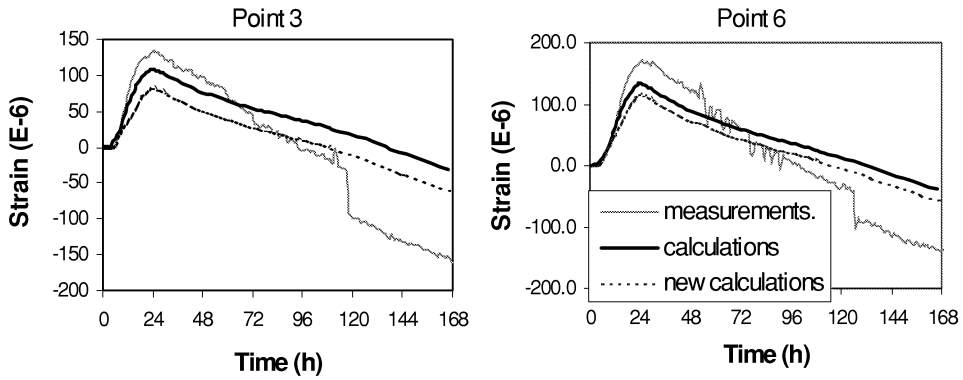

Figure 7.42: Strains in the bottom of the wall in Section 42 for two different temperature histories

The stresses and the strains in the bottom of the wall for two different temperature histories are presented in Figure 7.41 and Figure 7.42 respectively. It can be seen that slightly different temperature histories cause cc 15 % difference in tensile stresses.

The other reason of disagreement is the inadequate modelling of mechanical properties of concrete. The most obvious shortcoming is modelling of the total deformation (the sum of thermal dilation and autogenous deformation). In the lack of models for autogenous deformation and thermal coefficient the total free deformation measured for a typical temperature history is used for the whole wall. A constant value for the thermal coefficient is assumed ($8x10^{-6}$) and autogenous deformation is obtained by substracting thermal dilation from the total free deformation. This approach is correct when the TSTM test is performed because of the uniform temperature in the specimen. In a structure, where the temperature varies from point to point it may produce an error.

Cracks are observed in the walls in both sections, and according to the measurements (see Figure 7.37 and Figure 7.33) they probably appeared ca 5 days after casting. The highest calculated cracking risk in both section is slightly above 0.9, which means that predicted stresses are lower than the real stresses. This can also be observed when the TSTM tests are simulated, see Figure 7.25. Lower tensile strength than predicted can also be a part of the explanation.

Modelling of the structure and the support conditions are probably not the reason of discrepancy between calculations and measurements. The structure is modelled as realistically as possible, by means of 3D model, and in the previous chapter it was shown that the influence of the ground stiffness on the stresses in both walls is very small. But, the influence of the joint between the walls and the foundations is interesting to examine. The fact that the development of the strains in the upper part of the wall agree much better with the measurements than the strains close to the foundation may be explained by a possible slip in the joint.

In the subsequent analysis the joint is modelled by means of interface elements between the wall and the foundation. In the absence of experimental data on stiffness in the joint, the following assumption is used: transferring of restraint in the joint from the old concrete to the young one is done only by means of the through reinforcement. The concrete contribution in the joint is completely neglected. That is the most extreme situation, not likely to happen in practice, but the results of this numerical analysis are interesting because they represent some kind of "upper limit" and give an idea about maximal influence of casting joint on thermal stresses in this structure. All the other "realistic" situation will be between these two extreme cases: rigid bond between the wall and the foundation and no concrete contribution in the joint.

Figure 7.43 shows the influence of the slip in the joint on the strain development in the bottom and in the top of the wall in Section 42. It can be seen that the strains in the bottom are more affected by the joint slip than the strains in the top, and that the strains change in the "right" direction comparing to the measurements. That can not be said for the stresses. Slip in the joint reduces already low calculated stresses, see Figure 7.44, meaning that the deviation between measured and calculated strains can not be explained by a joint slip only.

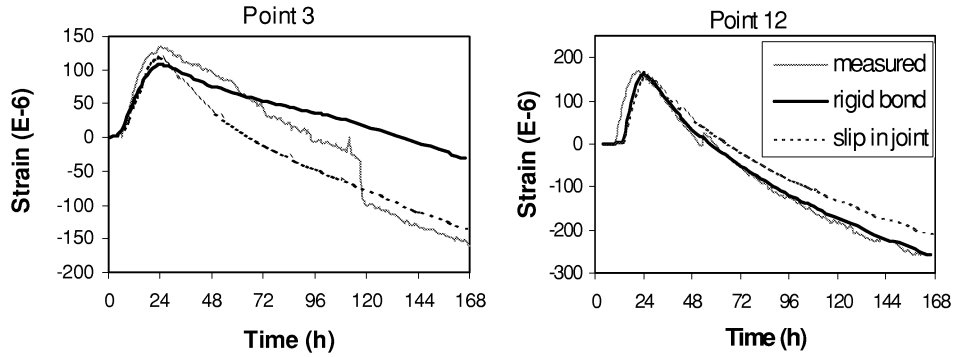

Figure 7.43: Influence of the slip in the joint on the strains in the wall in Section42

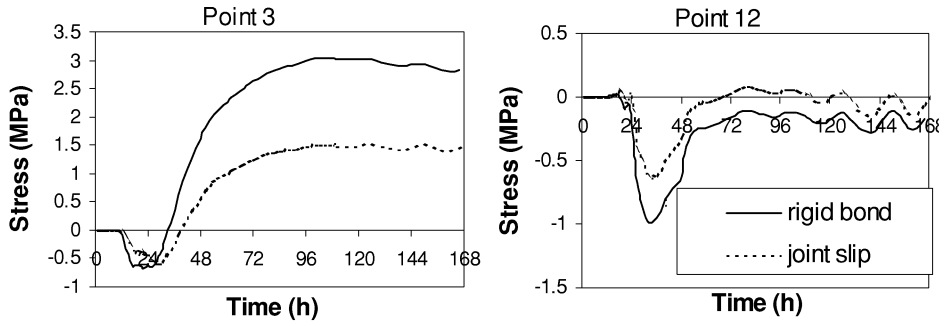

Figure 7.44: Influence of the slip in the joint on the stresses in the bottom and in the top of the wall in Section42

The starting point in this comparison between the measured and the calculated strains is that the measurements are correct and thus serve as the correct solution for the numerical simulation. But accuracy of the measurements can also be questioned. When different strain gauges were compared in the wall in Section 2, (see Figure 7.8), it could be seen that the deviation between results of the Geokon vibrating wire and the welded strain gauges was as large as $\pm 50 \times 10^{-6}$, i.e. of the same magnitude as the deviation between the calculations and the measurements.

7.5 Conclusions

Temperature and strain/stress development in two sections of the Maridal culvert is simulated and the calculation results are compared with measurements.

The deviation between calculated and measured temperature is generally within the range of $\pm 5^0 C$. The reasons for disagreement are: different initial temperatures due to variations in fresh concrete temperature and casting history, difficulties in modelling of the casting history and environmental conditions, differences between properties of the concrete in situ and in laboratory, etc.

The calculated strains are in general smaller in magnitude than the measured ones. The deviation between the calculations and the measurements is largest for the strains in the bottom of the wall. When the increase of strain due to crack is neglected, the deviation is about $\pm 50 \times 10^{-6}$ both in tension and compression.

The main reasons of disagreement between the calculated and the measured strains are:

- difference between the calculated and the measured temperature in the wall
- modelling of mechanical behaviour of hardening concrete, especially thermal dilation coefficient and autogenous deformation,
- possible slip in the joint between the hardening part and the adjacent restraining part of the structure
- accuracy of the measurements

The temperature is a very important factor in the stress simulation, and even a relatively small deviation between the measured and calculated temperature, f. i. 4^0C, may cause a considerable difference in tensile stresses. Unfortunately, it is difficult to obtain a “perfect” agreement between calculated and measured temperature, due to the previously mentioned reasons.

More research is needed if the thermal dilation coefficient and autogenous deformation will be more accurately modelled. The approach of using the total free deformation determined for a typical temperature history is justified when the TSTM tests are performed; in simulation of a structure, it produces an error.

Slip failure in the casting joints will reduce the restraint stresses and cracking risk, and therefore the correct modelling of casting joints is of great interest. However, knowledge of the behaviour of casting joints is very limited and more research must be done to clarify that.

The deviation between different measuring methods is of the same magnitude as the deviation between the calculated and the measured strains, which is unacceptable if these results are used as a correct answer for the numerical simulation. As long as the reliability of the measurements is not improved, comparison between calculations and measurements should mainly have a character of guidance.

A suitable limit for prevention of cracking is according to (Emborg 1994) 0.7, and according to (Rostasy 2000) 0.75. The predicted cracking risk is slightly above 0.9, what means that the cracking criterion is not satisfied.

When all uncertainties in the modelling of hardening concrete behaviour as well as uncertainties in the measuring methods are taken into account, it can be concluded that the results of the present simulations are satisfying.

Chapter 8

Conclusions

8.1 Summary and conclusions

This thesis deals with prediction of early age cracking caused by restrained temperature dilation and autogenous deformation. Traditionally, prediction of early-age cracking has been based on temperature criteria. The temperature criteria alone are, however, not sufficiently accurate for cracking prediction because they do not consider crucial factors as thermal dilation, autogenous deformation, mechanical properties and restraint conditions. For a reliable crack prediction at early ages stress-strain criteria must be applied.

The main purpose of this study is to extend the general applicability of stress/strain based cracking prediction, and to contribute to better understanding and better prediction of stresses during hardening of concrete structures.

The hydration process in hardening concrete is governed by two coupled diffusion processes: temperature development and development of the water distribution. A common assumption, also adopted here, is that influence of the development of water distribution on the hydration process and mechanical properties may be neglected and that only influence of temperature is considered. The maturity principle is adopted, according to whom the rate of hydration at a given degree of hydration is a function of temperature only. Hence, the behaviour of early age concrete is considered as a thermomechanical problem. Because of the small influence of stresses on the hydration process, the problem may be decoupled. The thermal problem is solved first, and the results are used in the subsequent stress analysis.

The temperature development in hardening concrete structure may be calculated by the Fourier differential equation for heat conduction in a homogenous and isotropic body. Traditionally, two parameters are used to describe the state of the hydration process: degree of hydration and equivalent age. Modelling of hydration process and material properties by means of degree of hydration is not common in engineering practice. To make DIANA program more applicable to the engineering practice, equivalent age is introduced. The simpler and more common equivalent-time based model for the heat of hydration development is implemented and it is shown that it can describe temperature development with the same accuracy as the degree of hydration based model. In addition, a constant activation energy is replaced by a temperature dependent activation energy.

Implementation of the equivalent age gives the possibility of expressing all material properties as functions of equivalent age. To describe development of E-modulus, a modified CEB equation is implemented, where it is assumed that the E-modulus starts developing at a certain time t_0. This means that before t_0 volume changes do not induce any stresses, so

t_0 is a "zero-point" for stress calculation. The concept of concrete age t_0 bellow which no stresses can be generated is convenient and practical from several reasons, specially when the Double Power Law creep model is used in calculations.

Mathematical description for the mechanical response is given in form of the constitutive equations for different strain components. An additional component is included to take into account the transitional thermal creep - increase in creep due to the transient temperature.

The finite element method is used to solve the differential equations. Special attention is paid to the numerical integration of the viscoelastic constitutive relation. Numerical method based on the differential formulation is used and storage of the entire stress/strain history is avoided.

Creep is a major factor of mechanical behaviour of young concrete, and understanding of the creep influence on thermal stresses is therefore of essential importance in prediction of cracking risk. The influence of creep on self-induced stresses is examined. Emphasis is put on creep importance in different periods of the hardening process and following conclusions are made:

For internally restrained structures, prone to surface cracking in the early period, creep obviously reduces the cracking risk. Creep in the second period of hardening is not relevant for cracking risk.

Influence of creep in externally restrained structures is more complex. In the early period (heating phase) creep reduces the compressive stresses, and consequently increases the tensile stresses in the subsequent cooling period, thus having a negative effect on cracking risk. In the cooling phase creep is beneficial because it reduces the tensile stresses. These two effects are counteracting, and in some cases they annul each other. Then significantly different creep properties may give approximately the same tensile stresses, what may lead to the wrong conclusion that creep is not important for calculation of stresses in hardening concrete. To the contrary, creep is very important, and correct prediction of creep during the whole period of hardening is necessary for reliable prediction of cracking risk.

Three models for creep of hardening concrete are compared: Double Power Law, Maxwell chain and Burgers model. The models are calibrated to the same set of experimental data, and used in simulation of self-induced stresses in hardening concrete. A good agreement is found between the Double Power Law and the Maxwell chain, whereas the Burgers model and the Double Power Law gives different results. The reason of disagreement can partly be explained by different temperature dependence of these models, partly by the nature of the test the models are calibrated against. The comparison arises the question: what kind of test is most appropriate for determination of creep in hardening concrete?

Different test methods and approaches in creep modelling are discussed, with the emphasis on the TSTM test. The shortcomings of using this type of tests in prediction of creep parameters are shown. Conclusion is that TSTM test can not be used in determination of creep parameters. It can be used in modelling of mechanisms and nonlinearities, whereas creep parameters should be determined from the independent tests, i. e. standard creep tests with constant stress loaded at different ages, performed at a reference temperature, which completely define compliance function within the linearity range.

The most general approach of modelling structure at early ages is 3D FEM analyses with realistic modelling of the ground and the bond between the structure and the ground and between the different parts of structure. The method is very complex and therefore in practice it is replaced by different simplified methods. One of them, Compensation Plane method is compared to 3D analysis. Two methods are used to calculate stress development in a wall cast on previously cast foundation. Several calculations are performed for walls with different geometry and different support conditions. In the case of long structures ($L/H>5$) two methods give similar results. For short structures results of the Compensation Plane method deviates from the results of the 3D analysis, and the deviation is dependent of support conditions. It is largest if the structure is prevented to rotate around horizontal axis in the cross section. Choice of method does not affect considerably the size of the maximum stresses, i. e. cracking risk. However, stresses in the upper part of the wall are significantly different.

The influence of parameters describing geometry of the structure and stiffness of the ground on the stresses in hardening structure is also investigated by means of the three-dimensional non-linear analyses.

In the end, the attention is moved from verification analyses on small laboratory specimens to a real structure. The temperature and stress/strain development is simulated in two sections of Maridal culvert in Oslo. To identify material parameters necessary for calculation, a comprehensive test program has been carried out at NTNU. Both the thermal and mechanical properties were tested and the material models were checked in the Temperature-Stress Testing Machine. The culvert was instrumented within the Brite-Euram project and temperature and strain development were recorded from the casting. The results of three-dimensional calculations are compared with the measurements. Deviation between calculated and measured temperature is within range of $\pm 5^{0}C$. Deviation between calculated and measured strains is about $\pm 50\times 10^{-6}$ both in tension and compression. It can be explained, among other things, by difference between the calculated and the measured temperature, modelling of mechanical behaviour of hardening concrete, specially thermal dilation coefficient and autogenous deformation and possible slip in the joint between the hardening part and the adjacent restraining part of the structure. The accuracy of the measurements can also be questioned. Predicted cracking risk is about 0.9, what is considered to be higher than the limit for prevention of cracking.

Taking into account all uncertainties in the modelling of hardening concrete behaviour and uncertainties in the measuring methods, it can be concluded that the results of the present simulations are satisfying.

8.2 Suggestions for further research

In modelling of hardening concrete behaviour many simplifications and assumptions have been made. They are often adopted in the absence of the full understanding of the physical mechanism and processes at the micro level, or because of its practical applicability. Some assumptions, justified in the case of hardened concrete, are also applied for hardening concrete without experimental evidence. One problem connected with modelling of hardening concrete behaviour is that experimental data are often lacking or are very scarce.

In the present section some suggestions for more research and further improvement of modelling of concrete at early ages are given. They are based on the results and the limitations of the present work.

In hardening concrete creep in tension is of great interest. However, experimental data about creep in tension at early ages are very scarce due to difficulties connected with performance of this type of tests. The most obvious problem is separation of creep deformation and relatively high autogenous deformation. In hardened concrete drying shrinkage is well-known phenomenon, which may be avoided by preventing concrete from drying. In hardening concrete autogenous deformation takes place independently on environmental conditions and can not be influenced from the exterior, so simultaneous creep and shrinkage are always present. When the autogenous deformation measured on unloaded specimen is substracted from the total deformation, different values for creep strain may be obtained in tension and compression. Consequently, the assumption about equal creep in tension and compression, applied for hardened concrete, may not be true here. More research is necessary to clarify that.

Also more research is necessary to investigate the temperature influence on creep. In the absence of experimental data, the TSTM tests are used to calibrate model for transient creep in the present work. The approach has some limits, what is discussed in Chapter 5. There is a need for more creep tests at different temperatures.

Thermal dilation and autogenous deformation are major contributors to the stress generation in hardening concrete. However, there are no generally accepted models for thermal dilation coefficient and autogenous deformation. Therefore the total deformation (sum of the thermal dilation and autogenous deformation) determined for a representative temperature history is used in the calculations in this work. The approach has several drawbacks, what is discussed in Chapter 7. It is clear demand for more research on this topic.

More experimental data are also needed to investigate high-stress nonlinearity in tension and low-stress nonlinearity for young concrete.

References

ACI Comitee 207 (1973), "Effect of restraint, volume changes and reinforcementon cracking of massive concrete", *ACI Journal*, 70(45)

Andersen, M. E. (1995), *Design and Construction of Concrete Structures in View of Early-Age Thermal Effects*, Ph.D. thesis, Department of Structural Engineering, Technical University of Denmark.

Andersen, M. E., Jensen, H. J., Pedersen, E. S., and Spange, H. (1997), "*HETEK, Control of Early Age Cracking in Concrete, Phase 8: Modelling of Support Conditions*", Department of Structural Engineering and Materials, Technical University of Denmark.

Atrushi, D. and Bosnjak, D. (2000), "Tensile Creep of Young High Performance Concrete", International PhD Symposium in Civil Engineering, Vienna

Bazant, Z. P. and Wu, S. T. (1974a), "Rate-type creep law of aging concrete based on Maxwell chain", *Materials and Structures*, 7(37)

Bazant, Z. P. (1975), "Theory of creep and shrinkage in concrete structures: a precis of recent developments", *Mechanics Today* 2

Bazant, Z. P. and Wu, S. T. (1974b), "Creep and Shrinkage Low for Concrete at Variable Humidity", *Journal of the Engineering Mechanics Division*, 100(6)

Bazant, Z. P. and Osman, E. (1975), "Double Power Law for Basic Creep of Concrete", *Materials and Structures*, 9(49).

Bazant, Z. P. and Panula, L. (1978), "Practical prediction of time-dependent deformations of concrete,":

Part I and II, *Materials and Structures*, 11(65), 1978

Part III and IV, *Materials and Structures*, 11(66), 1978

Part V and VI, *Materials and Structures*, 12(69), 1979

Bazant, Z. P. and Kim, S. S. (1979), "Nonlinear Creep of Concrete - Adaptation and Flow", *Journal of the Engineering Mechanics Division*, 105(3)

Bazant, Z. P. and Wittman, F. H. (1982), *Creep and Shrinkage in Concrete Structures*, John Wiley and Sons.

Bazant, Z. P. and Chern, J. C. (1985a), "Concrete creep at variable humidity", *Material and Structures*, 18(103)

Bazant, Z. P. and Chern, J. C. (1985b), "Triple Power Law for Concrete creep", *Journal of Engineering Mechanics*, 111(1)

Bazant, Z. P., editor (1986), *Mathematical Modeling of Creep and Shrinkage of Concrete*, Fourth RILEM International Symposium on Creep and Shrinkage of Concrete: Mathematical modeling, John Wiley and Sons.

Bernander, S. and Emborg, M. (1994), "Risk of cracking in massive concrete structures-New developments and experiences", International RILEM Symposium T*hermal Cracking in Concrete at Early Ages* in Munich

Bernander, S. (1994), Practical Measures to Avoiding Early Age Thermal Cracking in Concrete Structures, State-of-the-art reports prepared by RILEM Technical Comitee 119, *Prevention of Thermal Cracking in Concrete at Early ages*

Bjøntegaard, Ø., Kanstad, T., Sellevold, E. J., and Hammer, T. A. (1998), "Stressinducing deformation and mechanical properties of high performance concrete at very early ages", 5th International Symposium on *Utilization of High Strength/ High Performance Concrete*, Sandefjord, Norway

Bjøntegaard, Ø. (1999), *Thermal Dilation and Autogenous Deformation as Driving Forces to Self-Induced Stresses in High Performance Concrete*, Ph.D. thesis, NTNU, Trondheim, Norway

de Borst, R. and van den Boogard, A. H. (1995), "Finite-Element Modeling of Deformation and Cracking in Early-Age Concrete", *Journal of Engineering Mechanics*, 120(12).

Bosnjak, D. and Kanstad, T. (1997), "*Analysis of hardening high performance concrete structures*", Second International DIANA Conferance on Finite Elements in Engineering and Science, Amsterdam

Brameshuber, W. and Hilsdorf, H. K. (1987), "Development of strength and deformability of very young concrete", in Proceedings of the SEM/RILEM International Conference on *Fracture of Concrete and Rock* in Houston, Texas

Breugel, K. van (1980), "*Artificial cooling of hardening concrete, Delft University of Technology"*, Research Report No 5-80-9, The Netherlands (quoted from Breugel 1994)

Breugel, K. van (1991), *Simulation of Hydration and Formation of Structure in Hardening Cement-based Materials*, Ph.D. thesis, Delft University of Technology, The Netherlands.

Breugel, K. van (1994), Prediction of Temperature Development in Hardening Concrete, State-of-the-art reports prepared by RILEM Technical Comitee 119, *Prevention of Thermal Cracking in Concrete at Early ages.*

Brown, T.D. and Javaid, M.Y. (1970), "The thermal conductivity of fresh concrete",*Materials and Structures*, 3(18)

Byfors, J. (1980), "*Plain concrete at early ages*", CBI Research, Swedish Council for Building Research, Stockholm.

Comite Euro-International du Beton (1990), *CEB-FIP model code 1990*

Cook, R. D., Malkus, D.S. and Pleisha M.E. (1989), "*Concepts and applications of finite element analysis*", John Wiley and Sons

Coutinho, A. S. (1977), "A contribution to the mechanics of concrete creep", *Materials and structures*, 10(55) (quoted from Neville 1983)

4C-Temp & Stress Manual Version 2 (1998), DTI Building Technology, Denmark

DIANA Manual - Release 7 (1998), TNO Building and Construction Research, Department of Engineering Mechanics and Information Technology, Delft, The Netherlands

DTI (1996), "Nyt fra Betoncentret. Ung beton kryber", *Dansk Beton*, No 4, November 1996 (in Danish)

Emborg, M. (1989), "*Thermal stresses in concrete structure at early ages*", Ph.D. thesis, Division of Structural Engineering, Luleå University of Technology, Sweden.

Emborg, M. (1994a), "Models and methods for computation of thermal stresses and cracking risk", State-of-the-art reports prepared by RILEM Technical Comitee 119, *Prevention of Thermal Cracking in Concrete at Early ages*

Emborg, M. (1994b), "Development of mechanical behaviour at early ages including mathematical models", State-of-the-art reports prepared by RILEM Technical Comitee 119, *PreventionPrevention of Thermal Cracking in Concrete at Early ages*

Eurocode 2 (1991), "*Design of concrete structures - Part 1-1, General rules and rules for buildings*", ENV 1992-1-1:1991

Freiesleben Hansen, P. and Pedersen E. J. (1977), "*Måleinstrument til kontrol af betons hærdning*", Nordisk Betong 1, Stockholm (in Danish)

Freiesleben Hansen, P. (1978) *Hærdeteknology1. Portlandcement*, Aalborg Portland og BKF-centralen, Lyngby (in Danish)

Freiesleben Hansen, P. and Pedersen, E. J. (1984), "*Curing of concrete structures*", CEB report, Bulletin d'information, 166

Gutsch, A. and Rostasy, F.S. (1994), "Young concrete under high tensile stresses - creep, relaxation and cracking", in *Thermal Cracking in Concrete at Early Ages*, Proceedings of the International RILEM Symposium in Munich

Gutsch, A. (1998), "*Stoffeigenschaften jungen Betons - Versuche und Modelle"* , Ph.D. thesis, Technical University of Braunschweig, Germany

Gutsch, A. (2000), "*Influence of elevated temperature on creep and relaxation of early age concrete*", IPACS report, preliminary version

Gutsch, A. and Rostasy, F.S. (2000), "*Mechanical models of the stress-strain behaviour of young concrete in axial tension and compression*", IPACS report

Han, N. (1996), "*Time Dependent Behaviour of High Strength Concrete*", Ph.D. thesis, Delft University of Technology, The Netherlands.

Hauggaard, A. B., Damkilde, L., Freiesleben Hansen, P., Hougaard Hansen, J., Nielsen, A., and Christensen, S.L. (1997a), "*HETEK, Control of Early Age Cracking in Concrete, Phase 3: Creep in Concrete*", Department of Structural Engineering and Materials, Technical University of Denmark.

Hauggaard, A. B., Damkilde, L., Freiesleben Hansen, P., Pedersen, E. S., and Nielsen, A. (1997a), "*HETEK, Control of Early Age Cracking in Concrete, Phase 4 and 5: Material*

Modeling, Continuum Approach", Department of Structural Engineering and Materials, Technical University of Denmark.

Hauggaard, A. B. (1997), "*Mathematical Modelling and Experimental Analysis of Early Age Concrete*", Ph.D. thesis, Department of Structural Engineering and Materials, Technical University of Denmark.

Hedlund, H. (1996), "*Stresses in High Performance Concrete due to Temperature and Moisture Variations at Early Age*", Licentiate thesis, Division of Structural Engineering, Luleå University of Technology, Sweden

Heimdal, E., Kanstad, T., and Kompen, R. (1999), "*Early age concrete field tests at the Maridal culvert. Project description and test results*", NOR-IPACS report STF22 A99763. ISBN 82-14-01044-6

Heimdal, E., and Kanstad, T. (2000), "*Maridal culvert, Field tests, Part 2*", NOR-IPACS report, preliminary version

Helland, S. (2000),"Round-Robin tests performed on strength development, temperature dependency, heat release and time of setting", NOR-IPACS report, preliminary version

Illston, J. M. and Sanders, P. D. (1973), "The effect of temperature change upon the creep of concrete under torsional loading", *Magazine of Concrete Research*, 25(84)

Jonasson J. E. (1977), "*Datorprogram for icke-linjæra berækningar i betong med hænsin till svinn, krypning och temperature*", Swedish Cement and Concrete Research Institute, Stockholm (in Swedish)

Jonasson, J. E. (1984), "*Slipform Construction - Calculations for Assessing Protection Against Early Frezing*", Swedish Cement and Concrete Research Institute, CBI Forskning/Research 4.84, Stockholm, Sweden.

Jonasson, J. E. (1994), "*Modelling of Temperature Moisture and Stresses in Young Concrete*", Ph.D. thesis, Division of Structural Engineering, Luleå University of Technology, Sweden.

Jordaan, I. J., England, G. L., and Khalifa, M. A. (1977), "Creep of Concrete: A Consistent Engineering Approach", *Journal of the Structural Division*, 103(3)

Kanstad, T. (1994), "*Early Age Behaviour of Concrete and Reinforced Concrete Structures*", Department of Structural Engineering, Norwegian Institute of Technology, Trondheim, Norway.

Kanstad T., Hammer, T. A., Bjøntegård, Ø. and Sellevold, E. J. (1999), "*Mechanical properties of young concrete: Evaluation of test methods for tensile strength and modulus of elasticity. Determination of model parameters.*", NOR-IPACS report STF22 A99762. ISBN 82-14-01062-4.

Kanstad, T., Bosnjak, D., Bjøntegaard, Ø., Sellevold, E., Petkovic, G. and Heimdal, E. (1999a), "Early age concrete field tests at the Maridals Culvert. Part two: Model parameter identification and numerical simulation", 5th International Symposium on *Utilization of High Strength/ High Performance Concrete*, Sandefjord, Norway

Kanstad, T. (2000), "*Verification of Skanska's Engineering Method by Timedependent full 3D DIANA-analyses*", IPACS report, preliminary version.

Khan, A. A., Cook, W. D. and Mitchel, D. (1998), " Thermal properties and transient thermal analysis of structural members during hydration", *ACI Materials Journal*, 95(3)

Khoury G. A., Grainger, B. N., and Sullivan, P. J. E. (1985), "Transient thermal strain of concrete: literature review, conditions within specimen and behaviour of individual constituents", *Magazine of Concrete Research*, 37(132)

Kjellman O. and Olofsson J. (1999), "*3D Structural Analysis of Crack Risk in Hardening Concrete Structure*", IPACS report, TG4/N2

Liang, R. Y. and Niu, Y. Z. (1997), "Numerical modeling of Early-Age Concrete Behavior", in Proceeding of the 1997 *ASME-ASCE-SES Joint Summer Meeting* in Evanston, USA

Lindgård J. and Sellevold, E. J. (1993), "Is high strength concrete more robust against elevated curing temperatures?" in *High Strength Concrete 1993*, Proceedings of the Third International Symposium on Utilization of High Strength Concrete in Lillehammer, Norway.

Lokhorst, S. J. and van Breugel, K. (1994), "From microstructural development towards prediction of macro stresses in hardening concrete", in *Thermal Cracking in Concrete at Early Ages*, Proceedings of the International RILEM Symposium in Munich

Mangold M. (1994), "Methods for Experimental Determination of Thermal Stresses and Crack Sensitivity in the Laboratory", State-of-the-art reports prepared by RILEM Technical Comitee 119, *Prevention of Thermal Cracking in Concrete at Early ages*

Mareschal, J. C. (1972), "*Determination simultanee da la diffusivite et da la conductivite thermique du beton pendant son hydratation*", Contribution to the Task Group W 40 of the Conseil International du Batiment, Holzkirchen (quoted from Breugel 1994)

Morabito P. (1994), "Methods to Determine the Heat of Hydration of Concrete", State-of-the-art reports prepared by RILEM Technical Comitee 119, *Prevention of Thermal Cracking in Concrete at Early ages*

Neville, A. M., Dilger, W. H., and Brooks, J. J. (1983), *Creep of Plain and Structural Concrete*, Construction Press.

Neville, A. M., and Brooks, J. J. (1987), *Concrete Technology*, Longman

Nillson, M. (2000), "*Thermal Cracking of Young Concrete*", Licentiate thesis, Division of Structural Engineering, Luleå University of Technology, Sweden.

Normaler: Vegbygging, Vegvesenets håndbokserie 018, Statens vegvesen 1992 Oslo (in Norwegian)

NS 3656 (1993) *Concrete testing. Rate of reaction as a function of temperature*, Norwegian Building Research Institute, NBR, first edition

Olofsson, J., and Uhlan, M. (1999), "*Round-Robin simulation. Ground Slab examples*", IPACS report, TG4/N3.

Olofsson, J., Bosnjak, D., and Kanstad, T. (2000), "*Crack Control of Hardening Concrete Structures - Verification of a Three-step Engineering Method*", 13th Nordic Seminar on Computational Mechanics, Oslo

Oluokun, F. A., Burdette, E. G. and Deatherage, H. J. (1991a), "Elastic modulus, Poisson's ratio and compressive strength relationship at early ages", *ACI Materials Journal*, 88(1)

Oluokun, F. A., Burdette, E. G. and Deatherage, H. J. (1991b), "Splitting tensile strength and compressive strength relationship at early ages", *ACI Materials Journal*, 88(2)

Onken, von P. and Rostasy, F. S. (1995), "*Wirksame Betonzugfestigkeit im Bauwerk bei fruh einsetzendem Temperaturezwang*", Deutcher Ausschuss Fur Stahlbeton, Heft 449, Institute for Building Materials, Concrete Construction and Fire Protection, Technical University of Braunschweig, Germany

Parrot, L. J. (1979), "A study of transitional thermal creep in hardened cement paste", *Magazine of Concrete Research*, 31(107)

Pedersen, J. E. (1994), "Prediction of temperature and stress development in concrete structures", in *Thermal Cracking in Concrete at Early Ages*, Proceedings of the International RILEM Symposium in Munich

Pettersson, D. (1998), *Stresses in Concrete Structures from Ground Restraint*, Licentiate thesis, Division of Structural Engineering, Lund Institute of Technology, Lund University, Sweden

Pettersson, D. (2000), *Control of Cracking due to Imposed Strains in Concrete Structures*, Ph.D. thesis, Division of Structural Engineering, Lund Institute of Technology, Lund University, Sweden

Reinhardt, H. W., Blaauwendraad, J., and Jongedijk, J. (1982), "Temperature development in concrete structures taking account of state dependent properties", in *Concrete at Early Ages*, Proceedings of the International Conference in Paris.

Rostasy, F.S., Gutch, A., and Laube, M. (1993), "Creep and Relaxation of Concrete at Early Ages -Experiments and Mathematical Modelling", in *Creep and Shrinkage of Concrete*, Proceedings of the 5th International RILEM Symposium in Barcelona.

Rostasy, F.S., Tanabe, T., and Laube, M. (1994), "Assessment of External Restraint", State-of-the-art reports prepared by RILEM Technical Comitee 119, *Prevention of Thermal Cracking in Concrete at Early ages*

Rostasy, F.S., Gutsch, A., and Krauss, M. (1999), "*Restraint Interaction of Slabs with Soil and Piles during Early Age*", IPACS report, preliminary version

Rostasy, F.S., Krauss, M. and Gutsch, A. (2000), "*Computation of stresses and cracking criteria for earlu age concrete - methods of IBMB*", IPACS report, preliminary version

Schutter, G. D. and Taerwe, L. (1996), "Degree of hydration-based description of mechanical properties of early age concrete", *Materials and structures*, 29

Schutter, G. D. and Taerwe, L. (1997), "Towards a more fundamental non-linear basic creep model for early age concrete", *Magazine of Concrete Research*, 49(180)

Smeplass S. (2000), "*Herdekassen - bestemmelse av avkjølingstallet*", NOR-IPACS report, preliminary version (in Norwegian)

Spange, H. and Pedersen, E. S. (1996), "*HETEK, Control of Early Age Cracking in Concrete, Phase 1: Early Age Properties of Selected Cncrete*", Department of Structural Engineering and Materials, Technical University of Denmark.

Springenschmid, R., Breitenbucher, R, and Mangold, M. (1994). "Development of the Cracking Frame and the Temperature-Stress Testing Machine", in T*hermal Cracking in Concrete at Early Ages*, Proceedings of the International RILEM Symposium in Munich, E & FN SPON

Takacs, P. F. (1999), "I*mplementation of an additional thermal strain term in FE program DIANA*", Internal notate, NTNU, Trondheim, Norway

Tazawa, E. and Miyazawa, S. (1994), "Autogenous shrinkage of concrete and its importance of concrete technology", in *Creep and Shrinkage of Concrete*, Proceedings of the 5th International RILEM Symposium in Barcelona.

Thelandersson, S. (1987), "Modeling of Combined Thermal and Mechanical Action in Concrete", *Journal of Engineering Mechanics,* 113(6)

Thomassen, A. K. (1999), "*Temperature and strain calculations related to the field tests at the Maridals Culvert*", NOR-IPACS report, STF22 A99761. ISBN 82-14-01062-4

Umehara, H., Uehara, T., Iisaka, T., and Sugiame, A. (1994), "Effect of Creep in Concrete at Early Ages on Thermal Stress", in T*hermal Cracking in Concrete at Early Ages*, Proceedings of the International RILEM Symposium in Munich, E & FN SPON

Westman, G. (1995), *Thermal Cracking in High Performance concrete*, Licentiate thesis, Division of Structural Engineering, Luleå University of Technology, Sweden.

Westman, G. (1999), *Concrete Creep and Thermal Stresses*, Ph.D. thesis, Division of Structural Engineering, Luleå University of Technology, Sweden

Wittmann, F. H. (1995), "Influence of drying induced damage on the hygral diffusion coefficient", in Proceedings of the *Second International Conference on Fracture Mechanics of Concrete Structures* (FRAMCOS 2) in Zurich

Zienkiewicz, O. C. and Taylor, R. L. (1977), *The Finite Element Method*, Mc Graw Hill, 2 edition.

Appendix 1

Comparison of the Double Power Law and Maxwell chain

- Model parameters for the Double Power Law:

  $E_c(28) = 40693$ MPa, $t_0 = 9$ h, $s = 0.148$, $n_E = 0.383$,

  $\varphi_0 = 0.415$, $d = p = 0.26$

- Model parameters for Maxwell chain:

  Elasticity moduli are given as multilinear functions of equivalent age.

  Maturity [s]:

  .0000000E+00 .3231360E+05 .4104000E+05 .8841800E+05 .1904908E+06 .4104000E+06 .8841800E+06 .1904908E+07 .4104000E+07 .8841800E+07 .1904908E+08

  E_1[N/m^2]:

  .1000000E+08 .1000000E+08 .1242022E+09 .2633184E+09 .3052653E+09 .2944363E+09 .1061126E+09 .3672968E+09 .5842503E+10 .1039536E+11 .1435616E+11

  E_2[N/m^2]:

  .1000000E+08 .1000000E+08 .1177327E+10 .1579673E+10 .1493248E+10 .1323893E+10 .1134327E+10 .9496971E+09 .7914299E+09 .6534430E+09 .5391292E+09

  RELTIM [s]: .4320000E+03

  E_3[N/m^2]:

  .1000000E+08 .1000000E+08 .7473856E+09 .1706907E+10 .1832038E+10 .1748812E+10 .1605346E+10 .1447524E+10 .1217662E+10 .1013603E+10 .8402315E+09

  RELTIM [s]: .4320000E+04

  E_4 [N/m^2]:

  .1000000E+08 .1000000E+08 .5065013E+10 .4613249E+10 .4212973E+10 .3717531E+10 .3140489E+10 .2553273E+10 .2182590E+10 .1838898E+10 .1544209E+10

  RELTIM [s]: .4320000E+05

E_5 [N/m^2]:

.1000000E+08 .1000000E+08 .1136315E+10 .2019031E+10 .2502456E+10 .2957151E+10 .3406975E+10 .3736752E+10 .3287301E+10 .2843112E+10 .2426791E+10

RELTIM [s]: .4320000E+06

E_6[N/m^2]:

.1000000E+08 .1000000E+08 .1263127E+10 .3342962E+10 .4269256E+10 .4907862E+10 .5449269E+10 .5855638E+10 .5205799E+10 .4636440E+10 .4108629E+10

RELTIM [s]: .4320000E+07

E_7[N/m^2]:

.1000000E+08 .1000000E+08 .1840460E+10 .4218884E+10 .5290067E+10 .6042748E+10 .6652764E+10 .7048762E+10 .6169014E+10 .5432176E+10 .4821999E+10

RELTIM [s]: .4320000E+08

E_8[N/m^2]:

.1000000E+08 .1000000E+08 .4369009E+10 .1039456E+11 .1309291E+11 .1496462E+11 .1646488E+11 .1740734E+11 .1514326E+11 .1317861E+11 .1147991E+11

RELTIM [s]: .4320000E+09

Comparison of the Double Power Law and Burgers model

- Model parameters for the Double Power Law:

  $E_c(28) = 38628$ MPa, $t_0 = 4.95$ h, $s = 0.24$, $n_E = 0.43$,

  $\varphi_0 = 0.61$, $d = p = 0.3$

- Model parameters for Burgers model:

$$\eta_1 = 1.77 \cdot 10^6 + 1.98 \cdot 10^8 \cdot \exp\left[-\left(\frac{1438}{t_{eq}}\right)^{0.562}\right]$$

$$\eta_2 = 2.38 \cdot 10^5 \cdot \exp(4.16 \cdot 10^{-3} \cdot t_{eq})$$

$$E_2 = 1.302 \cdot 10^5 \cdot \exp(1.22 \cdot 10^{-3} \cdot t_{eq})$$

In the calculation of the strains the E-modulus determined in the creep tests is used in stead of model. These values and other concrete properties are reported in:

Spange, H. and Pedersen, E. S. (1997), "*HETEK, Control of Early Age Cracking in concrete. Phase1: Early Age Properties of Selected Concrete*", Department of Structural Engineering and Materials, Technical University of Denmark.

The BASE concrete

Parameters used in simulation of the TSTM test results:

- Activation energy parameters:
  A = 25000, B = 1470
- Model parameters for the Double Power Law:
  $E_c(28)$ = 34300 MPa, t_0 = 11 h, s = 0.173, n_E = 0.394,
  φ_0 = 0.75, d = 0.24, p = 0.2
  ρ = 0.27 (transient creep)
- Model parameters for the tensile strength development
  f_t = 4.44 MPa, n_t = 0.658
- Thermal dilation coeficient
  α_T = 8.5 E-6

DEPARTMENT OF STRUCTURAL ENGINEERING
NORWEGIAN UNIVERSITY OF SCIENCE AND TECHNOLOGY

N–7491 TRONDHEIM, NORWAY
Telephone: +47 73 59 47 00 Telefax: +47 73 59 47 01

"Reliability Analysis of Structural Systems using Nonlinear Finite Element Methods",
C. A. Holm, 1990:23, ISBN 82-7119-178-0.

"Uniform Stratified Flow Interaction with a Submerged Horizontal Cylinder",
Ø. Arntsen, 1990:32, ISBN 82-7119-188-8.

"Large Displacement Analysis of Flexible and Rigid Systems Considering Displacement-Dependent Loads and Nonlinear Constraints",
K. M. Mathisen, 1990:33, ISBN 82-7119-189-6.

"Solid Mechanics and Material Models including Large Deformations",
E. Levold, 1990:56, ISBN 82-7119-214-0, ISSN 0802-3271.

"Inelastic Deformation Capacity of Flexurally-Loaded Aluminium Alloy Structures",
T. Welo, 1990:62, ISBN 82-7119-220-5, ISSN 0802-3271.

"Visualization of Results from Mechanical Engineering Analysis",
K. Aamnes, 1990:63, ISBN 82-7119-221-3, ISSN 0802-3271.

"Object-Oriented Product Modeling for Structural Design",
S. I. Dale, 1991:6, ISBN 82-7119-258-2, ISSN 0802-3271.

"Parallel Techniques for Solving Finite Element Problems on Transputer Networks",
T. H. Hansen, 1991:19, ISBN 82-7119-273-6, ISSN 0802-3271.

"Statistical Description and Estimation of Ocean Drift Ice Environments",
R. Korsnes, 1991:24, ISBN 82-7119-278-7, ISSN 0802-3271.

"Turbidity Current Modelling",
B. Brørs, 1991:38, ISBN 82-7119-293-0, ISSN 0802-3271.

"Zero-Slump Concrete: Rheology, Degree of Compaction and Strength. Effects of Fillers as Part Cement-Replacement",
C. Sørensen, 1992:8, ISBN 82-7119-357-0, ISSN 0802-3271.

"Nonlinear Analysis of Reinforced Concrete Structures Exposed to Transient Loading",

K. V. Høiseth, 1992:15, ISBN 82-7119-364-3, ISSN 0802-3271.

"Finite Element Formulations and Solution Algorithms for Buckling and Collapse Analysis of Thin Shells", R. O. Bjærum, 1992:30, ISBN 82-7119-380-5, ISSN 0802-3271.

"Response Statistics of Nonlinear Dynamic Systems",
J. M. Johnsen, 1992:42, ISBN 82-7119-393-7, ISSN 0802-3271.

"Digital Models in Engineering. A Study on why and how engineers build and operate digital models for decisison support",
J. Høyte, 1992:75, ISBN 82-7119-429-1, ISSN 0802-3271.

"Sparse Solution of Finite Element Equations",
A. C. Damhaug, 1992:76, ISBN 82-7119-430-5, ISSN 0802-3271.

"Some Aspects of Floating Ice Related to Sea Surface Operations in the Barents Sea",
S. Løset, 1992:95, ISBN 82-7119-452-6, ISSN 0802-3271.

"Modelling of Cyclic Plasticity with Application to Steel and Aluminium Structures",
O. S. Hopperstad, 1993:7, ISBN 82-7119-461-5, ISSN 0802-3271.

"The Free Formulation: Linear Theory and Extensions with Applications to Tetrahedral Elements with Rotational Freedoms",
G. Skeie, 1993:17, ISBN 82-7119-472-0, ISSN 0802-3271.

"Høyfast betongs motstand mot piggdekkslitasje. Analyse av resultater fra prøving i Veisliter'n",
T. Tveter, 1993:62, ISBN 82-7119-522-0, ISSN 0802-3271.

"A Nonlinear Finite Element Based on Free Formulation Theory for Analysis of Sandwich Structures",
O. Aamlid, 1993:72, ISBN 82-7119-534-4, ISSN 0802-3271.

"The Effect of Curing Temperature and Silica Fume on Chloride Migration and Pore Structure of High Strength Concrete",
C. J. Hauck, 1993:90, ISBN 82-7119-553-0, ISSN 0802-3271.

"Failure of Concrete under Compressive Strain Gradients",
G. Markeset, 1993:110, ISBN 82-7119-575-1, ISSN 0802-3271.

"An experimental study of internal tidal amphidromes in Vestfjorden",
J. H. Nilsen, 1994:39, ISBN 82-7119-640-5, ISSN 0802-3271.

"Structural analysis of oil wells with emphasis on conductor design",
H. Larsen, 1994:46, ISBN 82-7119-648-0, ISSN 0802-3271.

"Adaptive methods for non-linear finite element analysis of shell structures",

K. M. Okstad, 1994:66, ISBN 82-7119-670-7, ISSN 0802-3271.

"On constitutive modelling in nonlinear analysis of concrete structures",
O. Fyrileiv, 1994:115, ISBN 82-7119-725-8, ISSN 0802-3271.

"Fluctuating wind load and response of a line-like engineering structure with emphasis on motion-induced wind forces",
J. Bogunovic Jakobsen, 1995:62, ISBN 82-7119-809-2, ISSN 0802-3271.

"An experimental study of beam-columns subjected to combined torsion, bending and axial actions",
A. Aalberg, 1995:66, ISBN 82-7119-813-0, ISSN 0802-3271.
"Scaling and cracking in unsealed freeze/thaw testing of Portland cement and silica fume concretes",
S. Jacobsen, 1995:101, ISBN 82-7119-851-3, ISSN 0802-3271.

"Damping of water waves by submerged vegetation. A case study of laminaria hyperborea",
A. M. Dubi, 1995:108, ISBN 82-7119-859-9, ISSN 0802-3271.

"The dynamics of a slope current in the Barents Sea",
Sheng Li, 1995:109, ISBN 82-7119-860-2, ISSN 0802-3271.

"Modellering av delmaterialenes betydning for betongens konsistens",
Ernst Mørtsell, 1996:12, ISBN 82-7119-894-7, ISSN 0802-3271.

"Bending of thin-walled aluminium extrusions",
Birgit Søvik Opheim, 1996:60, ISBN 82-7119-947-1, ISSN 0802-3271.

"Material modelling of aluminium for crashworthiness analysis",
Torodd Berstad, 1996:89, ISBN 82-7119-980-3, ISSN 0802-3271.

"Estimation of structural parameters from response measurements on submerged floating tunnels",
Rolf Magne Larssen, 1996:119, ISBN 82-471-0014-2, ISSN 0802-3271.

“Numerical modelling of plain and reinforced concrete by damage mechanics”,
Mario A. Polanco-Loria, 1997:20, ISBN 82-471-0049-5, ISSN 0802-3271.

“Nonlinear random vibrations - numerical analysis by path integration methods”,
Vibeke Moe, 1997:26, ISBN 82-471-0056-8, ISSN 0802-3271.

“Numerical prediction of vortex-induced vibration by the finite element method”,
Joar Martin Dalheim, 1997:63, ISBN 82-471-0096-7, ISSN 0802-3271.

“Time domain calculations of buffeting response for wind sensitive structures”,
Ketil Aas-Jakobsen, 1997:148, ISBN 82-471-0189-0, ISSN 0802-3271.

"A numerical study of flow about fixed and flexibly mounted circular cylinders",
Trond Stokka Meling, 1998:48, ISBN 82-471-0244-7, ISSN 0802-3271.

“Estimation of chloride penetration into concrete bridges in coastal areas”,
Per Egil Steen, 1998:89, ISBN 82-471-0290-0, ISSN 0802-3271.

“Stress-resultant material models for reinforced concrete plates and shells”,
Jan Arve Øverli, 1998:95, ISBN 82-471-0297-8, ISSN 0802-3271.

“Chloride binding in concrete. Effect of surrounding environment and concrete composition”,
Claus Kenneth Larsen, 1998:101, ISBN 82-471-0337-0, ISSN 0802-3271.

“Rotational capacity of aluminium alloy beams”,
Lars A. Moen, 1999:1, ISBN 82-471-0365-6, ISSN 0802-3271.

“Stretch Bending of Aluminium Extrusions”,
Arild H. Clausen, 1999:29, ISBN 82-471-0396-6, ISSN 0802-3271.

“Aluminium and Steel Beams under Concentrated Loading”,
Tore Tryland, 1999:30, ISBN 82-471-0397-4, ISSN 0802-3271.

"Engineering Models of Elastoplasticity and Fracture for Aluminium Alloys",
Odd-Geir Lademo, 1999:39, ISBN 82-471-0406-7, ISSN 0802-3271.

"Kapasitet og duktilitet av dybelforbindelser i trekonstruksjoner",
Jan Siem, 1999:46, ISBN 82-471-0414-8, ISSN 0802-3271.

“Etablering av distribuert ingeniørarbeid; Teknologiske og organisatoriske erfaringer fra en norsk ingeniørbedrift”, Lars Line, 1999:52, ISBN 82-471-0420-2, ISSN 0802-3271.

“Estimation of Earthquake-Induced Response”,
Símon Ólafsson, 1999:73, ISBN 82-471-0443-1, ISSN 0802-3271.

“Coastal Concrete Bridges: Moisture State, Chloride Permeability and Aging Effects”
Ragnhild Holen Relling, 1999:74, ISBN 82-471-0445-8, ISSN 0802-3271.

”Capacity Assessment of Titanium Pipes Subjected to Bending and External Pressure”,
Arve Bjørset, 1999:100, ISBN 82-471-0473-3, ISSN 0802-3271.

“Validation of Numerical Collapse Behaviour of Thin-Walled Corrugated Panels”,
Håvar Ilstad, 1999:101, ISBN 82-471-0474-1, ISSN 0802-3271.

“Strength and Ductility of Welded Structures in Aluminium Alloys”,
Miroslaw Matusiak, 1999:113, ISBN 82-471-0487-3, ISSN 0802-3271.

“Thermal Dilation and Autogenous Deformation as Driving Forces to Self-Induced Stresses in High Performance Concrete”, Øyvind Bjøntegaard, 1999:121, ISBN 82-7984-002-8, ISSN 0802-3271.

“Some Aspects of Ski Base Sliding Friction and Ski Base Structure”,
Dag Anders Moldestad, 1999:137, ISBN 82-7984-019-2, ISSN 0802-3271.

"Electrode reactions and corrosion resistance for steel in mortar and concrete",
Roy Antonsen, 2000:10, ISBN 82-7984-030-3, ISSN 0802-3271.

"Hydro-Physical Conditions in Kelp Forests and the Effect on Wave Damping and Dune Erosion. A case study on Laminaria Hyperborea",
Stig Magnar Løvås, 2000:28, ISBN 82-7984-050-8, ISSN 0802-3271.

"Random Vibration and the Path Integral Method",
Christian Skaug, 2000:39, ISBN 82-7984-061-3, ISSN 0802-3271.

"Buckling and geometrical nonlinear beam-type analyses of timber structures",
Trond Even Eggen, 2000:56, ISBN 82-7984-081-8, ISSN 0802-3271.

”Structural Crashworthiness of Aluminium Foam-Based Components”, Arve Grønsund Hanssen, 2000:76, ISBN 82-7984-102-4, ISSN 0809-103X.

“Measurements and simulations of the consolidation in first-year sea ice ridges, and some aspects of mechanical behaviour”, Knut V. Høyland, 2000:94, ISBN 82-7984-121-0, ISSN 0809-103x.